Stony Brook University

THE EFFECT OF COMBINED FLUID SHEAR STRESS AND CYCLIC TENSILE STRETCH ON VASCULAR ENDOTHELIAL CELLS

A Dissertation Presented

by

Daphne Meza

to

The Graduate School

in Partial Fulfillment of the

Requirements

for the Degree of

Doctor of Philosophy

in

Biomedical Engineering

Stony Brook University

May 2017

Stony Brook University

The Graduate School

Daphne Meza

We, the dissertation committee for the above candidate for the

Doctor of Philosophy degree, hereby recommend

acceptance of this dissertation.

Dr. Wei Yin – Dissertation Advisor
Associate Professor
Department of Biomedical Engineering

Dr. Stefan Judex - Chairperson of Defense
Professor
Department of Biomedical Engineering

Dr. Mary D. (Molly) Frame
Associate Professor
Department of Biomedical Engineering

Dr. Carlos Colosqui
Assistant Professor
Mechanical Engineering Program
Department of Mechanical Engineering

This dissertation is accepted by the Graduate School

Charles Taber

Dean of the Graduate School

Abstract of the Dissertation

THE EFFECT OF COMBINED FLUID SHEAR STRESS AND CYCLIC TENSILE STRETCH ON VASCULAR ENDOTHELIAL CELLS

by

Daphne Meza

Doctor of Philosophy

in

Biomedical Engineering

Stony Brook University

2017

Vascular wall endothelial cells (ECs) are continuously subject to blood flow-induced shear stress and vasodilation-constriction induced tensile (or compressive) stress/strain. Altered mechanical environment can trigger EC activation and lead to atherosclerosis. Atherosclerosis is the main cause of coronary artery disease, which is the leading cause of death in the US. The functional and morphological response of ECs to fluid shear stress (FSS) or cyclic strain (CS) has been well documented. However, the responses of ECs to concomitant FSS and CS, have not been well characterized. A better understanding of this process can lead to more targeted preventive and therapeutic solutions for vascular diseases such as atherosclerosis.

To investigate and better quantify the relationship between biomechanics and atherosclerosis formation, a patient-specific fluid-structure interaction (FSI) model of the left coronary artery was developed. The model incorporated transient blood flow, blood vessel cyclic bending and stretching, as well as myocardial contraction, to provide a physiologically relevant simulation of blood flow, shear stress and tensile strain conditions within the left coronary artery. Blood flow-induced FSS and CS on the vascular wall under various physiological and pathological conditions were estimated.

In parallel, a novel shearing-stretching device was developed, to apply physiologically relevant FSS and CS concomitantly to cultured human coronary artery endothelial cells. Upon mechanical stimulation, endothelial cell morphological and functional responses were characterized. Changes in cell morphology were evaluated through cell area and elongation. Changes in EC functional responses were evaluated by characterizing EC activation, (i.e., ICAM-1 and phosphorylated PECAM-1 expression) and associated mechanotransduction (MAPK) pathway activation. Cells subjected to pathological FSS and CS mechanical conditions, in comparison to cells subjected to physiological conditions, were significantly bigger in area and presented significantly increased EC activation. Concomitant FSS and CS stimulation induced significant changes in endothelial cell function, compared to when cells were exposed to only FSS or CS alone. These findings demonstrate the complex interplay between altered FSS and CS, and suggest both FSS and CS need to be considered to investigate how mechanical stress/strain affects endothelial cell mechanotransduction, pathophysiological responses and disease initiation.

To my family, especially my parents, Elvin Meza and Liliana Sanchez.

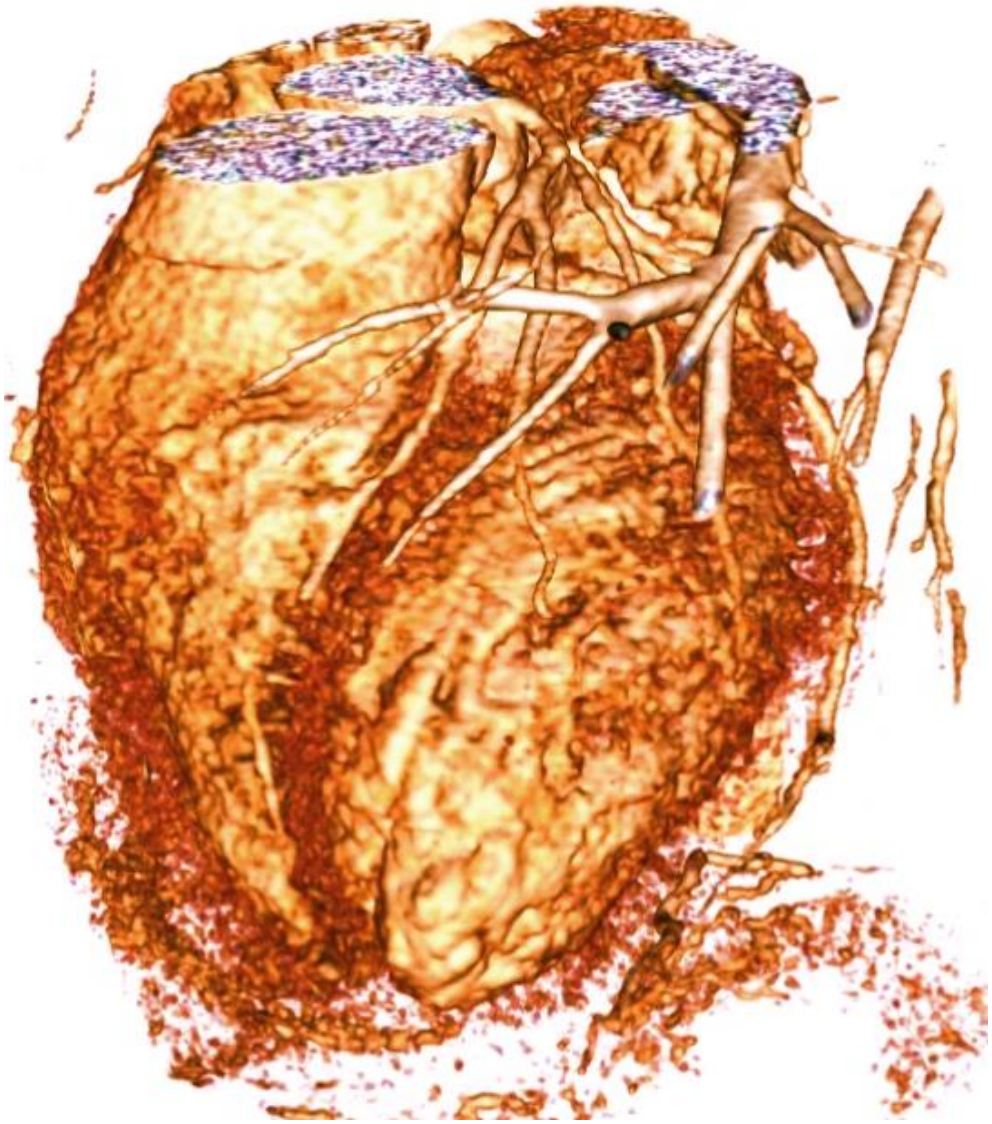

Frontispiece: Computed Tomography of a patient's heart, from which much of this work was based on.

TABLE OF CONTENTS

List of Figures

List of Tables

List of Abbreviations

ALE – Arbitrary Langragian
ANOVA – Analysis or variance
BCA – Bicinchoninic acid assay
CAD – Cardiovascular Disease
CFD – Computational fluid dynamics
CS – Cyclic Strain
CT – Computed Tomography
DAPI – 4',6-Diamidino-2-phenylindole
EC – Endothelial cell
ERK - Extracellular-signal-regulated kinase
eNOS – Endothelial nitric oxide synthase
FSI – Fluid-structure interaction
g – Gravitational field 9.81 m/s^2
HCAEC – Human coronary artery endothelial cells
Hz – cycle / second
ICAM – Intercellular-Adhesion Molecule
IVUS – Intravascular ultrasound
JNKs – C-Jun N-terminal kinases
LAD – Left Anterior Descending
LDL –Low density lipoproteins
MAPK – Mitogen-activated protein kinases
MR – Mooney Rivlin
mRNA – Messenger ribonucleic acid
NA – Numerical aperture
NKκB – Nuclear factor kappa-light-chain-enhancer of activated B cells
NO – Nitric oxide
PECAM – Platelet-Endothelial Cell Adhesion Molecule
RT-PCR – Reverse transcriptase-polymerase chain reaction
WSS – Wall Shear Stress

Acknowledgments

First and foremost I would like to thank my advisor, Dr. Wei Yin, for making this dissertation and research experience possible. She shared invaluable one-on-one time with me, either teaching lab protocols, discussing current projects, or planning future goals. She gave me freedom in research but at the same time kept me focused. Importantly, she also managed a lab environment and culture which stimulated creativity, curiosity, progress, and friendliness. This made an already enjoyable research task even more enjoyable, and also provided relief when things weren't going as planned. She not only guided me in lab work, but was also a few steps away if I ever needed advice in anything else. She provided me with the guidance, knowledge, and materials needed to start off and grow as a scientist. Her love for research is inspiring and I was lucky enough to have been allowed to share in with some of it.

I want to thank Dr. Rubenstein for being a mentor to me as well, for being open to conversation and between jokes, help me in different aspects of my dissertation. Apart from scientific advice, Dr. Rubenstein lightened the lab environment and provided everyone with much needed laughter. He entertained us in between experiments with daily life stories that I will always remember. As a mentor, he was also a door knock away, for help in any area of my life, even to the extent of teaching us how to change our own car oil.

Thank you so much to my committee members who shared with me their time and knowledge through this process. Dr. Judex, thanks for your great support in award nominations, and for being available if I ever needed it. Thanks for being open to conversation, and for being a great teacher. Dr. Frame, thanks for your scrutiny in my work, and for asking questions which force me to think about my work through different perspectives. Dr. Colosqui, thanks for your guidance in the computer modeling, for your support and eagerness to help.

I am grateful for the graduate and undergraduate students who helped me complete different parts of my dissertation or whom I shared lab time with. I enjoyed the time spent together and the relationships that came out of it. Louie Abejar, Bryan Musmacker, Wo Sun, Elisabeth Steadman, Stephen Leung, Samuel Lederer, Marina Fandaros, Thomas Stransky and Yie Ding, thanks for the helping hands provided. Sarah Hom, Kirstin Barber, Ioana Soaita, Sehar Laljee, and everyone aforementioned, thanks for the friendships built.

Thanks also to the people who believed in me and pushed me into research, even before graduate school. They had a great influence in my life and set a career path for me which I love and am immensely grateful for. Dr. Ashok Puri, head of the Louisiana Alliance for Minorities Program at University of New Orleans, help me attain my first research experience at Brookhaven National Laboratory. He advised me to attend conferences and supported me always. Dr. Lisa Miller was the person with which I had my first biomedical research experience. I loved the work and really appreciated working with her. I don't think I would be in graduate school if it wasn't for her. Thanks for continuing to be there. I am grateful I got to learn about GEM through friends at BNL. I am also grateful for Toni Sperzel who recruited me from BNL.

To the Center for Inclusive Education, who 100% supported me, both morally and financially. Dr. Angel Gonzalez, thanks for being a great mentor and friend. Thanks for being someone I felt comfortable with bringing up any kind of issue. Thanks for guiding me through tough transitions here at Stony Brook, and thanks for knowing my story.

To Dr. Jonathan Liu, thanks for letting me learn about microscopy and participate in the development of medical devices. To Danni Wang, Ye Chen, Steven Leigh, Yu Wang, and Altaz Khan thank you for the time and work shared.

Thank you to my friends who were there either part of the time or through it all: Manisha Rao, Roshni Kothadia, Yesenia Miranda, Jeyannt San, Gaurav Lalwani, Ana Delgado, and everyone from the -1800YAS Papi group, thanks for the support and all the great times shared. Ronak Dholakia, thank you for being my ADINA mentor, for all the discussions and teachings along the way.

Special thanks to my boyfriend, Frank Celeste, who has been there for me, supporting me and helping me along the way. I am thankful he has been there through happy, tough, stressful, and joyous days. Thanks for carrying the burden with me and thanks for sharing your life with me and making ours happier.

Thanks to my family's unconditional love and support throughout these five years. Mom, thanks for always being there and providing me with much needed love and comfort during this time. Dad, thanks for believing in me. Nicole and Melanie, thanks for your love and support. Extended family, uncles, aunts, cousins, godparents, thanks for loving me, even at a distance and being 100% supportive.

Publications

1. **Daphne Meza**, Saravan K. Shanmugavelayudam, Arielys Mendoza, Coralys Sanchez, David Rubenstein, Wei Yin, 2017, “Platelets modulate endothelial cell response to dynamic shear stress through PECAM-1.” Thromb Res, 150, pp. 44-50.
2. **Daphne Meza**, David Rubenstein, Louie Abejar, Wei Yin, 2016, “A Shearing-Stretching Device That Can Apply Physiological Fluid Shear Stress and Cyclic Stretch Concurrently to Endothelial Cells.” J Biomech Eng-T Asme, 138(3).
3. **Daphne Meza**, Danni Wang, Yu Wang, Sabine Borwege, Nader Sanai, and Jonathan T. C. Liu, 2015, "Comparing high-resolution microscopy techniques for potential intraoperative use in guiding low-grade glioma resections," Lasers Surg Med, 47(4), pp. 289-295.
4. Danni Wang, **Daphne Meza**, Yu Wang, Liang Gao and Jonathan T. C. Liu, 2014, "Sheet-scanned dual-axis confocal microscopy using Richardson–Lucy deconvolution," Optics Letters, 39(18), pp. 5431-5434.
5. Jonathan T. C. Liu, **Daphne Meza**, and Nader Sanai, 2014, "Trends in fluorescence image-guided surgery for gliomas," Neurosurgery, 75(1), pp. 61-71.
6. Yu Wang, Altaz Khan, Steven Leigh, Danni Wang, Ye Chen, Steven Leigh, **Daphne Meza**, McVeigh, P. Z., Wilson, B. C., and Liu, J. T., 2014, "Rapid ratiometric biomarker detection with topically applied SERS nanoparticles," Technology (Singap World Sci), 2(2), pp. 118-132
7. Yu Wang, Altaz Khan, Steven Leigh, Danni Wang, Ye Chen, **Daphne Meza**, and Jonathan T. C. Liu, 2014, "Comprehensive spectral endoscopy of topically applied SERS nanoparticles in the rat esophagus," Biomed Opt Express, 5(9), pp. 2883-2895.

On Preparation:

1. **Daphne Meza**, David Rubenstein, Wei Yin, 2017, “A comprehensive fluid-structure interaction model of the left coronary artery.”
2. **Daphne Meza**, Elisabeth Steadman, Thomas Stransky, Bryan Musmacker, David Rubenstein, Wei Yin, 2017, “Effect of concurrent fluid shear stress and cyclic strain on endothelial cell activation.”

Chapter I

INTRODUCTION, SPECIFIC AIMS AND SIGNIFICANCE

Coronary artery disease (CAD) (also known as coronary heart disease) is the leading cause of death in the US [4]. Coronary arteries (**Figure 1A**) are the vessels that supply blood to the cardiac muscles. CAD occurs when the coronary arteries are blocked due to plaque accumulation, or atherosclerosis (**Figure 1B**). Decreased blood supply to the heart can cause myocardial infarction (heart attack).

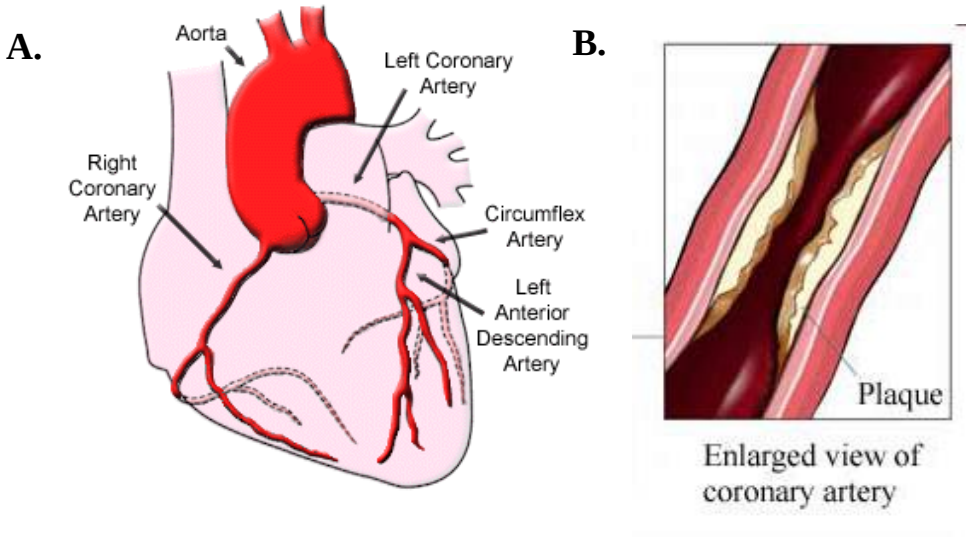

Figure 1. A) Coronary arteries supply blood to the heart muscles. [1] B) Enlarged view of an obstructed coronary artery due to plaque accumulation (atherosclerosis) [3]

There are two main coronary arteries which supply the heart: the right and the left coronary artery (**Figure 1A**). The left coronary artery divides into two branches, the circumflex artery and the left anterior descending (LAD) artery. The LAD's obstruction accounts for 40-50% of myocardial infarctions, as compared to 15-20% caused by circumflex artery blockage and 30-40% by right coronary artery obstruction [5].

Both biochemical and biomechanical factors play important roles in CAD development [6, 7]. The study of how biomechanical factors affect CAD development has had a growing interest in the last decades, and it is the focus of this dissertation.

The theory of the important role hemodynamics/biomechanics has on atherosclerosis formation was proposed by Mustard[8], Fox[9], Texon[10], Mitchell[11], Fry[12] and Caro et al[13], in the 1960-1970's [14, 15]. Their hypothesis was presented to account for the localization of atherosclerosis in the arterial system, evidenced in clinical and postmortem studies. These studies found that atherosclerotic lesions on human vessels do not develop randomly throughout the vasculature (**Figure 2**), instead lesions occur focally at bifurcations, branch ostia and curvatures in the arterial tree where blood flow is disturbed and flow separation from the vessel wall, along with formation of eddies are likely to occur[16-18] (also termed regions of recirculating or oscillatory flow). Fry[12] and Caro[13] specifically proposed low and high wall shear stresses induced by blood flow might be the cause of atherosclerosis localization. Since then, many *in vitro* and *in vivo* studies have validated their theory.

Shear stress, which is the frictional force induced by blood flow acting on the vessel wall is sensed and mechanotransduced by endothelial cells lining the inner portion of the vessel wall into a biochemical signal that results in either an atherogenic or atheroprotective response by the cells. Low shear stress (<10 dynes/cm^2), prevalent at atherosclerosis-prone sites, stimulates an atherogenic response, while normal shear stress, prevalent at disease-free regions along the vasculature (>10 dynes/cm^2, but <25 dynes/cm^2) induces an atheroprotective endothelial cell response[19-21]. Furthermore, high shear stress (>25 dynes/cm^2) prevalent at plaque protusions, or stenosis throats, is thought to elicit atherogenic responses as well[22], but more studies are needed to support this claim.

The mechanotransduction process is thought to start off with common mechanotransducers such as platelet-endothelial cell adhesion molecule (PECAM-1). Depending on the magnitude, frequency and duration of the mechanical signal, PECAM-1 can then phosphorylate and activate the mitogen-activated protein kinases (MAPK) pathway[23, 24] via the phosphorylation of extracellular signal-regulated kinases

(ERK)1/2, c-Jun N-terminal kinases (JNK) and p38. This MAPK activation would then result in the activation of transcriptional factors (such as nuclear factor kappa-light-chain-enhancer of activated B cells, NF-κB) [25, 26]. Subsequently, the expression of EC surface inflammatory proteins (such as intercellular-adhesion molecule, ICAM-1) would increase [26, 27], enhancing leukocyte transmigration and many other inflammatory responses [28, 29]. These inflammatory responses could potentially lead to atherosclerosis formation.

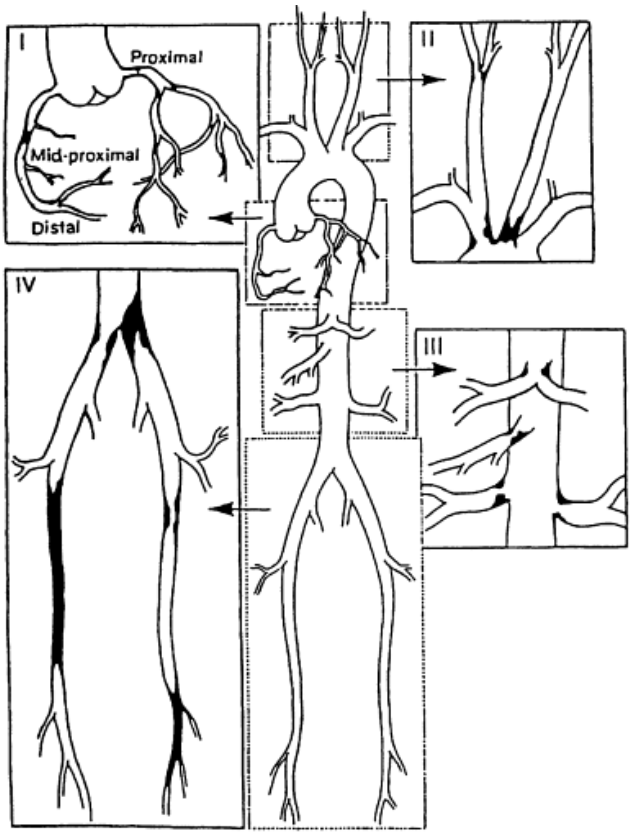

Figure 2. Distribution of atherosclerosis in humans. Atherosclerosis occurs preferentially at bifurcations where blood flow is disturbed and oscillatory. [2]

The EC change in function in response to mechanical stimuli, is also accompanied by an apparent morphological change. ECs adjust their cytoskeleton to maintain homeostasis. In disease-free regions of the vasculature, were flow is laminar, ECs align and elongate parallel to the direction of flow[30]. This alignment reduces their resistance to flow and activates atheroprotective mechanotransductory pathways. Along bifurcations and areas were flow is disturbed and oscillatory, ECs exhibit a cobblestone morphology, with no definite alignment[31]., which is thought to expose ECs to greater shear stress gradients and be responsible for the activation of atherogenic mechanotransductory pathways[32].

However, *in vivo*, ECs are exposed to a complex set of mechanical stimuli. Coronary artery endothelial cells are exposed to shear stress induced by blood flow, along with cyclic tensile strains induced by the artery's cyclic displacement, bending and contraction during the cardiac cycle [33, 34] (Refer to **Figure 3**). Cyclic strain varies in magnitude, frequency, direction, and can be isotropic and anisotropic in nature[35].

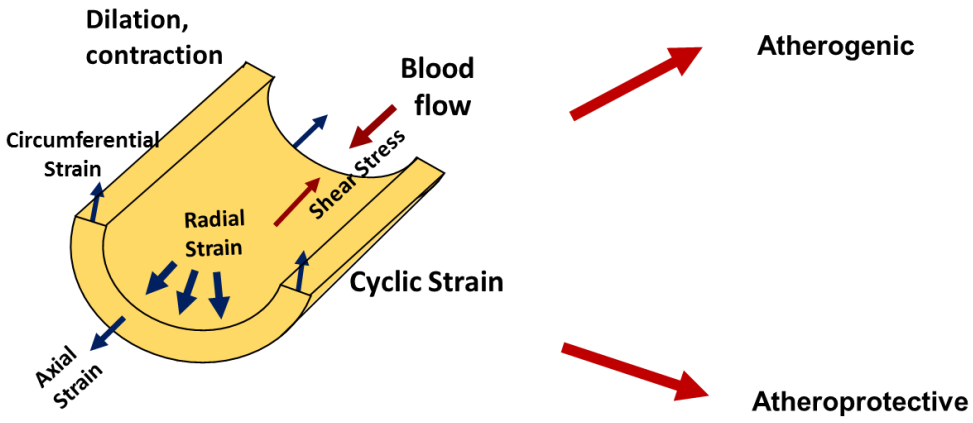

Figure 3. Endothelial cells lining the inner vessel wall are exposed to two major forces: A) cyclic strain and B) fluid shear stress. Cells can react in either an atherogenic or atheroprotective way to their mechanical environment.

ECs are sensitive to cyclic strain and also react in either an atherogenic or atheroprotective manner to this stimuli. Cyclic strain, similar to shear stress, is known to affect various cellular processes, including alignment, vascular angiogenesis, endothelial barrier function, proliferation, apoptosis and differentiation [35-38]. Physiological and pathological strain magnitudes depend on the type of endothelial cell and are not clearly distinguished. Some studies have shown physiological and pathological strains in pulmonary arterial endothelial cells, for example, are 5% and 18% respectively[36]. However, magnitudes for coronary artery endothelial cells have not been clearly distinguished.

Since ECs are sensitive to both shear stress and cyclic strain, and they are exposed to both concomitantly, studying EC response to both stresses is more physiologically relevant. The better this complex mechanical environment is mimicked in *in vivo* studies, the more natural *in vivo* cell behavior will be elicited. Changes in shear stress and tensile strain can lead to atherosclerosis development [39], yet how shear stress and tensile strain act together to affect endothelial cell function has not been well characterized. Understanding the relationship between mechanical stimuli and vascular pathology can lead to improved treatments. In order to be able to study the response of ECs to both stresses concomitantly, systems need to be designed that will allow for that.

Over the years, only a handful of systems have been developed to apply concurrent shear stress and cyclic stretch to ECs *in vitro*. In most of these systems, distensible tubes have been used to mimic veins or arteries [40-48]. Endothelial cells were seeded in the inner lining of the distensible tubes and flow and pressure were applied to simulate blood flow and circumferential stretching. Microfluidic cell culture channels then became popular in recent years [49]. Cells were cultured on suspended thin films inside channels which mimic segments of blood vessels. Some devices applied pressure and flow simultaneously to ECs cultured on thin flexible membranes, through pulse generator or other customized control systems [50-53]. These devices all applied a combination of uniaxial/biaxial strain and fluid shear stress concomitantly. Recently, Ravi Sinha et al.[54] developed a microfluidic device than can apply anisotropic

strain and fluid shear stress combinations. Even though this area of study is slowly growing, it remains underinvestigated.

These studies demonstrated that EC response to shear stress and cyclic stretch depends on whether the two stresses (or strains) are applied separately or simultaneously [55]. It was reported that both shear stress and cyclic stretch can equally affect the orientation and alignment of ECs [44], and that concurrent application of shear stress and tensile stretch may affect EC oxidative stress [56], intercellular junction protein expression, and EC permeability [57]. Furthermore, differences in phase relationship between the two mechanical stimuli can lead to significant differences in EC morphological response[58].

The **goal** of the present study was to characterize stress/strain (especially fluid shear stress and vascular wall tensile stress/strain) conditions in the left coronary artery, and to determine how these stresses/strain conditions affect endothelial cell pathophysiology. The underlying ***hypothesis*** was that ***the concurrent stimulation from altered shear stress and tensile strain may lead to significant changes in EC morphology and function, accelerating local inflammatory responses***.

Three specific aims were carried out to test the hypothesis.

Specific Aim 1: A fluid-structure interaction (FSI) model of the left anterior descending (LAD) coronary artery was developed under physiological and pathological conditions, to determine the dynamic fluid shear stress (FSS) and cyclic tensile strain (CS) distribution on the coronary artery wall. Patient-specific geometry, transient blood flow, blood vessel wall viscoelasticity, blood vessel cyclic bending, and myocardium contraction were incorporated into the FSI model to increase the physiological relevance of the model.

Specific Aim 2: A programmable shearing-stretching device that is capable of applying physiologically relevant dynamic fluid shear stress (FSS) and cyclic tensile strain (CS) simultaneously to endothelial cells (EC) was designed, fabricated, characterized and validated.

The system integrated a programmable vacuum-driven strain device with a programmable cone-and-plate shearing device, to allow concurrent application of pulsatile shear stress and cyclic strain to cultured ECs. Its main advantage over other similar systems is its ease of use and precise control of shear stress and strain. Stress/strain conditions generated by the device were validated experimentally, and the effectiveness of the device was evaluated through EC morphology changes under various mechanical loading conditions.

Specific Aim 3: Based on results obtained from Aim 1, physiological or pathological shear stress and/or tensile strain were applied to cultured human coronary artery endothelial cells (HCAEC) using the shearing-stretching device, developed in Aim 2. EC morphological and functional responses to single and combined stimuli were characterized. Changes in cell morphology were evaluated by cell area and elongation. Changes in EC inflammatory responses were evaluated by characterizing EC activation, i.e., cell surface ICAM-1 expression, PECAM-1 tyrosine phosphorylation, mechanotransduction pathway activation, i.e. MAPK pathway and associated transcription factor NF-κB activation.

Significance

The FSI model was the first model that incorporated patient specific geometry, transient blood flow, blood vessel motion, and myocardial contraction, to simulate blood flow and stress/strain conditions within the left coronary artery. The innovative shearing-stretching device enabled us to investigate EC mechanotransduction and inflammatory responses under dynamic FSS and CS simultaneously.

The results obtained from this study would help us to better understand how different mechanical stress/strain conditions interact to regulate EC function and disease initiation. New insight in EC mechanotransduction under physiological and pathological mechanical conditions will help to identify factors that are responsible for EC dysfunction, and lead to preventive and therapeutic solutions for cardiovascular disease [59].

Chapter II

FLUID-STRUCTURE INTERACTION MODEL OF THE HUMAN LEFT ANTERIOR DESCENDING CORONARY ARTERY

Manuscript in preparation:

Daphne Meza, David A. Rubenstein, Wei Yin, 2017, "A comprehensive fluid-structure interaction model of the left coronary artery," Biomechanics and Modeling in Mechanobiology

2.1 Abstract

A left coronary artery fluid-structure interaction (FSI) model was developed in this study. The model included not only transient blood flow conditions and cyclic motion of the artery (bending and stretching), but also pressure induced by myocardial contraction. A patient-specific 3D geometry of the left anterior descending (LAD) artery was constructed in ADINA, based on computed tomography angiography (CTA) data. To simulate disease conditions, a 70% stenosis was placed in the LAD. A physiologically relevant and fully developed velocity profile (0-12 cm/sec) was prescribed at the inlet of the LAD. The bending motion and displacement of the blood vessel were imposed based on the LAD's spatial information obtained from the CTA data. The cardiac muscle contraction-induced pressure (0-25 kPa) was applied to the outside of the vessel wall during systole. The inner blood vessel wall was defined as the fluid-structure interface. The fluid volume was solved using the Arbitrary Lagrangian-Eulerian formulation of the Navier-Stokes equations. The fluid and solid were fully coupled using a direct coupling method. The results demonstrated that myocardial contraction had a significant effect on the local hemodynamics. Specifically, it transiently increased blood flow velocity and fluid wall shear stress by approximately 4 folds. Under physiological conditions, fluid wall shear stress varied between 0 and 2.63 Pa, whereas under stenosis conditions, oscillating fluid wall shear stress occurred, and the maximum shear stress increased to 10.3 Pa in various regions near the stenosis throat. Circumferential strain developed in the blood vessel wall varied between 2-10.8% under physiological conditions and decreased to 0-4.5% under stenosis conditions. These results underscore the importance of incorporating transient flow, blood vessel motion and myocardial contraction when simulating coronary artery hemodynamics. With improved physiological relevance, this FSI model can help us to better understand the complex and dynamic mechanical environment within the left coronary artery, and elucidate how mechanical factors contribute to the initiation and development of coronary artery disease.

2.2 Introduction

The left anterior descending (LAD) coronary artery is considered the most critical vessel in terms of myocardial perfusion, since it supplies blood to 45-55% of the left ventricle [60]. The narrowing or blockage (severe occlusion of the artery) of the LAD due to atherosclerosis results in 40-50% of all heart attacks [5] and causes over 185,000 deaths in the US annually [61].

Besides genetic and life-style factors, biomechanics play a key role in atherosclerosis initiation and progression. Atherosclerosis only occurs at certain locations within the vasculature [15, 62, 63]. Atherosclerotic plaque tends to accumulate in areas with altered biomechanical conditions, such as altered fluid shear stress induced by disturbed blood flow, and/or altered tensile strain within the vascular wall due to changed local blood pressure or vessel compliance [64, 65]. Accelerated blood flow and elevated shear stress occur near a stenosis (i.e., blood vessel restriction due to atherosclerotic plaque accumulation), while stagnant flow and low shear stress are common near a bifurcation or within the recirculation zones downstream of a stenosis. With a plaque built up, the vascular wall tensile strain would change, due to the increased stiffness of the blood vessel wall. Pathological shear stress and/or tensile strain can cause atherogenic responses in vascular endothelial cells, by enhancing inflammatory protein expression and leukocyte transmigration [21, 37].

To better understand how atherosclerosis and coronary artery disease develop, the complex mechanical environment including, 1) shear stress induced by blood flow, 2) axial stretch due to cyclic bending, and 3) circumferential strain induced by blood pressure and myocardial contraction [66-68], within the coronary arteries need to be better characterized. Numerical simulation provides an effective solution to estimate fluid shear stress and vascular wall strain within the coronary artery, as neither can be effectively measured *in vivo.*

Current Ultrasound, Magnetic Resonance Imaging (MRI), and fused Intravascular Ultrasound (IVUS) Computed Tomography (CT) based methods have various limitations to measure wall shear stress (WSS). UItrasound is restricted by limited spatial resolution and therefore can only be used to estimate fluid shear stress in relatively straight arteries [69]. 4D MRI can considerably underestimate wall shear stress magnitude due to a lack in spatiotemporal resolution [70, 71]. Fused IVUS CT methods are "invasive" in nature [72], and can only be applied to patients who are already undergoing catheterization.

Methods to measure strain *in vivo* are more common, since these are typically used to identify vulnerable plaques (plaque at risk of rupture). These methods include ultrasound based variants such as Dobutamine Stress Echocardiography (DSE)[73], Doppler Stress Imaging (DSI) [74], 2D Speckle Tracking Ecocardiography (STE) [73, 74], Ultrasound Palpography [75], Non-invasive Vascular Ultrasound Elastography (NIVE) [76], Automatic Function Imaging (AFI) [77], among others [78]. Ultrasound scanning is always a compromise between resolution and penetration. Given that the coronary arteries are located relatively deep inside the body, invasive intraluminal echocatheters are needed to image them. Therefore, the greatest disadvantage of all these ultrasound techniques is all are invasive. These techniques can also affected by translational motion [79], angle dependent measurements [76, 80, 81] and subjective interpretation which is a result of both image quality and experience [82-84].

In recent years, many fluid-structure interaction (FSI) models of the coronary arteries have been developed to simulate blood flow-arterial wall interactions. The dynamic movement of the arterial wall influences the motion of the blood, and the arterial wall displacement is computed based on the force generated by the blood as it travels through the vessel. Many of those models were successful in elucidating stress-strain conditions in the coronary arteries, by including patient-specific geometry [85, 86], pulsatile flow, cyclic bending [87] and anisotropic material properties of the blood vessel wall [88].

However, few of those models have considered the effect of myocardial contraction on hemodynamics and blood vessel wall strain conditions [89]. A large portion of the left coronary artery is embedded within the myocardium. During systole, the cardiac muscles contract, which can constrict the

left coronary artery, and significantly reduce coronary blood flow [90]. The magnitude of this contraction, i.e., squeezing of the myocardium on the external blood vessel wall, can reach 40 kPa [67]. Ignoring the effect of such a huge contraction force would likely result in an underestimation of flow and strain conditions within the left coronary artery.

Zhang et al incorporated myocardial contraction into a 2D FSI model to compare the difference between epicardial and intramural arteries [91]. They reported that due to myocardial contraction, the maximum blood flow velocity increased slightly. However, simplified 2D geometry and flow conditions limited the physiological relevance of this model. Smith et al [92] developed a FSI model to investigate if myocardial contraction would inhibit coronary blood flow. Their model showed that a so-called "intramyocardial pump" played a dominant role in reducing systolic flow. However, the effects of cardiac muscle contraction on blood hemodynamics, fluid shears stress, or blood vessel wall tensile stress, were under investigated. In 2011, Ohayon et al [93] developed a patient-specific finite element (FE) model to study the effect of myocardial contraction on coronary blood vessel wall stress and strain distribution. They reported that wall strain stiffening induced by myocardial contraction, was an additional process contributing to the initiation of atherosclerosis. However, how blood flow interacted with the vessel wall was not considered in their study.

In the present study, a FSI model of the left contrary artery was developed based on a patient-specific LAD geometry. This model incorporated transient blood flow, blood vessel cyclic bending and stretching, as well as myocardial contraction, to provide a physiologically relevant estimation of blood flow, shear stress and tensile strain conditions within the left coronary artery, under physiological and pathological conditions.

2.3 Materials and Methods

The 3D geometry of a healthy left anterior descending artery (LAD) was constructed based on the anatomical CTA (Computed Tomography Angiography) data acquired from a patient at Tianjin First Center Hospital in China.

The myocardial area was isolated using 3D Slicer (Surgical Planning Labs, Boston), and LAD was segmented using the *colliding fronts segmentation algorithm* of the Vascular Modeling Tool Kit (VMTK, an open source software, www.vmtk.org). The 3-dimensional geometry of LAD was constructed and smoothed using SolidWorks (2015), and exported to ADINA (Version 9.2, ADINA R&D Inc., Watertown, MA) for mesh generation (**Figure 4A**). To simulate disease conditions, a 70% stenosis was added 8 mm downstream from the bifurcation of LAD and the left circumflex artery (LCX). The stenosed area (an intruding plaque) was positioned towards the arterial wall opposite to the myocardium (**Figure 4B**) [94]. The width of the lesion area was 3.05 mm and the length was 6.78 mm, which were typical for a 50-70% stenosis in the left coronary artery [95].

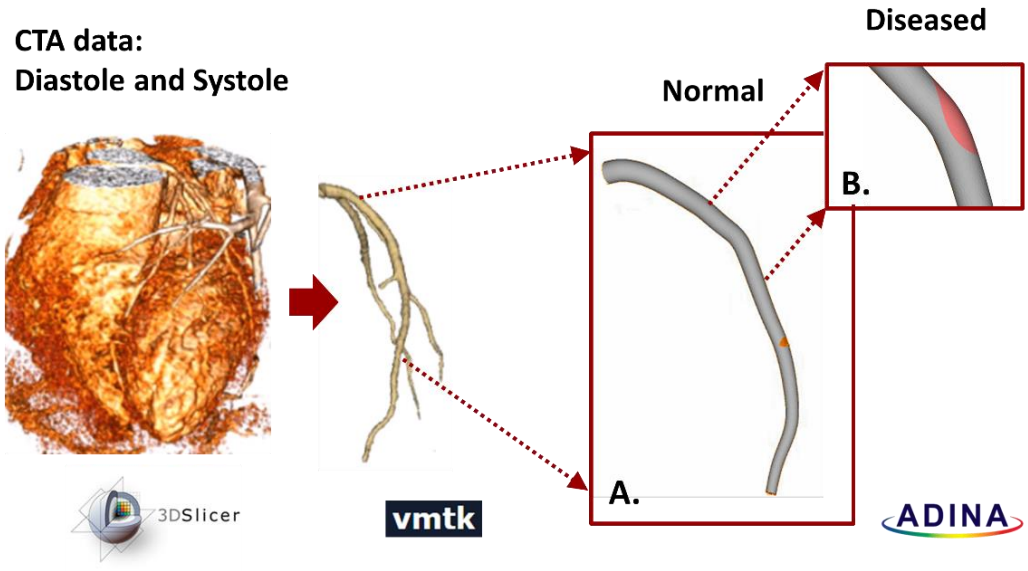

Figure 4. Patient-specific LAD segmentation workflow. Myocardium region was isolated from patient's CTA data. (A) The LAD was segmented and prepared for mesh generation. (B) Diseased condition was simulated by adding a 70% stenosis, 8 mm downstream from the LAD-LCX bifurcation.

Free-form triangular elements were generated for both the normal and the stenotic LAD geometries using the Delaunay meshing algorithm. The fluid domain (i.e., blood within the vessel) and the solid domain (i.e., the blood vessel wall) were meshed separately. To ensure mesh independence, mesh size (the number of elements) was increased gradually till the solution difference was less than 5%. In the present study, the normal LAD consisted of 39,284 elements in the solid domain and 373,903 elements in the fluid domain. In the 70% stenosis model, the solid domain included the vascular wall and the plaque. There were 39,214 elements in the wall, 30,778 elements within the plaque, and 374,517 elements in the fluid domain. For the stenosis model, adequate face linkage was employed to ensure nodal coincidence between the plaque and the arterial wall.

The diameter of LAD at the inlet was 3.82 mm, and that at the outlet was 1.59 mm. The total length of the model was 7.45 cm (**Figure 4A**). The arterial wall was defined as 3-D shell with a thickness of 0.25 mm [96]. During one cardiac cycle, LAD experienced large displacements due to cyclic bending and myocardial compression, which was prescribed based on the CTA data. **Figure 5A** depicts the centerline locations of LAD at the end of systole and diastole. The largest displacement occurred approximately 35 mm downstream from the inlet, and the outlet moved up/down by 7.5 mm.

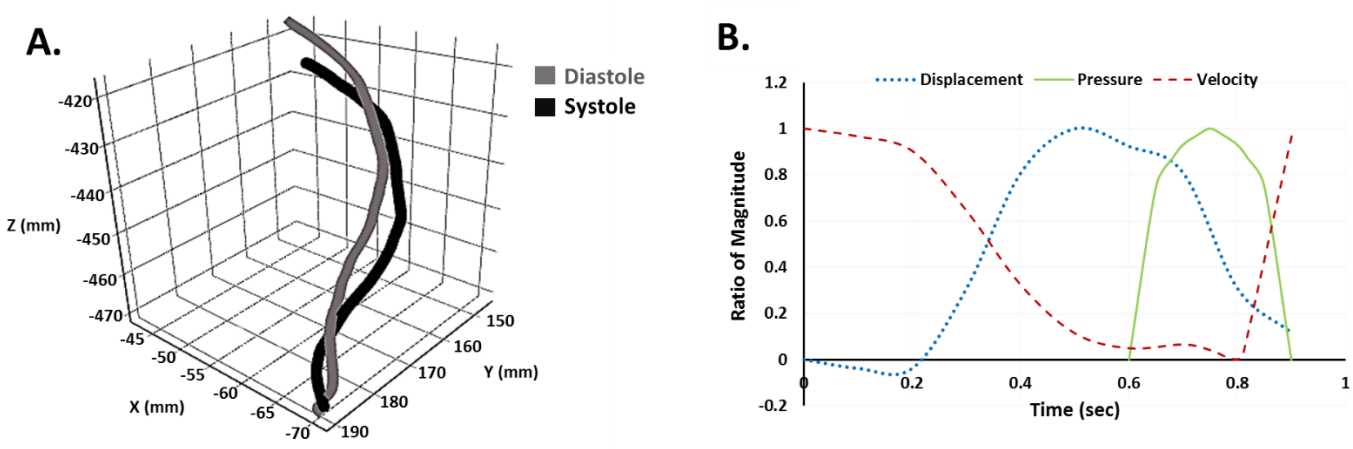

Figure 5. Input waveforms for the FSI model. (A) Cyclic displacement of LAD was computed by tracking centerline locations of the LAD at the end of diastole and systole. (B) Pressure waveform induced by myocardial contraction, inlet blood velocity waveform, and inner LAD wall displacement waveform during one cardiac cycle. Pressure induced by myocardial contraction changed between 0 and 25 kPa; inlet blood velocity varied between 0 and 12 cm/s; and displacement of the blood vessel varied between 0.3 mm and 7.5 mm. All waveforms are shown as ratio to the magnitude of displacement, pressure and velocity.

The arterial wall and the plaque were defined as nonlinear elastic, anisotropic, and incompressible materials. Their mechanical behavior was described using the hyper-elastic modified Mooney-Rivlin model with added anisotropic effects [97]. These anisotropic properties result from randomly oriented or aligned collagenous fibers within the blood vessel wall, which affect the response of the blood vessel to applied stress/strain significantly, especially when the strain is large.

The strain energy density function (W) for the Mooney-Rivlin model (stress-strain relationship) is given by [97, 98]:

$$W = c_{10}(I_1 - 3) + c_{01}(I_2 - 3) + c_{11}(I_1 - 3)(I_2 - 3) + c_{20}(I_2 - 3)^2 + c_{02}(I_2 - 3)^2 + D_1\left[e^{D_2(I_1-3)} - 1\right] + \frac{k_1}{2k_2}\{exp[k_2(J_1 - 1)^2] + exp[k_2(J_2 - 1)^2] - 2\}$$

(Equation 1)

where I_i are strain invariants of the Cauchy-Green deformation tensor and are defined as the following [97, 98]:

$$I_1 = \sum C_{ii} \quad \text{(Equation 2)}$$

$$I_2 = \frac{1}{2}(I_1^2 - C_{ij}C_{ij}); \quad \text{(Equation 3)}$$

$$I_3 = \det \boldsymbol{C} \quad \text{(Equation 4)}$$

$$I_4 = C_{ij}(n_a)_i(n_a)_j; \quad \text{(Equation 5)}$$

$$I_5 = C_{ij}(n_b)_i(n_b)_j; \quad \text{(Equation 6)}$$

$J_i's$ are the reduced invariants [97, 98], defined as the following:

$$J_1 = I_4 I_3^{-1/3} \quad \text{(Equation 7)}$$

$$J_2 = I_6 I_3^{-1/3} \quad \text{(Equation 8)}$$

The direction of the collagenous fibers are described by the normal vectors $\boldsymbol{n}_a$ and $\boldsymbol{n}_b$ with components $(n_a)_i$ and $(n_b)_i$ respectively [97, 98]. c_i, D_i and K_i are material constants chosen to match the experimental data (tensile stretch and histology) from human coronary arteries and calcified plaque, reported by Kural et al [99] and Karimi et al [100]. In those studies, the artery and plaque samples were pre-elongated (5%) during mechanical testing, simulating pre-stress conditions [99, 100]. **Table 1** summarizes the constants of the Mooney-Rivlin model and the added anisotropic properties.

Table 1. The Mooney-Rivlin constants and anisotropic constants for the normal vascular wall and the plaque.

	Mooney-Rivlin constants (MPa)							**Anisotropic constants (KPa)**	
	C_{10}	C_{01}	C_{20}	C_{11}	C_{02}	D_1	D_2	K_1	K_2
Vascular Wall[99]	-1.31	0.115	0	0	0	0.63	2	3.6	23.5
Plaque[100]	-0.49	0.50	3.63	1.19	4.73	0	0	-	-

The inlet of the arterial wall was fixed in all translational and rotational directions through the calculation to allow for model convergence.

To simulate the cyclic bending motion of the blood vessel, a displacement waveform (**Figure 5B**) calculated based on the CTA data was prescribed along the inner LAD wall. During one cardiac cycle, the maximum radius of curvature displacement was 7.5 cm (occurring at 0.5 sec).

The pressure induced by myocardial contraction was also included in the model. As depicted in **Figure 5B**, the squeezing of the cardiac muscles took place during systole, and the maximum pressure generated was approximately 25 kPa [67]. This load was imposed on LAD through the outside blood vessel wall.

A transient blood flow velocity input was applied at the inlet of LAD. During one cardiac cycle, the flow rate within the LAD varied between 0 and 100 mL/min, corresponding to a mean velocity of 0-12 cm/sec [101]. The maximum flow occurred during early diastole when the ventricles were relaxing and the extravascular compression of the coronary arteries was absent. Blood flow was assumed laminar, and blood was modeled as an incompressible and Newtonian fluid with a density of 1060 kg/m^3 and a dynamic viscosity of 3.5 cP. The LAD outlet was defined as a pressure outlet, with zero normal traction.

The inner surface of the LAD wall, and the outer boundary of the fluid volume were defined as the fluid-structure interface. At the interface, velocity and traction conditions were equal. The fluid domain was solved using the Arbitrary Lagrangian-Eulerian formulation of the Navier-Stokes equations. The fluid and solid were fully coupled using a direct coupling method with a coupling composite time step of 0.0025 sec. Default convergence criteria (10^{-3} tolerance) were used for both the force and the displacement calculation.

Following numerical simulation, blood flow velocity, wall fluid shear stress, and blood pressure distribution were analyzed for the fluid domain. Blood vessel wall circumferential and axial strains were calculated for the solid domain. Results obtained from the normal LAD model were compared to that of the stenosis model.

2.4 Results

2.4.1 Blood Flow Velocity

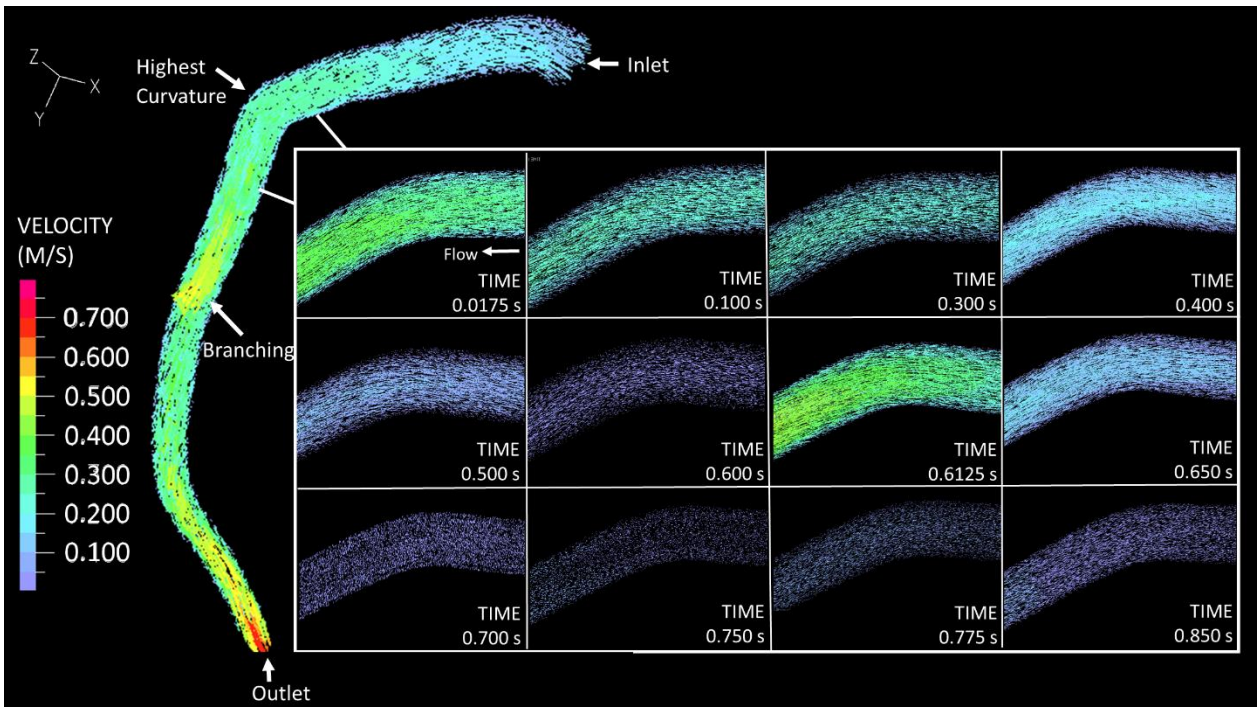

Figure 6. Blood flow velocity within the LAD under normal conditions. During diastole, blood flow was unidirectional within the normal LAD, with an average velocity of 0.21 m/s.

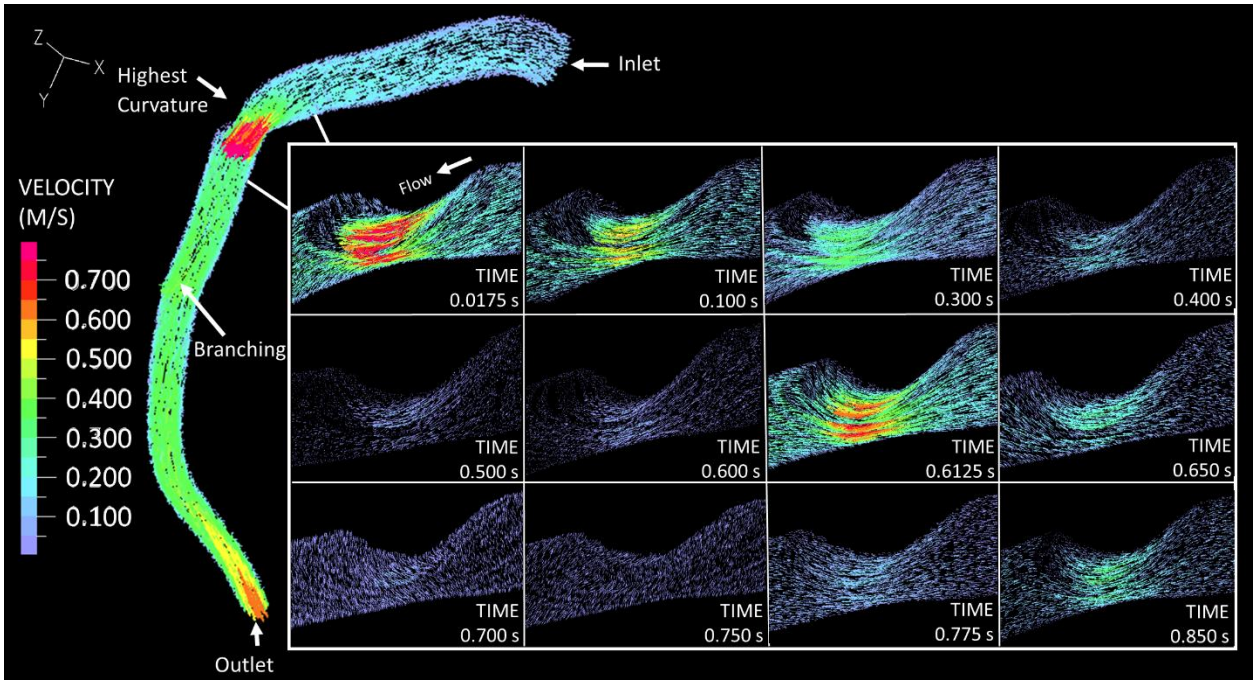

Figure 7. Blood flow velocity within the LAD under stenosis conditions. The plaque obstruction resulted in an increased velocity (to 0.8 m/s) at the stenosis throat. Flow detachment occurred downstream of the plaque, causing the development of a recirculation region, where flow was oscillatory and with a maximum velocity magnitude of about 0.225 m/s.

Transient velocity input (**Figure 5B**, the velocity waveform) was prescribed at the inlet of the LAD. As the blood vessel dislocated and the myocardium compressed, blood flow velocity changed. 0.0175 sec into the diastole (the beginning of diastole was defined as t=0), and approximately 8 mm downstream from the inlet (enlarged area in **Figure 6**), blood flow velocity reached its maximum, i.e., 0.40 m/s, in the normal LAD (**Figure 6**). For the rest of the diastole, as blood pressure decreased, blood velocity decreased gradually. At the beginning of systole (t=0.61 sec), myocardial contraction started, which caused a surge in blood flow velocity, bringing it back up to 0.42 m/s. Through the cardiac cycle, blood flow was laminar, with the Reynolds number varying between 27.6 and 551. Blood flow under the stenosis conditions (70%) followed a similar trend, but appeared more complex (**Figure 7**). At the stenosis throat (about 8 mm from the inlet), the maximum flow velocity (magnitude was 1.0 m/s) occurred at approximately 0.02 sec, followed by a gradual decrease until the end of diastole. As systole started (t=0.61

sec), myocardial compression caused blood flow acceleration, and the velocity went up to 0.83 m/sec. Flow detachment occurred downstream of the stenosis, resulting in a recirculation region. The average velocity of the oscillatory flow within the recirculation region (approximately 0.6 cm in length) was 0.075m/s. With the presence of a 70% stenosis, the maximum Reynolds number increased to 757. The maximum and mean velocity, as well as the maximum Reynolds number of blood flow under normal and stenosis conditions are summarized in **Table 2**.

Table 2- The maximum and mean velocity, maximum Reynolds number, maximum shear stress, maximum/mean wall fluid shear stress, and maximum/mean tensile strain values in the normal (point of interest is located 8 mm downstream from the inlet) and stenotic (stenosis throat and recirculation region) LAD models

	Normal	**Stenosis Throat (on plaque)**	**Recirculation Region**
Maximum velocity (m/s)	0.42	1.05	0.225
Mean velocity (m/s)	0.21	0.35	0.11
Maximum Reynolds number	551	757	310
Maximum shear stress (Pa)	7.50	24.46	1.51
Maximum wall fluid shear stress (Pa)	2.63	10.3	0.9
Mean wall fluid shear stress (Pa)	1.2	3.7	0.3
Maximum circumferential strain (%)	10.8	4.50	9.00
Mean circumferential strain (%)	8.00	3.3	7.00
Maximum axial strain (%)	14	3.5	15.5
Mean axial strain (%)	8.5	1.3	10.5

2.4.2 Maximum Shear Stress

The maximum shear stress (MSS) at the wall was calculated. The maximum shear stress was defined as one-half of the difference between the maximum and minimum principal stress. The MSS along the normal LAD wall is depicted in **Figure 8**. MSS in areas near the inlet was in general less than 7 Pa. MSS was close to 4.5 Pa at the point of the highest curvature, 5 Pa before and after the branching, and 9 Pa near the outflow of the model. During diastole, MSS decreased as blood flow velocity decreased, and increased back again during systole. Approximately 8 mm downstream of the LAD inlet, MSS reached a magnitude of 6 Pa at the beginning of systole (**Figure 8**, t = 0.6125 sec). Arterial bending did not seem to impact MSS much. With the presence of a 70% stenosis (located 8 mm downstream of the inlet), MSS increased significantly (**Figure 9**). At the stenosis throat, the MSS increased by 2.5 folds, to 15 Pa (compared to 6 Pa under normal condition) during systole. In the recirculation zone downstream of the stenosis, MSS was low (1.51 Pa) and oscillatory.

Wall fluid shear stress (WSS) was also calculated based on the local shear strain rate and effective viscosity. The maximum and mean WSS values are summarized in **Table 2**.

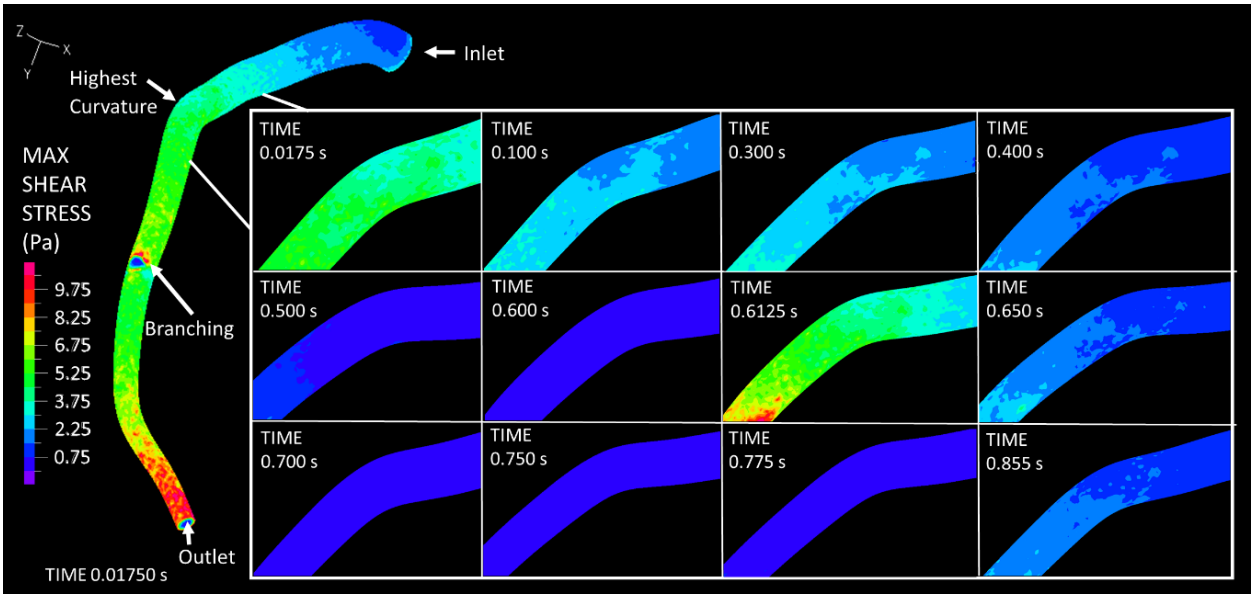

Figure 8. The maximum shear stress along the LAD wall under normal conditions through the cardiac cycle. Wall shear stress was significantly increased by myocardial compression (0.6125 s). The white arrows indicate the inflow, outflow, point of highest curvature and branching point (the branching artery is not shown).

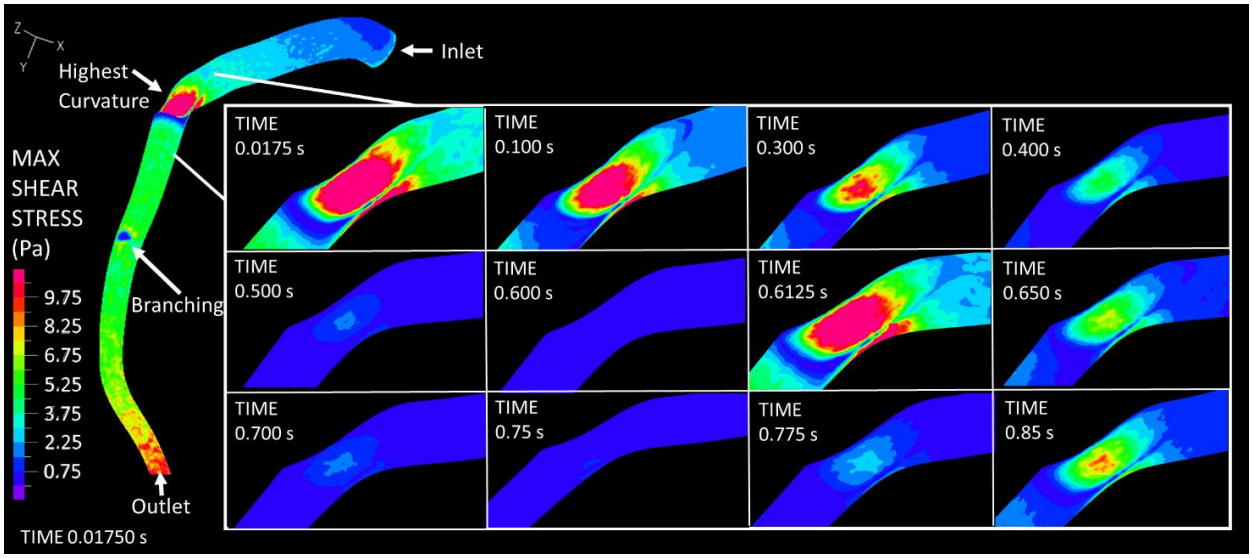

Figure 9. The maximum shear stress along the LAD wall under stenosis conditions. The maximum wall shear stress significantly increased during systole due to myocardial compression. The white arrows indicate the inflow, outflow, point of highest curvature and branching point (the branching artery is not shown).

2.4.3 Strain

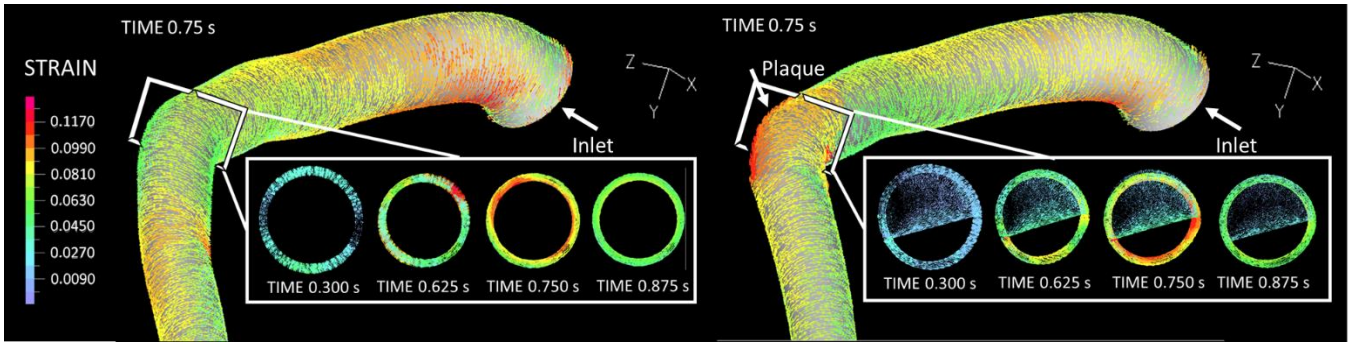

Figure 10. Blood vessel wall circumferential strain in the normal LAD model. At t=0.75 sec (mid systole), the vessel wall is subject to up to 10.8% blood vessel wall circumferential strain. With the presence of stenosis, the circumferential strain in the plaque area decreased to a maximum of 4.5%.

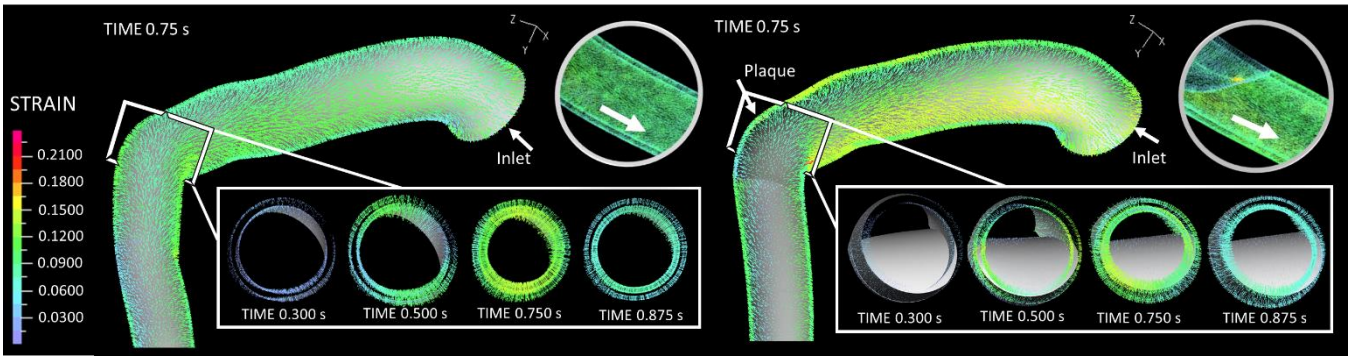

Figure 11. Blood vessel wall axial strain in the normal and stenotic LAD model. Both normal and stenotic models are subject to up to 15.5% axial strain during systole. Axial strain in the plaque area decreases to a maximum of 3.5%.

The cyclic bending and stretching motion of LAD contributed greatly to the axial and circumferential strain developed within the blood vessel wall. **Figure 10** depicts the circumferential strain distribution within the blood vessel wall at t = 0.75 sec (mid systole), when myocardial contraction generated the most compression. 8 mm downstream from the inlet in the normal artery, myocardial contraction resulted in a maximum circumferential strain of 10.8%, which decreased to 2% during

diastole. The maximum axial strain was 14%, and the minimum was 1.5% (**Figure 11**). In the stenosis model, due to the presence of the plaque (8 mm downstream from the inlet), the maximum circumferential strain decreased to 4.5% (**Figure 10**), and the maximum axial strain to 3.5% (**Figure 11**). Within the recirculation region downstream of the stenosis, the maximum circumferential strain was approximately 9%, and the maximum axial strain was 15.5%. Blood pressure in early diastole (minimum bending, no myocardial contraction) only caused very small circumferential and axial strain (<2%), compared to that induced by the vessel motion.

Both WSS and tensile strain can significantly affect vascular wall endothelial cell functions. Therefore, WSS and tensile strain distribution within the LAD was carefully examined. **Figure 12** depicts representative WSS and tensile strain waveforms as a function of time, from randomly selected wall elements under normal and stenosis conditions. During one cardiac cycle, a wall element within a normal LAD was exposed to pulsatile shear stress and tensile strain. The magnitude of WSS was 1 Pa, and that of the circumferential strain and axial strain were 7% and 8.4% respectively (**Figure 12, Normal**). With a 70% stenosis, due to the increased stiffness of the plaque, WSS of a wall element located in the plaque area increased to 3.7 Pa, circumferential strain decreased to 3%, and axial strain to 2.8% (**Figure 12, Stenosis throat**). For a wall element within the recirculation zone, WSS decreased to 0.7 Pa, circumferential strain to 5% and axial strain to 7.2% (**Figure 12, Recirculation region**).

To determine how myocardial contraction affected blood vessel wall fluid shear stress and tensile strain distribution, the normal and stenosis LAD models were also run without myocardial compression, i.e., in these models, the deformation of the blood vessel wall was mainly induced by the bending motion of the vessel and changes of blood pressure. Typical WSS and tensile strain waveforms are demonstrated in **Figure 13**. In the normal LAD model without compression, the magnitude of wall fluid shear stress was similar to that observed in the model with myocardium compression, **Figure 12, Normal**), which was approximately 1 Pa (**Figure 13, Normal**). During systole, however, differences occurred. The second

surge in shear stress due to myocardial contraction disappeared. Axial strain remained similar (7.3%) since axial strain was mostly induced by the bending motion of the vessel. Circumferential strain decreased to 2.9% since the vessel was no longer compressed during systole.

Similar trend was observed with the stenosis model. Near the plaque, the WSS magnitudes remained almost the same compared to the compressed model (i.e., 3.68 Pa compared to 3.7 Pa at the stenosis throat, and 0.74 Pa compared to 0.7 Pa within the recirculation region). However, the second shear stress peak disappeared in the non-compressed model. The axial strain values slightly differed from the compressed model (i.e., 3.1% compared to 3% at the stenosis throat, and 6.6% compared to 7.2% within the recirculation region). The lack of compression resulted in a large decrease in circumferential strain within the recirculation and stenotic throat region, from 5% to 3.7%, and from 3% to 1.9% respectively.

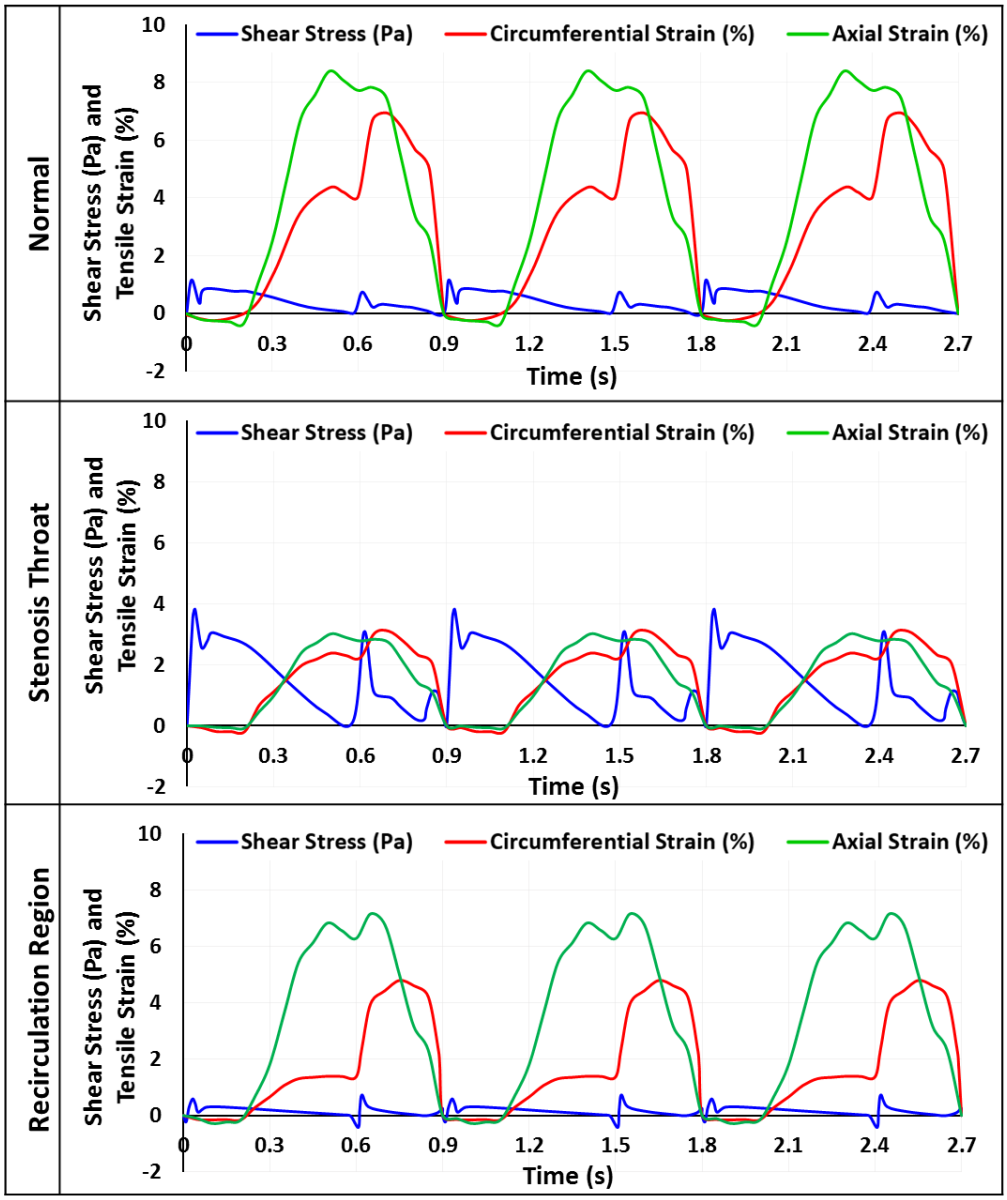

Figure 12. Wall shear stress and tensile strain along normal, recirculation and stenosis throat regions in the LAD, with myocardium compression

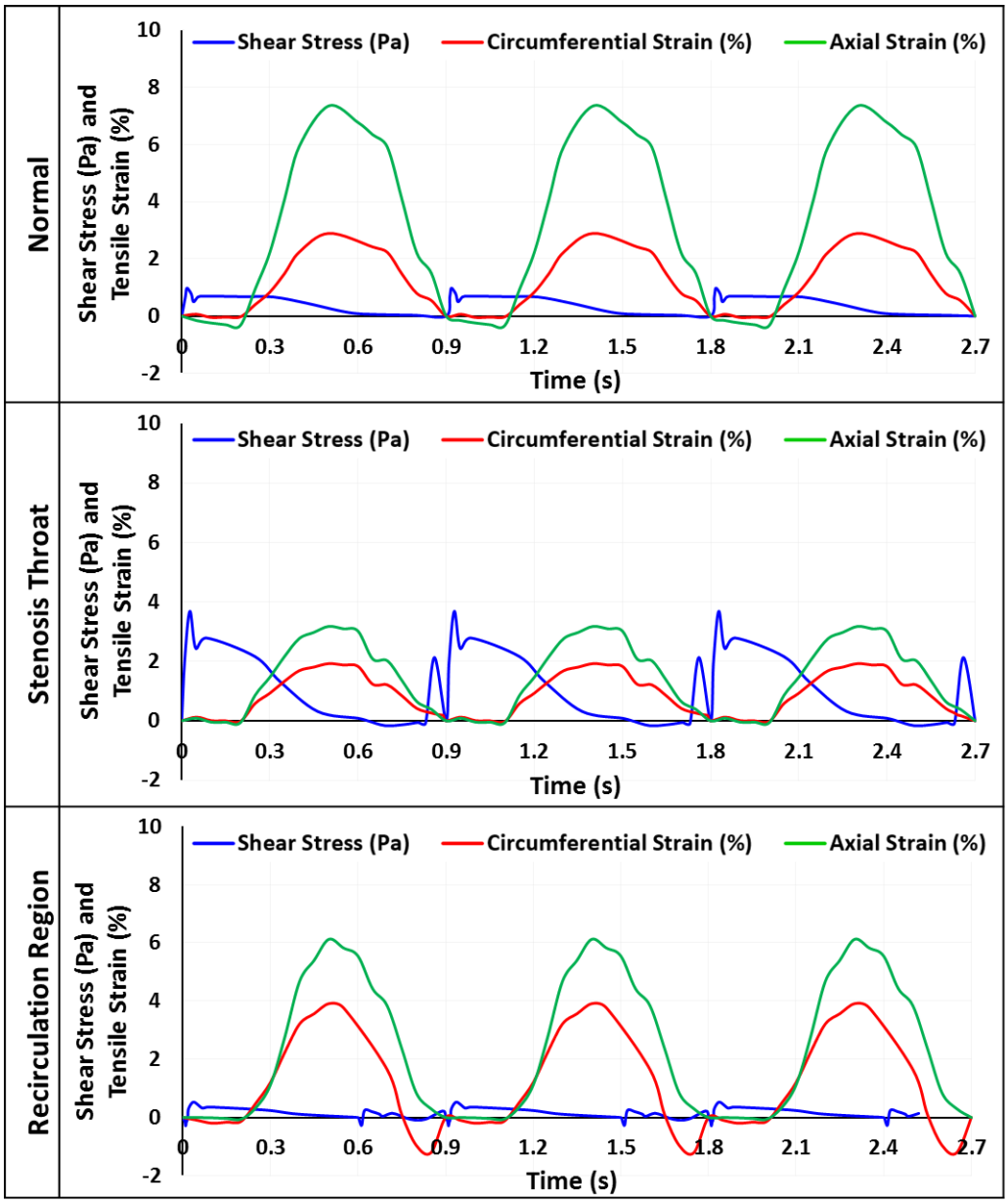

Figure 13. Wall shear stress and tensile strain along normal, recirculation and stenosis throat regions in the LAD, without myocardium compression.

2.5 Discussion

The left coronary artery models developed in this study incorporated transient blood flow, blood vessel motion (bending and stretching), and myocardial contraction. The effect of blood flow, vessel motion and cardiac muscle contraction collectively on coronary artery hemodynamics and vascular wall stress/strain distribution was investigated.

The lab has previously reported a left coronary artery FSI model considering both dynamic blood flow and vessel stretching-bending motion[87]. The present study improved the physiological relevance of the previous model by incorporating myocardial contraction. The results indicated that myocardial contraction had a significant effect on all hemodynamic parameters. It not only transiently increased blood flow velocity (by 4 folds) during systole, but also caused a second velocity peak during the cardiac cycle (**Figure 12**).

The present model estimated that the velocity magnitudes in the normal LAD varied between 0 and 0.42 m/s, which was in agreement with echo Doppler measurements in patients with normal coronary blood flow [102]. As expected, with the presence of a 70% stenosis, a prominent velocity increase occurred near the stenosis throat due to the decrease in lumen size. A recirculation region formed after the stenosis, and the size of the recirculation zone varied between 0.07 mm (during systole) and 0.6 mm (during systole). Compared to our previously reported FSI model (where myocardial contraction was not considered), velocity magnitudes estimated by the current model were much higher. In the previously reported model, the maximum blood velocity within the normal LAD was 0.18 m/s and that in the stenosed model was 0.31 m/s [87]; in the current model, the maximum blood velocity increased to 0.42 m/s and 1 m/s respectively. These differences may due to the inconsistencies in geometry[103], boundary conditions and degrees of freedom[104] between the two models.

Fluid shear stress at the vascular wall was also calculated using the present model. Within a normal LAD, wall fluid shear stress varied between 0 and 2.63 Pa. With a 70% stenosis, wall fluid shear stress near the stenosis throat went up to 10 Pa, and that within the recirculation region was always less than 0.9 Pa. These values are comparable to those reported in literature, that fluid shear stress below 1 Pa was considered pathologically low, between 1 and 2.5 Pa was considered normal (or physiological), and over 2.5 Pa was considered pathologically high [19, 105-108].

Besides changes in blood flow velocity and fluid shear stress, myocardial contraction also caused a 50% increase in the maximum shear stress within the vascular wall. The current model estimated that within a normal LAD, the maximum shear stress varied between 0.75 and 7.5 Pa, which is similar to that has been reported in literature [105].

In terms of strain, myocardial contraction caused a large increase in both axial and circumferential strain. Axial strain was more prominent during the bending motion, while circumferential strain changed largely during systole once the compression started. Yamamoto T, et al. measured the amount of compression in the LAD associated with cardiac contractions, using multi-planar reconstruction and enhanced cross sectional CT images. They reported an axial strain of 15.6 ± 26.4% (mean ± standard deviation) under normal conditions, which increased to 17.1 ± 30.8% with a stenosis [109]. Ohayon et al also reported similar axial strain values of -13.90 ± 8.92 [93]. These axial strain values are in concordance with that estimated by our model. Under normal conditions, the axial strain within the LAD reached a maximum value of 14%, which increased to 15.5% under stenotic conditions. Circumferential strain values obtained from the present LAD model were also comparable to those reported by *in-vivo* studies using intravascular ultrasound. Liang et al reported a 5-10% circumferential strain in normal regions of the LAD wall, while a 0-2% strain in the luminal area facing an eccentric plaque [110]. Our model estimated circumferential strains of 8% and 3% in normal LAD and near stenosis, respectively. The slight

difference here could be due to different plaque compositions, as mechanical properties of plaques change with their composition (calcified, soft or mixed), which varies greatly among patients [111].

In summary, this is the first large LAD FSI simulation model (>3mm) that included the effect of myocardium contraction. The results indicated that along with LAD cyclic stretching and bending motion [87, 112, 113], myocardial contraction exerted a substantial mechanical stress/strain on the artery and had a significant effect on coronary hemodynamics/mechanics. Values estimated using this model agreed well with that reported in literature (numerical simulation or *in vivo* measurement), validating the improved physiological relevance and accuracy of the model.

Coronary artery shear stress and tensile strain conditions estimated using this FSI model can be employed by *in vitro* studies to investigate how coronary biomechanics affect blood cell and vascular wall endothelial cell pathophysiological responses during atherosclerosis development.

2.7 Limitations

The FSI model has the following limitations.

1. The model does not take into account the multi-layered structure of arterial walls, instead it assumes a single layer with uniform material properties.
2. The vascular wall was assumed to have a uniform thickness, which is not always the case *in vivo*. However, the effect of thickness variation (+/- 10% as measured by high-frequency transthoracic and epicardial echocardiography [114]) on hemodynamic parameters such as wall shear stress and wall stiffness is still not fully understood, therefore it may or may not have affected the model estimation on hemodynamic parameters [93, 96, 115, 116].
3. Torsion effects were not included in the model which could improve the accuracy of the resultant hemodynamics in terms of WSS by ~3%[117]. The effect of torsion on the resultant strain distribution is not certain.
4. The model does not take into account the effect of anisotropy on the plaque area. The addition of anisotropic properties to the plaque area, could further enhance the resultant strain distribution estimation.

Chapter III

A SHEARING-STRETCHING DEVICE THAT CAN APPLY CONCURRENT FLUID SHEAR STRESS AND CYCLIC STRETCH TO ENDOTHELIAL CELLS

Portions of this chapter have been reproduced from:

> **Daphne Meza**, Louie Abejar, David A. Rubenstein, Wei Yin, 2016, "A Shearing-Stretching Device That Can Apply Physiological Fluid Shear Stress and Cyclic Stretch Concurrently to Endothelial Cells," J Biomech Eng, 138(3), p. 4032550.

3.1 Abstract

Endothelial cell (EC) morphology and functions can be highly impacted by the mechanical stresses these cells experience *in vivo*. In most areas in the vasculature, ECs are continuously exposed to blood flow induced shear stress, and vasodilation-contraction induced tensile stress/strain simultaneously. Investigations on how ECs respond to combined shear stress and tensile strain will help us to better understand how altered mechanical environment affects EC mechanotransduction, dysfunction and associated cardiovascular disease development. In the present study, a programmable shearing and stretching device that can apply dynamic fluid shear stress and cyclic tensile strain simultaneously to cultured ECs was developed. Flow and stress/strain conditions in the device were simulated using a fluid structure interaction (FSI) model in ADINA. To characterize the performance of this device and the effect of combined shear stress-tensile strain on EC morphology, human coronary artery ECs were exposed to concurrent shear stress and cyclic tensile strain in the device. Changes in EC morphology were evaluated through cell elongation, cell alignment and cell junctional actin accumulation. Results obtained from the numerical simulation indicated that in the "in-plane" area of the device, both fluid shear stress and bi-axial tensile strain was uniform. Results obtained from *in vitro* experiments demonstrated that shear stress, alone or combined with cyclic tensile strain, induced significant cell elongation. Biaxial tensile strain alone did not cause any noticeable change in EC elongation. Fluid shear stress and cyclic tensile strain had opposite effects on EC actin filament alignment and accumulation. By combining various fluid shear stress and cyclic tensile strain conditions, this device can provide a physiologically relevant mechanical environment to study EC responses to physiological and pathological mechanical stimulation.

3.2 Introduction

Vascular wall endothelial cells (ECs) are continuously subject to blood flow induced shear stress and vasodilation-contraction induced tensile (or compressive) stress/strain. Altered mechanical environment can trigger various pathological responses in ECs and lead to atherosclerosis [118-121]. To investigate how different mechanical conditions affect EC functions and activities, multiple *in vitro* models have been developed to apply shear stress, or tensile strain to ECs. It is well established that under physiological flow, ECs align their cytoskeleton proteins with the blood flow direction which reduces effective resistance of the flow [30]. Pathological flow can result in altered (e.g., elevated, reduced or oscillatory) shear stress on ECs, causing EC activation. Activated ECs can express increased amount of surface adhesion molecules (such as ICAM-1) [122], which promote monocyte recruitment and initiate atherosclerosis. Cyclic stretch (sometimes compression) can also affect EC functions greatly. It was reported that in the absence of shear stress, cyclic axial stretch of blood vessels can cause EC actin fibers to align with the circumferential direction, reducing endothelium-dependent vasodilatability [123]. Large cyclic strain can lead to EC activation [124] and apoptosis [125]. Cyclic stretch can also activate EC ion channels, affecting EC mechanotransduction [126] and enhancing EC pro-inflammatory responses associated with atherosclerosis [127].

However, under pathological conditions, how altered shear stress and cyclic strain work together to affect EC functions was under investigated. Over the years, only a handful of systems have been developed to apply concurrent shear stress and cyclic stretch to ECs *in vitro*. In most of these systems, distensible tubes were used to mimic veins or arteries [40-48], making cell culture and accurate control of stress/strain waveforms challenging. Furthermore, to visualize cells, the tubes need to be cut open to flatten following stress/strain treatment, which could induce additional changes in the results. Microfluidic cell culture channels have become popular in recent years [49]. Cells can be cultured on a suspended thin film inside a channel that mimics a segment of a blood vessel wall. However, the lack of control worsens as

the channel area increases. Switching between biaxial and circumferential strain application would require changes in the lithographed microfluidic channel geometry, and the need in frequent film loading and characterization made such systems low throughput. Some other devices could apply pressure and flow simultaneously to ECs cultured on thin flexible membranes, through pulse generator or other customized control systems [50-53]. However, the complex experimental setup and inability to generate physiologically relevant dynamic stress/strain conditions made these devices/systems less applicable.

In spite of the limitations associated with the above mentioned systems, it has been demonstrated that EC response to shear stress and cyclic stretch depends on whether the two stresses (or strains) are applied separately or simultaneously [55]. It was reported that both shear stress and cyclic stretch can equally affect the orientation and alignment of ECs[44], and the concurrent application of shear stress and tensile stretch may affect EC oxidative stress[56], intercellular junction protein expression, and EC permeability [57].

In the present study, a programmable shearing-stretching device that can apply precisely controlled dynamic shear stress and cyclic tensile strain to ECs simultaneously was developed, in order to characterize EC responses. The device integrated a piston-driven vacuum system and a cone-and-plate shearing device, and was able to apply physiologically relevant dynamic shear stress and tensile strain to cultured ECs on flexible membranes. The effectiveness of the device was evaluated through numerical simulation and EC morphological responses. Using this device, the hypothesis that ECs may respond to shear stress or tensile strain differently if the two simulations are applied concurrently was tested.

3.3 Materials and Methods

3.3.1 The Dynamic Shearing-Stretching Device

The dynamic shearing-stretching device was designed based on a cone-and-plate shearing device [128] and a vacuum-driven membrane stretching system [129, 130] . As depicted in **Figure 14**, the device is composed of three components: 1) the housing for a culture plate with flexible membrane (**Figure 14A-B**), 2) shearing cones (**Figure 14C**), and 3) a piston vacuum system (**Figure 14D**). The culture plate with flexible membrane can be easily (and tightly) inserted into the housing and connected with the piston vacuum system. Circular-shaped supporting plates (**Figure 14E**) can be placed underneath the flexible membrane to ensure a 2D-equibiaxial strain in the "in-plane" area of the membrane [130, 131] when vacuum pressure is applied. The Teflon shearing cones are attached to stepper motors and can be placed right above the flexible membranes. The speed of the stepper motors and the piston can be programmed and precisely controlled using a computer, thus generating desired shear stress (through the change of cone speed) and bi-axial tensile strain (through the change of vacuum pressure) in the "in-plane" area of the membrane.

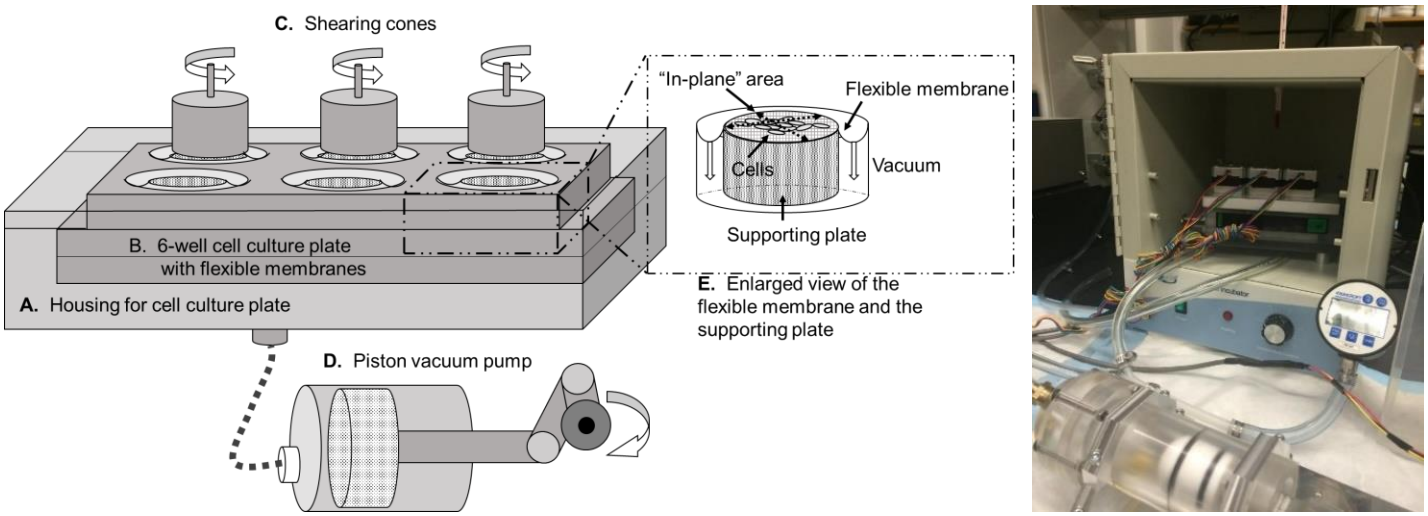

Figure 14. The shearing and stretching device. Left: a schematic drawing of the system. Right: a picture of the device in operation. (A) The housing for a cell culture plate; (B) The 6-well cell culture plate with flexible membrane; (C) Shearing cones; (D) The piston pump; (E) Enlarged view of the flexible membrane and the supporting plate.

3.3.2 Numerical Simulation of Shear Stress and Tensile Strain Distribution

To estimate shear stress and tensile strain distribution that can be generated on the flexible membrane, a 3D Fluid Structure Interaction (FSI) model was built using ADINA (8.9.3, ADINA R & D Inc.). The geometry of the numerical model matched that of the shearing-stretching device. The fluid around the cone will be modeled as a Newtonian fluid with the viscosity of 1 cP and density of 1 g/mL (matching that of culture media). The flexible membrane was modeled as the FSI interface with a Young's modulus of 600,000 Pa and a Poisson ratio of 0.49. The top of the supporting plate was defined as a rigid surface. The angular velocity of the cone was used as the velocity input of the fluid elements, and a cyclic vacuum pressure (frequency 1.1 HZ) was used as the transient pressure input on the flexible membrane, i.e., the FSI interface. To solve the numerical model, a maximum of 30 iterations were allowed at each time step. For both the fluid phase and the solid phase, the convergence tolerance was set as the default. To ensure

mesh-independence of the solution, mesh size for both the fluid phase and the solid phase was gradually increased until the difference in solution was less than 1%.

3.3.3 Cyclic Tensile Strain Measurement

The shearing component of the device has been well characterized experimentally in our lab [128, 132]. To determine the relationship between membrane strain and the applied vacuum pressure, and to validate strain uniformity, dots were marked on the flexible membrane and traced when vacuum pressure was applied. Real time motion of the dots on the membrane surface under vacuum pressure was recorded using an 8-megapixel iSight video-camera. Images were acquired at the rate of 120 frames per second and a resolution of 15×15 pixels per dot tracer. Each frame was then analyzed using an in-house MATLAB program. Circumferential strain (ϵ_θ) and radial strain (ϵ_r) were calculated as indicated by Equations 7 and 8, where r is the radial distance in the relaxed state and u is the radial displacement in the strained state [131, 133]. Equal circumferential and radial strains ($\epsilon_\theta = \epsilon_r$) would indicate strain field uniformity.

$$\epsilon_\theta = u/r \qquad \text{(Equation 9)}$$

$$\epsilon_r = \partial u/\partial r \qquad \text{(Equation 10)}$$

3.3.4 Endothelial Cell Culture

Human coronary artery ECs (HCAEC) were purchased from ScienCell Research Laboratories (Carlsbad, CA) and will be used between passages 2 and 7. Cells were maintained in endothelial cell basal medium supplemented with 5% fetal bovine serum, endothelial cell growth supplement, and 1% penicillin/streptomycin (all cell culture reagents were purchased from ScienCell Research Laboratories). Cells were grown to confluence in 6-well Flexcell culture plates (Flexcell International Corporation) pre-coated (2-3 hours at 37°C) with 5 μg/mL fibronectin (Sigma-Aldrich, St Louis, MO).

3.3.5 Applying concurrent shear stress and cyclic tensile strain to ECs

By setting the cone speed (18 rad/s) and the vacuum pressure (30 kPa, 1.1 Hz), a constant shear stress at 1 Pa and a cyclic tensile strain with a magnitude of approximately 3% were generated in the shearing-stretching device (**Figure 15**) and applied to a confluent monolayer of HCAEC simultaneously for 30 min at 37 °C. ECs that were not exposed to any stress or strain (resting cells) were used as the experimental control. To determine if the combined stimulation affected EC response differently than each single stimulation, ECs were also treated with pure shear stress (1 Pa), or pure cyclic tensile strain (3%).

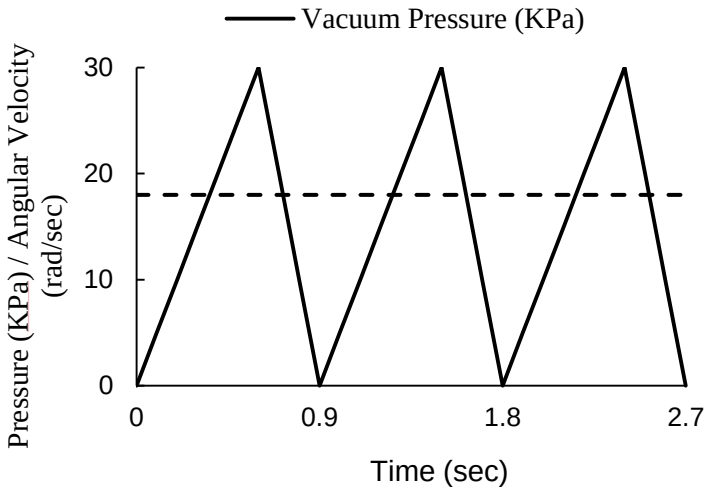

Figure 15. A constant angular velocity (18 rad/sec) was used as the velocity input of the cone, and a cyclic vacuum pressure (magnitude at 30 KPa) was used as the transient pressure input on the flexible membrane.

3.3.6 Immunofluorescence Microscopy

Following shear stress and/or tensile strain treatment, HCAECs were washed twice with PBS, fixed in 0.5% glutaraldehyde and neutralized with 100 mM glycine-BSA [134]. ECs were then stained with Alexa Fluor 488 conjugated Phalloidin for F-actin elements (Ambion, Life Technologies, NY). EC nuclei were stained with DAPI. Cell images were visualized using a Nikon Ti inverted microscope.

3.3.7 Cell Morphology Characterization

3.3.7.1 Cell Elongation

EC elongation following shear stress and/or tensile stretch treatment was determined using the Nikon Image Analysis Software. Cell elongation was quantified by the ratio of the long axis over the short axis of a cell, automatically determined by the software. Multiple cells were randomly chosen for each condition and the average of all the sampled cells was used as the elongation induced by that particular condition (control/untreated, shear, stretch, or combined). Cell elongation analysis was conducted by two individuals independently.

Additionally, EC nuclei elongation was assessed. Using MATLAB, cell nuclei images (DAPI stained) were converted to binary images and individual nuclei were randomly selected. Using a MATLAB built-in function, the long axis and short axis of each nucleus was determined. The elongation of the nucleus was defined as the ratio between long axis and short axis. Nucleus elongation analysis was also conducted by two individuals independently. MATLAB code is available in the supplemental information.

3.3.7.2 Cell Alignment

Cell alignment was quantified based on a method developed by Ng *et. al.* [135], which utilizes 2D Fast-Fourier transform (FFT) to determine orientation. Using the ImageJ software, F-actin fluorescence images (1082 by1082 pixels) of ECs were gray-scaled, background subtracted (using the "rolling ball' algorithm [136]), contrast enhanced (to ensure fiber visibility), and binarized. Orientation intensity histograms of F-actin fibers was generated using FFT. Following normalization (to the average intensity of each image), the alignment index (AI) was calculated. The AI refers to the fraction of actin fibers that are aligned within 20° of the peak angle [137]. A randomly aligned matrix would have an AI of 1. High AI would indicate a large fraction of actin fibers aligned around the peak angle.

3.3.7.3 F-actin Accumulation

Actin accumulation at cell junctions was measured using a custom MATLAB script. A line was placed across a randomly selected cell junction, from the outside to the inside of the cell. A plot of the intensities of the pixels along the line was generated and the signal (intensity at the junction) to background (intensity inside cell body) ratio was calculated and used to quantify actin accumulation. MATLAB script is available in the supplemental information section.

3.3.7.4 Statistical Analysis

Data analysis was conducted using SAS (9.3) or GraphPad Prism (v.6.01, San Diego, CA). Significant difference was defined as $\alpha = 0.05$. ANOVA was used to analyze cell elongation data. If significant difference ($P<0.05$) was detected, Student Newman Keuls post hoc test was conducted for further comparison. Student's *t*-test was used to analyze data on actin accumulation. For cell alignment, data was analyzed using Student's *t*-test with Welch's correction.

3.4 Results

3.4.1 The FSI model

Figure 16 depicts velocity vectors and shear stress distribution of the fluid phase as the cone was rotating (18 rad/s) and the membrane deformed under the cyclic vacuum pressure (0–30 kPa). In the flow field, the Reynolds number was low (< 1) throughout the stretching cycle, indicating that the flow was laminar. On the surface of the membrane, the fluid velocity gradient remained the same, resulting in a constant and uniformly distributed fluid shear stress (magnitude) in the in-plane area (1 Pa). **Figure 17A** depicts the membrane nodal displacement along the radial direction in the in-plane area at the maximum deformation (t=0.6 s). The displacement increased linearly as the radial distance increased (0–12 mm). Based on the displacement and original location of each node, circumferential and radial strain generated due to membrane deformation can be calculated using Eqs. (9) and (10). **Figure 17B** depicts the circumferential and radial tensile strain of one randomly chosen node (approximately 6 mm from the center of the membrane) as a function of time. The circumferential strain and radial strain were approximately the same (difference was less than 3%), with a maximum value of approximately 3% occurring at 0.6 s, indicating that a uniform equal-biaxial strain field was generated on the membrane surface in the in-plane area.

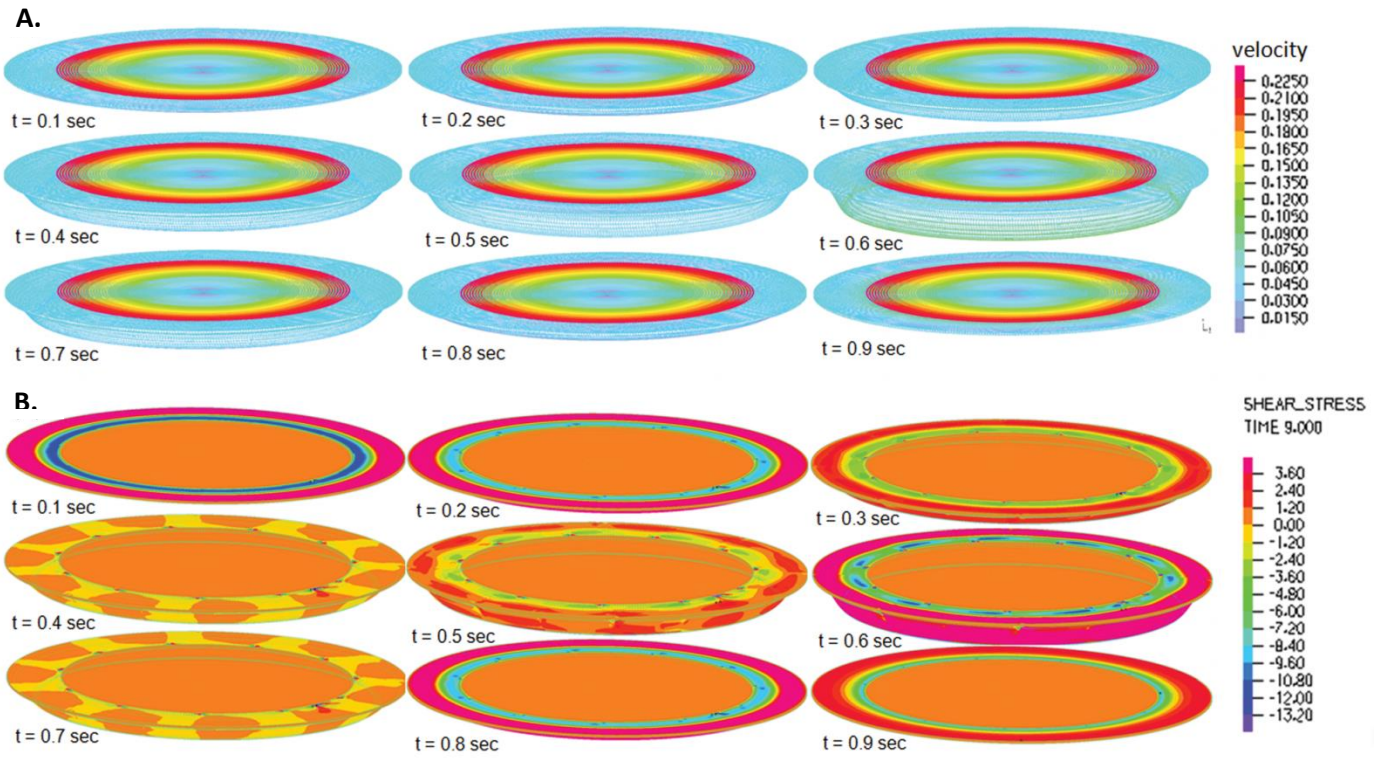

Figure 16. A) Velocity (m/s) vectors of the fluid phase as the vacuum pressure changed between 0 and 30 KPa in one stretching cycle. Simultaneously, the cone was rotting at a constant angular velocity of 18 rad/s. B) Corresponding shear stress (Pa) distribution in the flow field when both the cone and the membrane were moving.

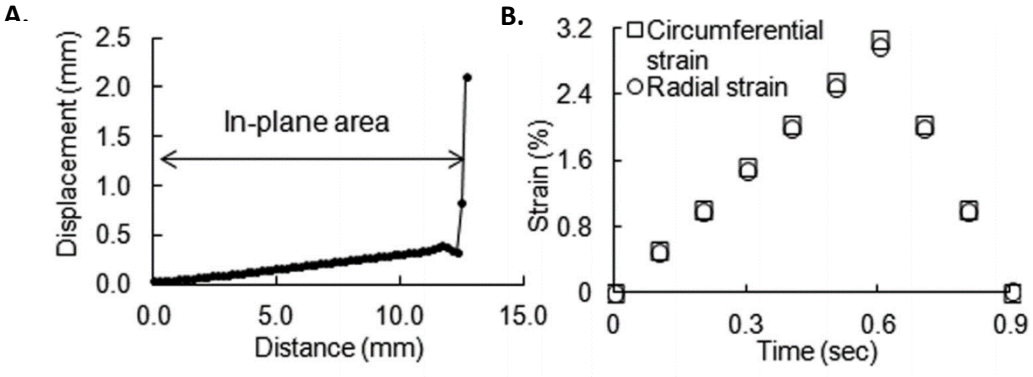

Figure 17. (A) Nodal displacement along the radial direction in the in-plane area of the membrane at t=0.6 sec. (B) Circumferential and radial strain of a randomly chosen node (6 mm from the center of the membrane) change as a function of time during one stretching cycle.

3.4.2 Experimental characterization of tensile strain

Based on the displacement of the dot tracers, radial strain (ϵ_r) and circumferential (ϵ_θ) strain along various angles (θ) and radial locations (r) were calculated and depicted in **Figure 18**. Using ANOVA, no significant difference (P >0.1, n=4) was detected in the circumferential or radial strain as location (angle θ and radial location r) changed. Moreover, no difference (P>0.1) was found between the radial strain (ϵ_r) and the circumferential (ϵ_θ) strain, indicating an equal-biaxial strain field. At the maximum vacuum pressure of 30 KPa, a uniform strain field was generated on the "in-plane" area of the membrane and the magnitude of the cyclic strain was approximately 3%, matching that calculated using the FSI model. Additionally, no significant change (P > 0.3) in membrane strain was detected after 30 min of continuous operation (cyclic stretch at 1.1 Hz).

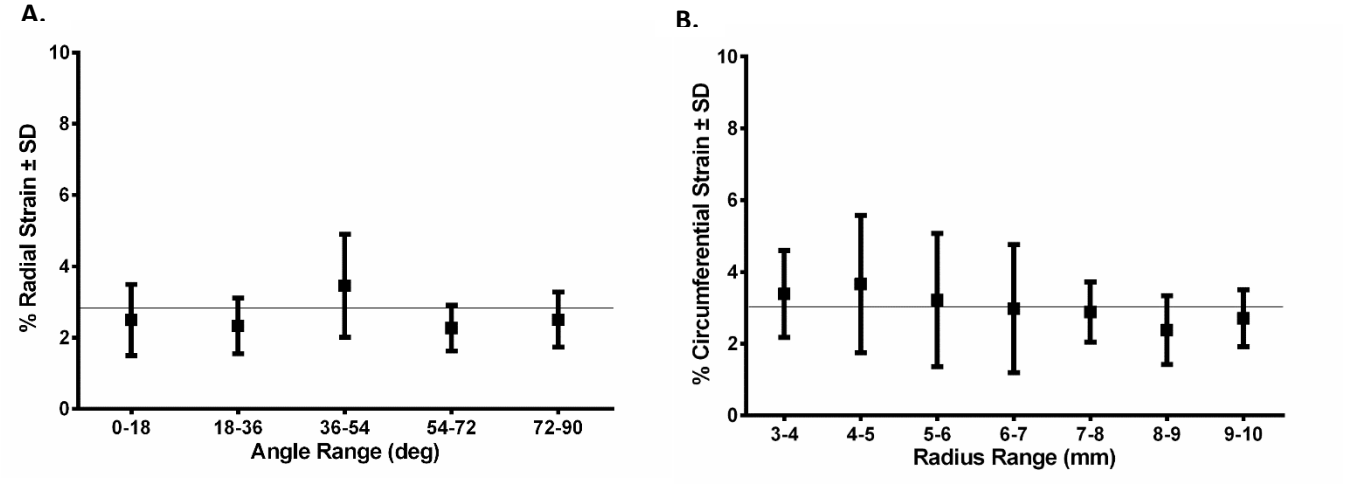

Figure 18. Measured circumferential and radial strain. (A) Radial strain did not vary significantly with angle (P>0.3); (B) circumferential strain did not vary significantly with radial distance (P>0.1). The circumferential and radial strains do not differ (P>0.1), indicating strain field uniformity.

3.4.3 Cell morphology characterization

Following shear stress (1 Pa) and/or cyclic tensile strain (3%) treatment, EC morphology was visualized using fluorescence microscopy. Representative images are depicted in **Figure 19** (magnification 40x). Untreated ECs (control) appeared relatively small and randomly oriented, without highlighted cell boundaries. ECs that were exposed to shear stress (alone or combined with tensile strain) looked enlarged and elongated; cell boundaries appeared more distinct. ECs exposed to cyclic tensile strain alone had a substantial increase in surface area and appeared more cuboidal.

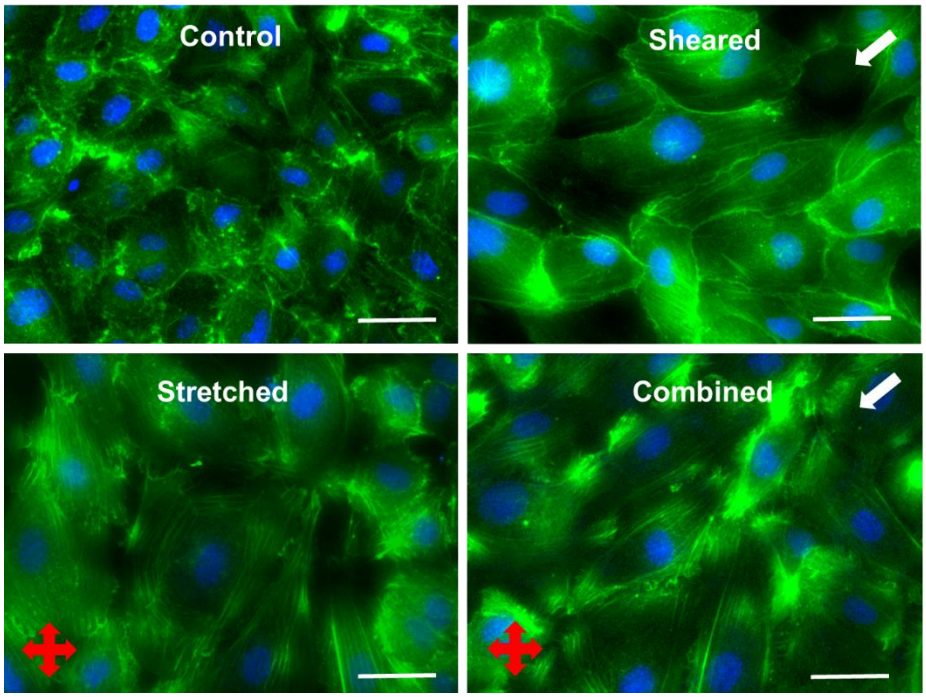

Figure 19. Representative images of ECs following shear stress and/or tensile strain treatment. White arrows indicate flow direction and red arrows indicate the directions of tensile strain. Scale bars represent 100 μm.

3.4.3.1 Cell elongation

EC elongation was quantified by calculating the ratio between cell long axis and short axis. The results (**Figure 20A**) demonstrated that shear stress, alone or combined with cyclic tensile strain, induced significant cell elongation ($P<0.05$), compared to untreated ECs. Cell elongation caused by concurrent shear stress and tensile strain was significantly lower ($P<0.05$) than that induced by shear stress alone. Equal-biaxial stretch alone did not cause any change in EC elongation. These results suggested that shear stress and bi-axial tensile strain may have opposite roles in cell elongation. In a similar manner, the elongation of EC nucleus was quantified by comparing the long axis and short axis of cell nucleus. The results (**Figure 20B**) showed that shear stress, alone or combined with cyclic tensile strain, induced a significant increase ($P<0.05$) in nucleus elongation, but no difference was detected between the two conditions. Biaxial tensile strain alone did not affect EC nucleus elongation. The mechanical stiffness of cell nucleus is in general ten times larger than that of the cytoskeleton [138], thus it requires high stress/strain or more time for significant changes to occur in nucleus. This might have contributed to the difference observed in cell elongation and nucleus elongation.

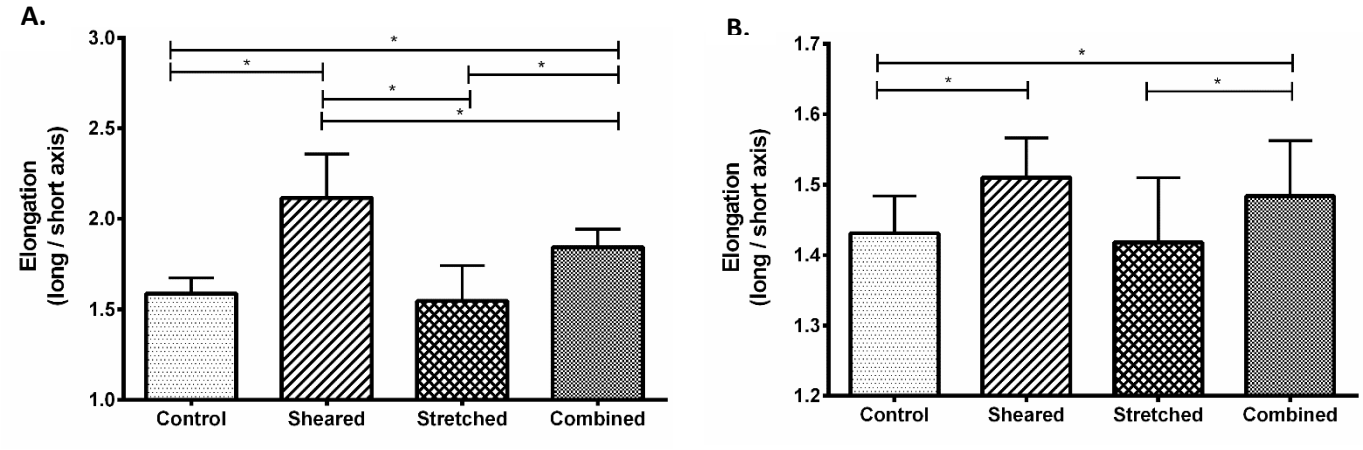

Figure 20. (A) Cell elongation and (B) Nucleus elongation after HCAEC were treated with shear stress and/or cyclic tensile strain. Data is presented as mean + standard deviation (n=24). * indicates significant difference ($P < 0.05$).

3.4.3.2 Actin filament alignment

The alignment of actin filaments was quantified using an in-house MATLAB program. The results (**Figure 21**) demonstrated that shear stress and biaxial tensile strain did not have the same effects on actin alignment. Under shear stress, EC actin filament's AI was significantly higher than that under biaxial tensile strain (ANOVA with Welch's correction, followed by Games-Howell post hoc test, $P<0.05$). However, shear stress and/or tensile strain did not cause any overall change in actin alignment when compared to untreated ECs, which may have resulted from the nature of the biaxial tensile strain and the fact that in a cone-and-plate shearing device, the shear stress direction is not uniform at different locations.

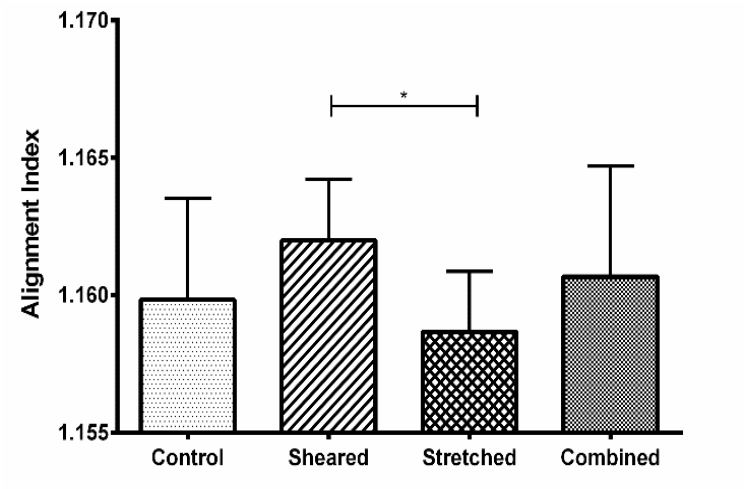

Figure 21. Actin alignment was quantified using FFT. Significant difference was detected between ECs that were treated with shear stress alone, and those treated with tensile strain alone ($P<0.05$, n=12-19). Data is presented as mean + standard deviation. * indicates significant difference ($P < 0.05$).

3.4.3.3 Actin accumulation at cell junctions

The accumulation of cortical actin, also referred to as junctional actin, is critical for the maintenance of cell junctional integrity. An increase in actin accumulation at the EC junction could be associated with increased endothelium permeability and enhanced monocyte transmigration [139]. It has been reported that the assembly, growth and maintenance of junctional actin depends on the mechanical stress ECs experience [140]. As the mechanical stress increases, the size of EC junctions could increase proportionally [141]. Using an in-house MATLAB program (see supplemental information section for written code), the intensity of pixels within the cell junction were compared to that within the cell body, and the ratio was used to quantify actin accumulation at cell junctions. ANOVA (with Welch's correction, P =0.012, n=31–93 images for each experimental condition) and Games Howell post hoc test demonstrated that there was a significant difference in actin accumulation between untreated cells (control) and cells treated with shear stress and tensile strain simultaneously (**Figure 22**). Independent student's t-test demonstrated that there was a significant difference (P=0.046) in actin accumulation between untreated cells and sheared cells. Student's t-test also demonstrated that there was a significant difference (P=0.011) in actin accumulation between tensile strain treated cells and stretch-and-shear treated cells (**Figure 22**)

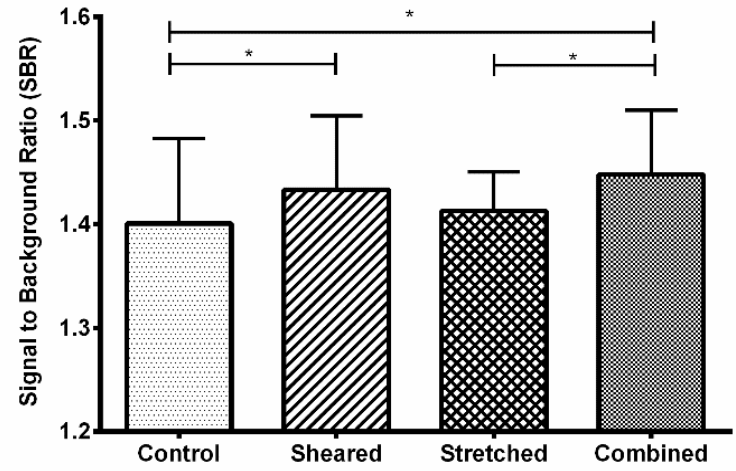

Figure 22. Actin accumulation along EC boundaries. Shear stress, alone or combined with tensile strain, induced significant increase in actin accumulation along cell boundaries ($P<0.05$, n=31-93). Biaxial tensile strain alone did not induce any changes in actin accumulation at cell junctions. Data is presented as mean + standard deviation.

3.5 Discussion

Mechanical stresses including fluid shear stress and blood vessel wall tensile stress/strain play important roles in EC morphology and functions. Altered mechanical environment can affect EC cytoskeleton arrangement, causing changes in cell alignment, migration, apoptosis, and protein/gene expression[142]. Evaluating changes in ECs induced by either fluid shear stress or cyclic tensile stretch alone would not provide comprehensive information on EC responses toward the dynamic mechanical environment in vivo. In the present study, a simple shearing-stretching device that can apply well-controlled and concurrent fluid shear stress and tensile strain to cultured ECs was developed, and its performance was examined through numerical simulation and in vitro experiments with HCAECs.

The results demonstrated that the shearing-stretching device can be precisely controlled to generate desired fluid shear stress and tensile strain at the same time. The concurrent fluid shear stress and tensile strain affected EC morphology, including cell elongation, alignment, and actin fiber accumulation, differently from shear stress or tensile strain alone. In large or medium sized arteries, physiological fluid shear stress is pulsatile and ranges from 1 to 7 Pa [143]. Under pathological conditions, fluid shear stress could deviate from the physiological range greatly: at an atherosclerotic lesion site, blood vessel wall fluid shear stress could elevate to well over 10 Pa [144], while within the recirculation zone or near a bifurcation, wall fluid shear stress may decrease significantly (less than 0.5 Pa) and oscillate [143]. Tensile strain induced by vessel dilation in blood vessels can vary greatly as well. With the presence of atherosclerosis, due to lipid deposition and/or calcification within the blood vessel wall, the extensibility of the blood vessel could decrease significantly, resulting in reduced tensile strain. In blood vessels like the coronary arteries, due to the large motion (bending and stretching) of the blood vessel, coronary artery

endothelial cells can experience a large variation in fluid shear stress and tensile strain in multiple directions (especially in the axial and circumferential direction) [87]. Even though it is still unclear if there is a threshold level of cyclic tensile strain that can induce significant EC morphology change and cause EC remodeling, many studies have chosen tensile strain between 2% and 10% to stimulate ECs *in vitro* [18, 145]. It was reported that 2% cyclic stretch could be as potent as shear stress at 8 Pa [44]. The effects from fluid shear stress and cyclic tensile strain could be additive or opposite, depending on the level of the stress/strain, pulsatility of the shear stress, or the phase angle between shear stress and tensile strain [44, 57].

In the present study, only simplified shearing-stretching conditions were tested to examine the performance of the shearing-stretching device. The results demonstrated that fluid shear stress alone had the largest effect on cell elongation, followed by the concurrent stimulation from shear stress and tensile strain. Cyclic bi-axial tensile strain hardly affected EC elongation. A similar trend was observed with EC alignment: cells had clearer alignment under fluid shear stress, compared to biaxial tensile strain. Shear stress, alone or combined with tensile strain, also induced a significant increase in actin accumulation along cell boundaries, while tensile stretch alone had no effect. These observations are in agreement with what has been reported in literature that ECs can elongate and align in response to shear stress [146-149], but not to a biaxial tensile strain[150]. In the present study, ECs also displayed a greater junctional actin accumulation under concurrent shear stress and strain, which is in agreement with a recent report showing that EC junction size can be modulated by cell–cell tugging forces [141] . Under concurrent shear stress and cyclic strain, ECs displayed a similar alignment, yet a reduced elongation when compared to ECs exposed to pure shear stress. This somewhat differs from alignment and elongation results obtained from the previous studies using distensible tubes [151], in which both alignment and elongation increased in response to concomitant shear stress and hoop stress. This discrepancy in results can be due to either the difference in the duration of mechanical stimulation (24 hours instead of 30 min in our study) or to the difference in strain magnitudes used (10% strain as opposed to 3% in our study).

In the in vitro experiments, 800 µl culture media was added to each well. In the numerical model, the same amount of media was modeled. To determine if the added media would affect the shear stress and/or strain distribution on the membrane, a stretching membrane model without the fluid phase (i.e., media) was conducted, and the results indicated that the presence of 800 µl media did not cause noticeable changes in membrane strain distribution. The in vitro experiments and the FSI numerical model supported the validity of the shearing-stretching system. In the in vitro experiments, the cells in the periphery area of the membrane could experience significantly elevated tensile strain, which may possibly cause large changes in EC morphology, function, and junctional integrity. These cells are not likely to affect cells within the in-plane area through cell–cell interaction, but could possibly release EC microparticles or activation markers/ proteins into the medium. These released microparticles or proteins could potentially affect the functions and behavior of the cells within the in-plane area. Effects from these released substances may need further investigation.

By modifying the shape of the supporting plate (**Figure 14E**), the strain generated through membrane stretch can be changed from equal-biaxial tensile strain to uniaxial strain, or other combinations of biaxial strain. By adjusting the motor speed and the cyclic vacuum pressure, this shearing-stretching device can generate various combinations of fluid shear stress and tensile strain, providing an easy solution to establish physiologically relevant mechanical environment. Examples include elevated pulsatile shear stress and decreased tensile strain that can occur at the stenosis throat within a stenosed blood vessel, or low oscillatory shear stress and reduced tensile strain that can occur in a recirculation zone downstream of the stenosis.

3.6 Conclusions

A simple programmable shearing-stretching device was developed in the present study, and its performance was validated through numerical simulation using an FSI model and in vitro experiments with HCAECs. The concurrent stimulation from fluid shear stress and cyclic tensile strain could induce different responses in EC morphology, compared to single stimulation from either fluid shear stress or tensile strain. By combining various fluid shear stress and cyclic tensile strain, the altered mechanical environment induced by disease conditions (such as atherosclerosis) can be achieved using this device and applied to cultured ECs, to investigate the role of changed mechanical stress/ strain in cardiovascular disease initiation and development.

3.6 Limitations

The shearing-stretching device has the following limitations.

1. Device setup does not allow for *in-situ* imaging.

   Monitoring the cell morphological and functional response over time would help further understand the cell's response to stimuli; however, given our device setup, this would not be possible.

2. Imaging upon mechanical stimulation can be challenging when using large numerical aperture (NA) objectives.

   The working distance of large NA objective is limited, and therefore in order to visualize cells with large NA objectives, the flexible membrane needs to be cut out the 6-well plate, which could potentially introduce more variability in the experimental design.

3. The device's capability to accurately reproduce the desired cyclic strain waveform depends on the vacuum's system response time.

   Since the cyclic strain being imposed to the cells is vacuum driven, the vacuum's response time, or the time needed for the vacuum to reach a specific pressure, determines the system's ability to accurately impose desired cyclic strain waveforms to cells.

4. Previous studies have demonstrated ECs are sensitive to differences in phase angles, or time lag between the application of one mechanical stimuli waveform and the other.

   In order to precisely control this, both the systems should be programmed through the same interface.

Chapter IV

EFFECT OF CONCURRENT FLUID SHEAR STRESS AND CYCLIC STRETCH ON ENDOTHELIAL CELL ACTIVATION

Manuscript in preparation:

Daphne Meza, Elisabeth Steadman, Bryan Musmacker, Thomas Stransky, David A. Rubenstein, Wei Yin, 2017, "Effect of concurrent fluid shear stress and cyclic stretch on endothelial cell activation,"

4.1 Abstract

Vascular wall endothelial cells (EC) are continuously exposed to complex mechanical loading conditions. Blood flow induced shear stress and blood vessel wall tensile/compressive strain may significantly alter EC morphology and function. The goal of this study was to investigate the effects of concurrent fluid shear stress and tensile strain on EC activation and morphology.

Using a custom designed shearing-stretching device, physiologically relevant shear stress and/or tensile strain waveforms were applied to endothelial cells. Three mechanical loading conditions were used: 1) Pulsatile shear stress at 1 Pa with 7% cyclic strain, simulating stress/strain conditions within a healthy coronary artery; 2) pulsatile shear stress at 3.7 Pa with 3% cyclic strain, simulating stress/strain conditions at the stenosis throat of a diseased artery; and 3) pulsatile shear stress at 0.7 Pa with 5% cyclic strain, simulating stress/strain conditions with the recirculation region downstream of a 70% stenosis.

EC morphology was evaluated by quantifying cell area and elongation. EC inflammatory responses were evaluated by characterizing EC activation, i.e., cell surface ICAM-1 expression, PECAM-1 tyrosine phosphorylation, mechanotransduction pathway (MAPK) activation, and associated transcription factor NF-κB activation.

Under all conditions, cells that were exposed to combined shear stress and tensile strain were much larger compared to untreated cells or cells that were exposed to either shear stress or tensile strain alone. Specifically, combined shear stress and tensile strain induced the greatest increase in cell area compared to normal or recirculation conditions. In contrast, cell elongation decreased significantly under combined shear stress and tensile strain, with the lowest values observed under recirculation conditions.

PECAM-1 phosphorylation was more responsive to tensile strain than shear stress. Low strain (3%), alone or combined with shear stress, caused lower PECAM phosphorylation compared to that under normal (7%) and recirculation conditions (5%). No significant changes were seen in ERK1/2 activation. However, combined shear stress and tensile strain under stenosis conditions caused a significant increase

in NF-κB activation. In terms of ICAM-1 expression, combined mechanical stimuli had a synergistic effect under pathological conditions (recirculation and stenosis), but not under physiological conditions (normal). Low recirculation shear (0.7 Pa) as well as low stenotic stretch (3%) significantly increased ICAM-1 expression compared to normal shear (1 Pa) and stretch (7%) conditions alone.

The results demonstrated that the simultaneous stimulation from shear stress and cyclic strain induced significant changes in endothelial cell activation and morphology compared to when cells were exposed to either shear stress or cyclic strain alone. These findings demonstrated the complex interplay between flow-induced shear stress and tensile strain. To better understand EC mechanotransduction and its effect on atherosclerosis formation, both fluid shear stress and cyclic strain should be considered.

4.2 Introduction

Endothelial cells along the vasculature display a distinct morphology and have a different function dependent on the mechanical environment they are subject to. Under physiological conditions, along one-dimensional flow regions where flow is laminar, cells align and elongate with flow direction which reduces their resistance to flow [152]. Under pathological conditions, in regions proximal and distal to atherosclerotic plaque (stenosis), where flow recirculation develops, cells present a cobblestone morphology with no definite alignment [31]. Moreover, on areas with high cyclic strain, cell remodeling diminishes, resulting in an increase in cell stiffness [153]. ECs respond to mechanical forces by adjusting their cytoskeleton, cell-junctions, and cell-matrix interactions to maintain hemostasis.

Apart from triggering structural modifications, mechanical forces also set off complex signal transduction cascades leading to functional changes within the cell. It is generally accepted that pathological stress/strain conditions can cause the activation of EC mechanotransducers such as PECAM-1, which can activate MAPK pathway via the phosphorylation of ERK1/2, and result in the activation of transcriptional factors (such as NF-κB) [25, 26] (See **Figure 23**). This would follow with an increase of EC surface inflammatory proteins (such as ICAM-1) [26, 27], which would enhance leukocyte transmigration, other inflammatory responses [28, 29], and can lead to atherosclerosis development.

The effect of altered shear stress or tensile strain on the MAPK pathway and ICAM-1 activation has been studied extensively[154]. However, the effect of simultaneous stimulation of shear stress and tensile strain on EC morphology, PECAM-1 activation, EC mechanotransduction and associated inflammatory responses is under investigated. Studies have previously reported that the combined effect of mechanical stresses on EC is not merely additive[155] [145] [156] [55] and have later shone light on the importance of the magnitudes and frequencies of the stresses when in combination[157].

Physiologically relevant shear stress and tensile strain waveforms need to be used when studying mechanotransduction induced inflammatory EC responses. This study utilizes physiologically relevant

shear stress and tensile strain values obtained from a patient-specific fluid-structure interaction model, developed in the first aim (Chapter 2). The shear stress and tensile strain value combinations utilized mimic the mechanical environment of a coronary artery under normal and diseased conditions. ECs were subjected to three mechanical stress combinations which simulated: 1) Normal conditions (1 Pa shear stress and 7% cyclic strain), 2) Recirculation region, downstream of 70% stenosis (0.7 Pa and 5% cyclic strain) and 3) Stenosis throat (3.7 Pa and 3% cyclic strain). EC morphology and inflammatory responses were evaluated through cell area, cell elongation, tyrosine phosphorylated surface PECAM expression, ERK1/2, NF-κB activation and resultant ICAM-1 surface protein expression.

A better understanding of the relationship between the combined effect of physiologically relevant fluid shear stress and tensile strain on EC response can lead to targeted preventive therapy for atherosclerosis, by helping to identify mechanical and intracellular transduction factors responsible for EC inflammatory responses and dysfunction.

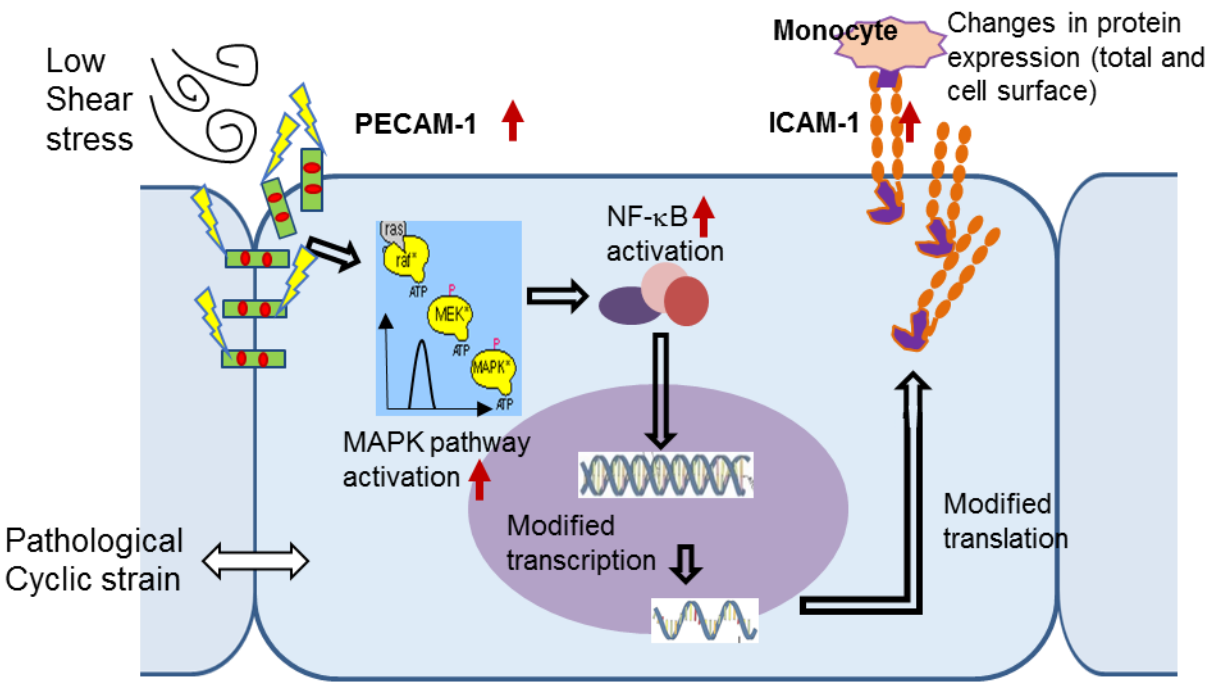

Figure 23. PECAM-1 on EC is believed to sense mechanical stimulation (shear stress / cyclic strain), phosphorylate and then pass the mechanical signal on by activating MAPK pathway and NF-κB, resulting in transcriptional changes and differential expression of proteins, such as ICAM-1.

4.3 Materials and Methods

4.3.4 Endothelial Cell Culture

Human coronary artery ECs (HCAEC) were purchased from ScienCell Research Laboratories (Carlsbad, CA) and were used between passages 2 and 7. HCAEC were maintained in endothelial cell medium supplemented with 5% fetal bovine serum, endothelial cell growth factors, and 1% penicillin/streptomycin (all cell culture reagents were purchased from ScienCell Research Laboratories). HCAEC were grown to confluence in 6-well Flexcell culture plates (Flexcell International Corporation) pre-coated (2-3 hours at 37°C) with 5 µg/mL fibronectin (Sigma-Aldrich, St Louis, MO).

Fibronectin was carefully added only in the center area of the well (approximately 25 mm in diameter, while the well diameter was 36.5 mm), in order to prevent cells from adhering to the peripheral area of the elastic membrane. Since the stretching is vacuum-driven, the peripheral area of the elastic membrane can experience up to 10-fold increase in tensile strain when being stretched [66](Refer to Aim 2 for a diagram of the shearing-stretching device setup). **Figure 24** shows cells adhere only on the fibronectin coated side of the elastic membrane.

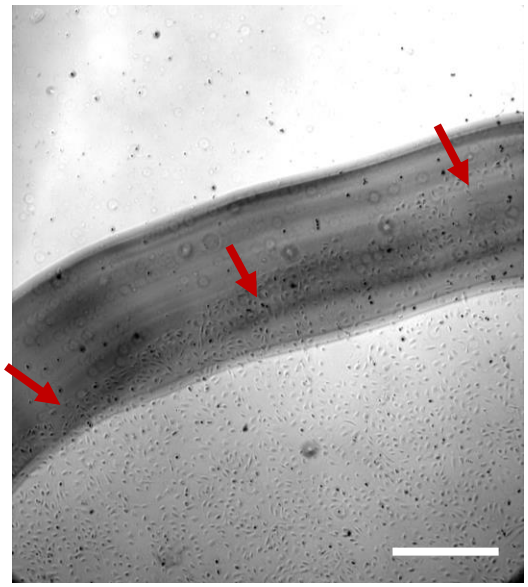

Figure 24. Wide-field 20X image of an elastic membrane area seeded with EC. Red arrows indicate the cell adhesion boundary. Cells only adhere to the fibronectin coated area.
Scale bar indicates 100 um.

4.3.5 Applying Concurrent Shear Stress and Cyclic Strain to ECs

Based on the fluid structure interaction model described in Chapter 2, physiological and pathological shear stress-tensile strain waveforms (**Figure 25**) were applied to EC monolayer using a custom-designed shearing-stretching device [66]. The piston vacuum pump from the original setup was replaced by a vacuum controller (Pressure Regulator, Part #QB3TANKKZN100KPG, ProportionAir, McCordsville IN), to enhance performance. Details of its characterization can be found in the Supplemental Information.

As depicted in **Figure 25**, three shear stress-tensile strain waveforms were used: 1) pulsatile shear stress varying between 0 - 1 Pa and cyclic tensile strain varying between 0 - 7%, mimicking normal mechanical loading conditions in a healthy coronary artery; 2) pulsatile shear stress varying between 0 - 3.7 Pa and cyclic tensile strain between 0 - 3%, mimicking pathological shear stress/strain conditions occurring at the stenosis throat (70%) in a diseased coronary artery; 3) pulsatile shear stress varying between 0 - 0.7 Pa and cyclic tensile strain between 0 - 5%, mimicking pathological shear stress/strain conditions in the recirculation zones developed downstream of a stenosis. One cardiac cycle lasted for 0.9 sec. Two shear stress peaks occurred in one cardiac cycle. The first peak was due to the increased blood flow rate during diastole, and the second peak was due to myocardial contraction during systole. The frequency of the cyclic tensile strain was approximately 1 Hz.

EC were exposed to concurrent shear stress and/or tensile strain for 1 hour at 37°C. Cells that were not treated (resting cells) were used as experimental control.

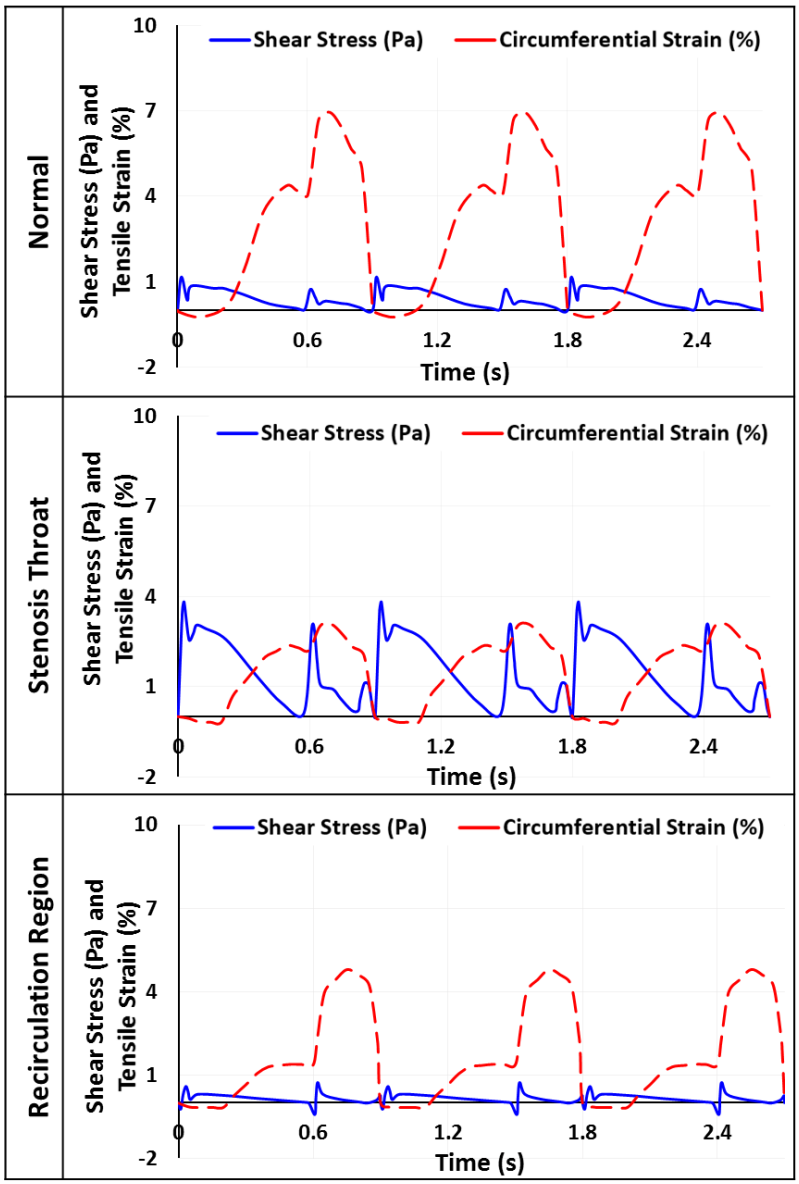

Figure 25. Shear stress and tensile strain waveforms applied to EC.

4.3.6 Immunofluorescent Microscopy

Following mechanical stimulation, HCAECs were washed twice with PBS, fixed in 0.5% glutaraldehyde and neutralized with 100 mM glycine-BSA. ECs were stained with Alexa Fluor 488 conjugated Phalloidin for F-actin elements (Ambion, Life Technologies, Carlsbad, CA). EC nuclei were stained with 4',6-diamidino-2-phenylindole (DAPI) (Life Technologies, Carlsbad, CA). Cell images were visualized using a Nikon Ti inverted microscope.

4.3.7 Cell Morphology Characterization – Cell Area and Elongation

EC area and elongation following shear stress and/or tensile stretch treatment were evaluated using *ImageJ* software (NIH). Cell elongation was quantified by the ratio of the long axis over the short axis of a cell, automatically determined by the software. Multiple cells were randomly chosen for each condition and the average of all the sampled cells were used as the elongation induced by that particular condition (untreated, shear, stretch, or combined).

4.3.8 Cell Functional Characterization

4.3.8.1 EC surface ICAM-1 expression

Following fluid shear stress and/or tensile strain treatment, HCAEC monolayer were washed and cell surface ICAM-1 expression was measured using a solid phase ELISA approach. A murine monoclonal anti-human ICAM-1 antibody (Abcam, Cambridge, MA) was used to detect endothelial cell surface ICAM-1 expression. Primary antibody binding was detected using an alkaline phosphatase conjugated

goat anti-mouse secondary antibody (Sigma-Aldrich, St. Louis, MO) and a P-nitrophenyl phosphate substrate. Absorbance was read at 405 nm using a SpectraMax i3 microplate reader (Molecular Devices, LLC, Sunnyvale, CA).

4.3.8.2 EC surface PECAM-1 phosphorylation

In a similar manner, following mechanical stimulation, EC surface PECAM-1 activation (phosphorylation) was also measured using solid phase ELISA. The primary antibody used was a polyclonal rabbit anti human phosphorylated PECAM-1 antibody (ABCAM).

4.3.8.3 ERK 1/2 (Extracellular signal-regulated kinases 1/2) Expression

Following mechanical treatment, HCAEC were washed and trypsinized. Collected cells were centrifuged at 1000 × *g* for 5 min. Cell pellet was then re-suspended in lysis buffer containing Triton X-100, protease and phosphatase inhibitors (Life Technologies, Carlsbad, CA), and incubated at 4 °C for 1 h.

Total protein concentration of the lysate was quantified using a standard BCA (bicinchoninic acid) assay (Thermo Scientific, Waltham, MA). EC ERK 1/2 activation was measured by Western Blot, using a monoclonal rabbit anti human phosphor-p44/42(ERK1/2) antibody (Cell Signaling Technology Inc., Danvers, Massachusetts). Primary antibody binding was detected using an EU-conjugated goat anti-rabbit secondary antibody (Molecular Devices). Expressed protein bands were visualized and quantified using the SpectraMax®i3 ScanLater™ Western blot detection system (Molecular Devices).

4.3.7.2 NF-κB activation

To determine if transcriptional changes would occur in shear stress- and/or tensile strain- treated EC, NF-κB activation was measured using a NF-κB pathway activation ELISA kit (eBioscience). It measured IκB proteins (phosphor-IκBa, IKKa and NFκBa) present in the cell lysate, using a sandwich approach. When NF-κB is inactive, IκB proteins bind to NF-κB transcription factor complex; upon extracellular stimulation such as mechanical stress/strain, IκB phosphorylates and dissociates from the complex, resulting in NF-κB activation and translocation to the nucleus.

4.3.7.4 Statistical analysis

Results are shown as mean + standard deviation. Statistical analysis was conducted using two-way ANOVA. If significant difference ($P < 0.05$) was detected, Tukey *post-hoc* test was used to conduct further comparisons between different treatment groups. All statistical analysis was conducted using GraphPad Prism (v.6.01, San Diego, CA).

4.3 Results

4.3.4 Cell Morphology

Following shear stress/tensile strain treatment, EC cytoskeleton F-actin filaments were detected by FITC-conjugated phalloidin using fluorescence microscopy. **Figure 26** (magnification 40x) depicts representative EC morphology under various stress/strain conditions. Untreated EC (control) appeared relatively small and randomly oriented, without distinct cell boundaries. EC that were exposed to

pathological low (0.7 Pa) or high (3.7 Pa) shear stress, alone or combined with pathological tensile strain, looked enlarged, elongated, with highlighted cell boundaries and/or stress fibers.

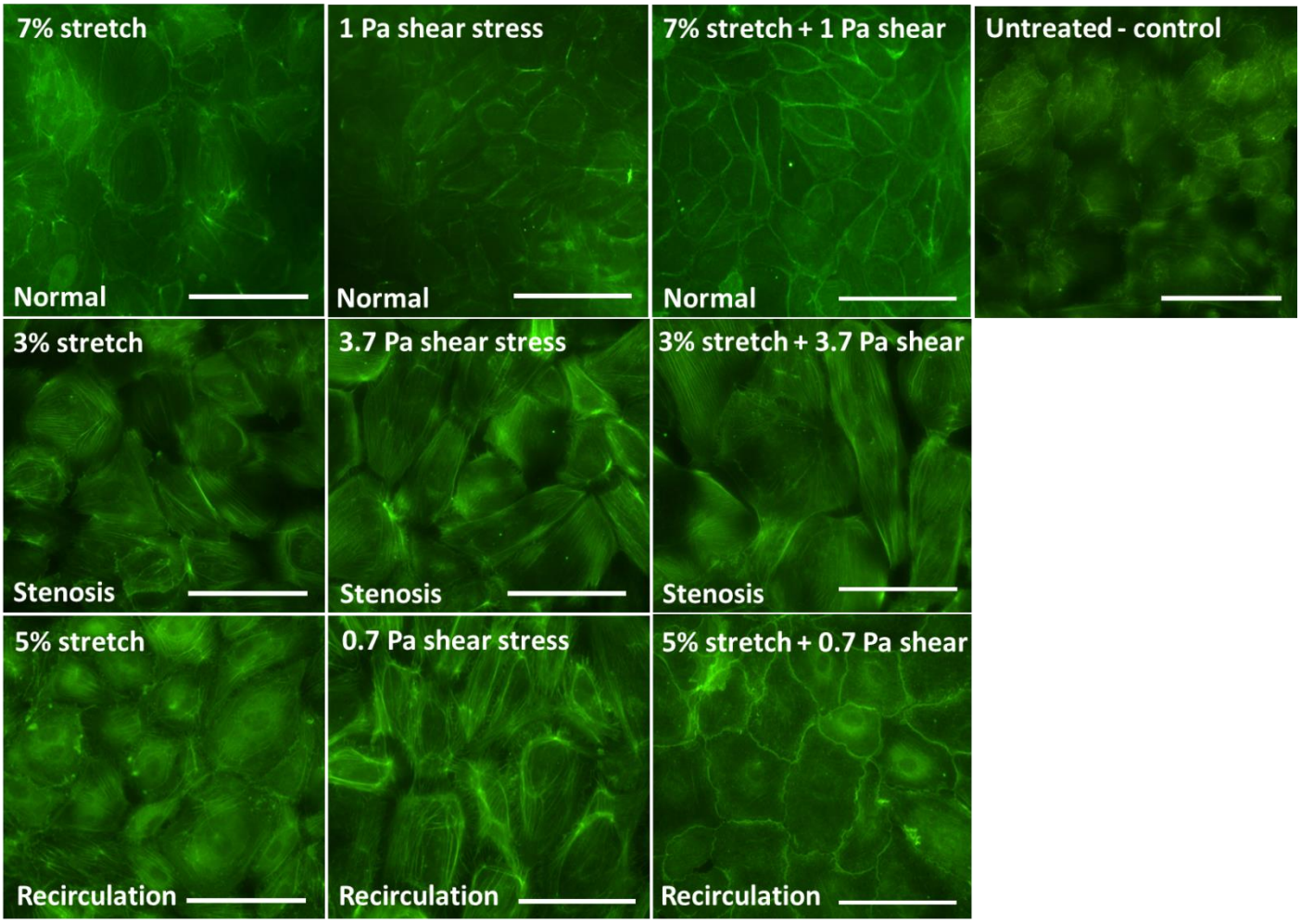

Figure 26. Representative images of EC morphology following mechanical stimulation. Pathological shear stress and/or tensile strain affected EC morphology greatly compared to physiological shear stress and/or tensile strain. Untreated EC were used as the experimental control. Scale bars represent 50 μm.

4.3.4.1 Cell Area

Changes in EC area induced by shear stress and/or tensile strain were quantified using the *Image J* software, and depicted in **Figure 27**. Two-way ANOVA indicated that both physiological/pathological conditions (i.e., normal, stenosis, or recirculation) and mechanical stimulation (i.e., fluid shear stress, cyclic tensile strain, or combined) had significant effects (P<0.001) on EC area. The comparisons between different treatment groups are summarized in **Table 3**.

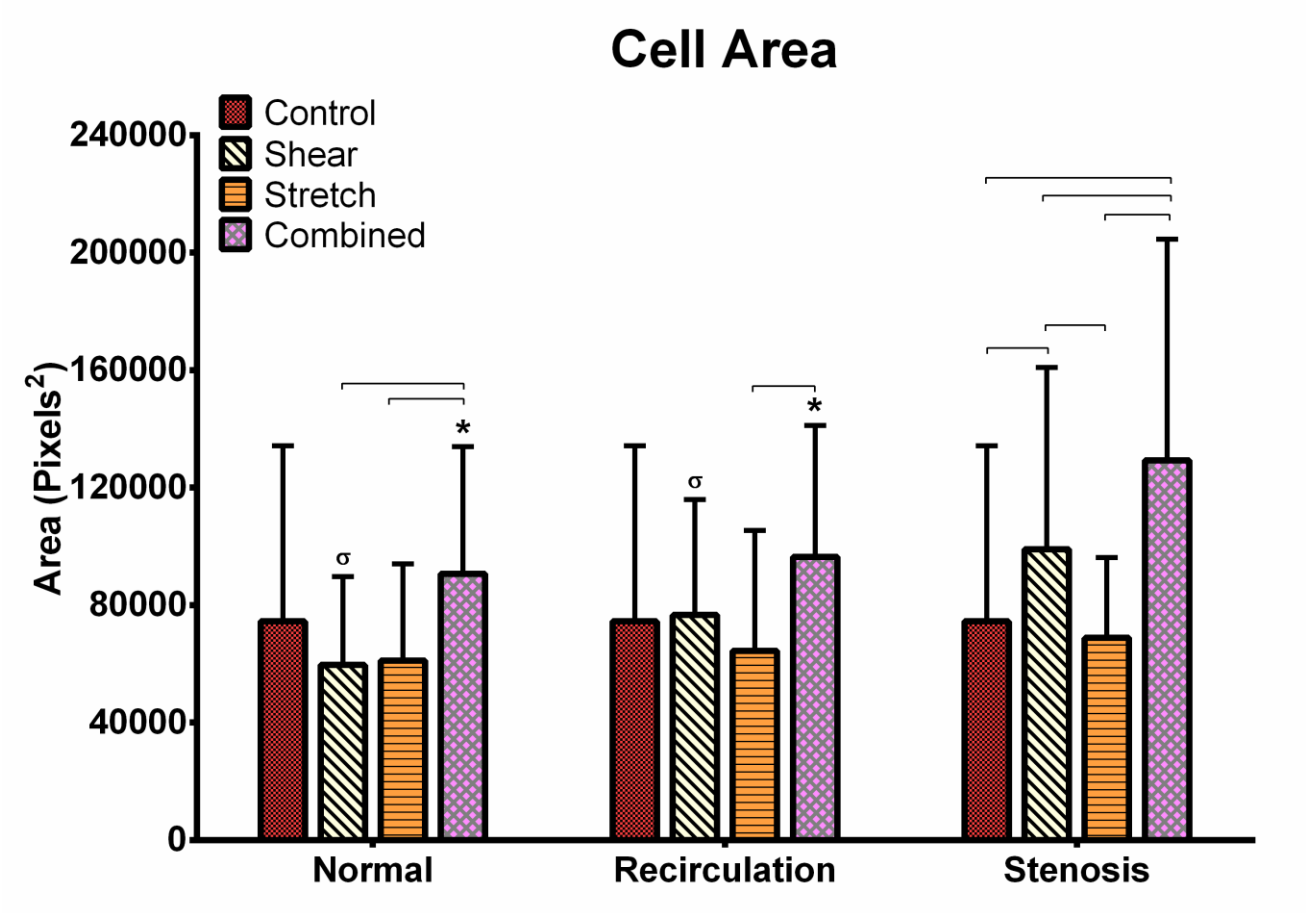

Figure 27. EC cell area after subjection to single or combined mechanical stimuli under physiological and pathological conditions. Combined stimuli significantly increased cell area compared to single stimulation. Data is presented as mean + standard deviation. * denotes significant difference from stenosis combined treatment; σ, significantly different from shear stenosis treatment. (Two-way ANOVA, *Tukey*, P <0.05)

Table 3- Two-way ANOVA indicate treatment (i.e., fluid shear stress, cyclic tensile strain, or combined) and condition (i.e., normal, stenosis, or recirculation effects), both had significant effects on EC area. Data is presented as mean ± standard deviation. Adjusted *P* values accounting for multiple comparison are presented. $P<0.05$ is considered significant.

0.3015
<.0001
<.0001
<0.0001
<0.0001
0.1032
0.0110
<.00001
<0.0001

	Normal	Stenosis	Recirculation
Control	66321.823 n = 79 ± 37110.3206	113199.794 n = 68 ± 76808.3980	29008.427 n = 60 ± 19702.6608
Shear	59644.716 n = 81 ± 30059.1125	99095.081 n = 221 ± 61809.9342	76630.775 n = 120 ± 39329.9670
Tensile Stretch	61163.696 n = 92 ± 32943.5352	68879.720 n = 118 ± 27294.1006	64503.286 n = 49 ± 40990.2216
Combined	91133.333 n = 84 ± 43286.1277	129308.258 n = 128 ± 75257.1909	90588.803 n = 49 ± 49122.5379

Elevated shear stress (3.7 Pa) significantly increased cell area as compared to normal (1 Pa) and low (0.7 Pa) pathological shear stress. On the contrary, tensile strain at 3%, 5% and 7% did not cause any significant change in cell area.

4.3.4.2 Cell Elongation

Similarly to cell area, two-way ANOVA indicated that both physiological/pathological conditions (i.e., normal, stenosis, or recirculation) and mechanical stimulation (i.e., fluid shear stress, cyclic tensile strain, or combined) had significant effects (P<0.001) on EC elongation. The comparisons between different treatment groups are summarized in **Table 4**.

Table 4- Two-way ANOVA results indicate treatment (i.e., fluid shear stress, cyclic tensile strain, or combined) and condition (i.e., normal, stenosis, or recirculation effects), both had significant effects on EC elongation. Data is presented as mean ± standard deviation. Adjusted P values accounting for multiple comparison are presented. P<0.05 is considered significant.

	Normal		Stenosis		Recirculation	
Control	1.9441 ± 0.5804	n = 133	1.9466 ± 0.5809	n = 68	1.6878 ± 0.3943	n = 60
Shear	2.2298 ± 0.8121	n = 97	2.0650 ± 0.7632	n = 221	2.0648 ± 0.6824	n = 120
Stretch	2.0036 ± 0.7466	n = 66	1.9262 ± 0.6069	n = 118	1.8023 ± 0.5172	n = 65
Combined	1.9849 ± 0.0915	n = 38	1.8053 ± 0.6185	n = 128	1.5608 ± 0.2993	n = 55

As shown in **Figure 28**, shear stress appears to have a dominant effect on cell elongation. Biaxial tensile strain alone caused no significant change in cell elongation. However, under combined tensile strain and shear stress, cell elongation reduced, compared to shear-alone conditions.

Under recirculation conditions, combined shear stress and tensile strain resulted in the least cellular elongation.

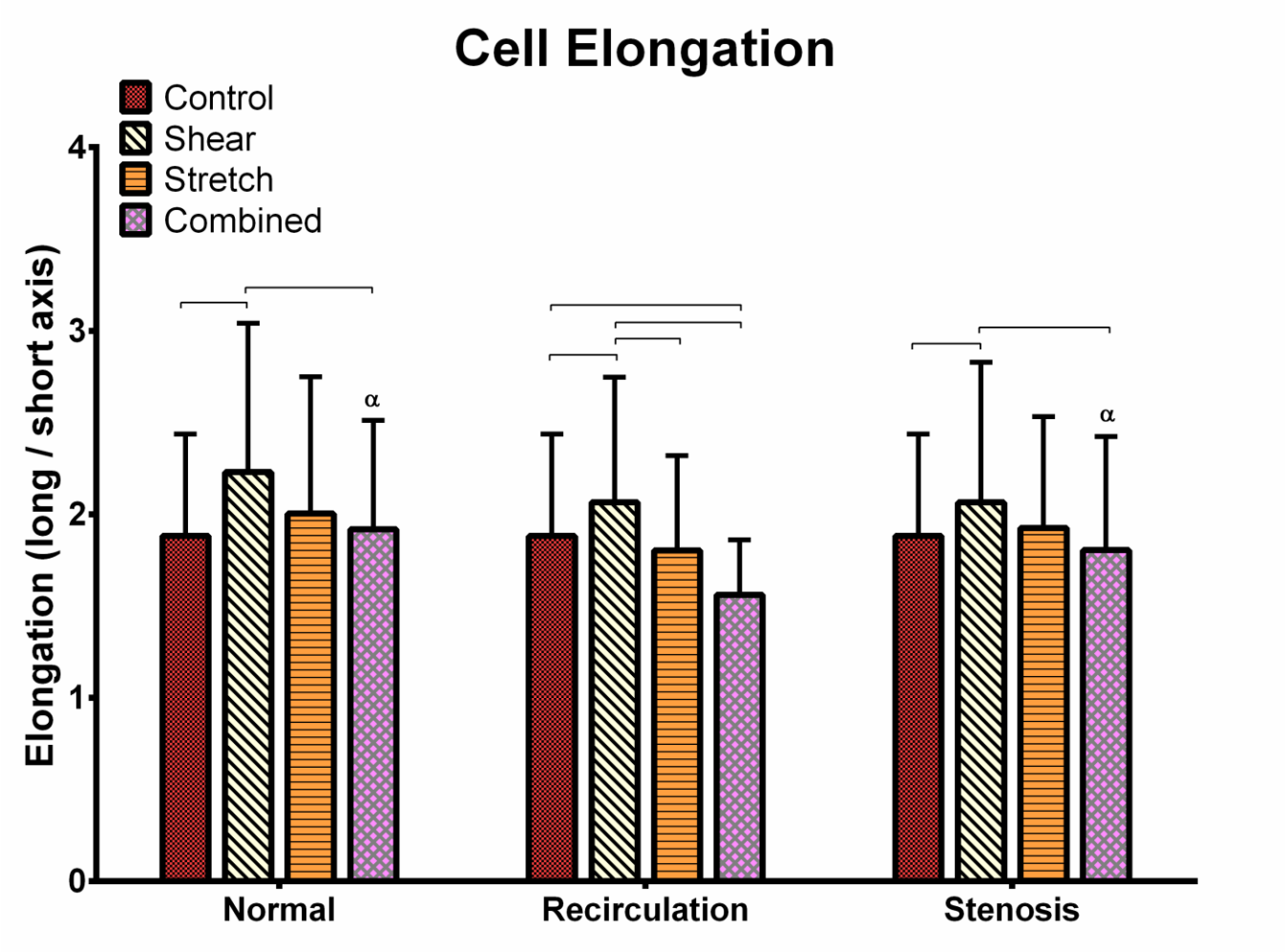

Figure 28. EC cell elongation upon subjection to single or combined mechanical stimuli under physiological and pathological conditions. Combined stimuli significantly decreased cell elongation as compared to single stimulation. Data is presented as mean + standard deviation. α, denotes significant difference from recirculation combined treatment (Two-way ANOVA, *Tukey*, $P<0.05$)

4.3.4 EC Activation

Following mechanical stimulation, EC responses were evaluated by characterizing EC PECAM-1 tyrosine phosphorylation, mechanotransduction pathway (MAPK) activation, transcription factor NF-κB activation, and cell surface ICAM-1 expression.

4.3.4.1 Phospho-PECAM

Two-way ANOVA indicated that both physiological/pathological conditions (i.e., normal, stenosis, or recirculation) and mechanical stimulation (i.e., fluid shear stress, cyclic tensile strain, or combined) had significant effects (P<0.001) on phospho-PECAM expression. The comparisons between different treatment groups are summarized in **Table 5**.

Table 5- Two-way ANOVA results indicate treatment (i.e., fluid shear stress, cyclic tensile strain, or combined) and condition (i.e., normal, stenosis, or recirculation effects), both had significant effects on phospho-PECAM expression. Data is presented as mean ± standard deviation. Adjusted P values accounting for multiple comparison are presented. P<0.05 is considered significant.

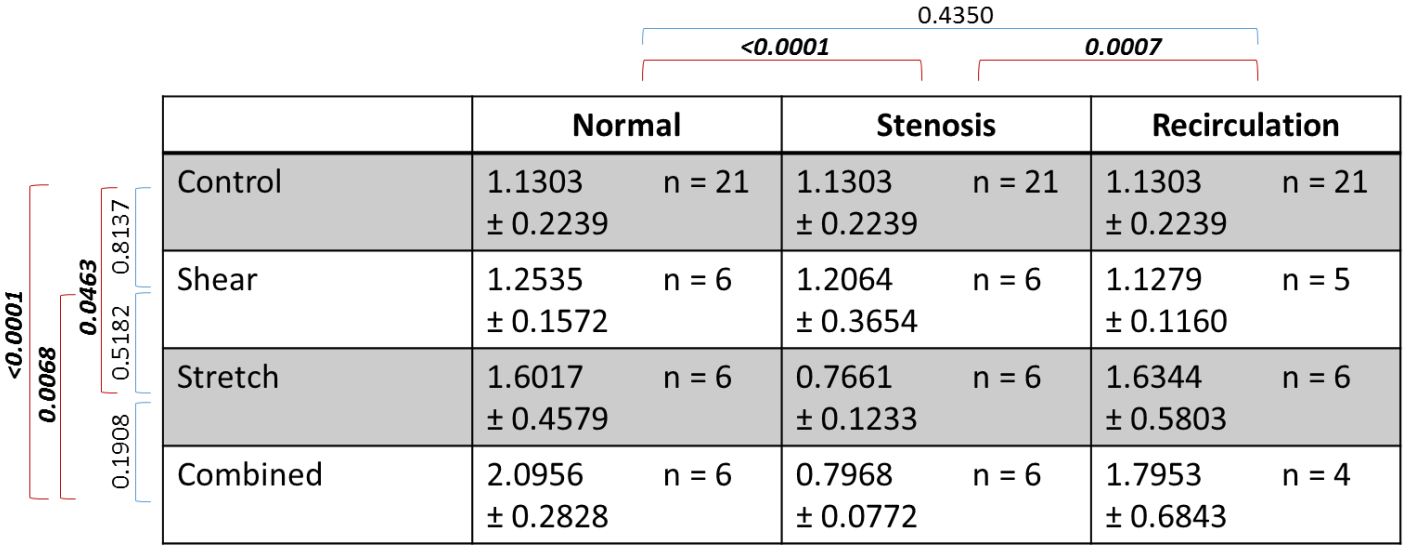

	Normal	Stenosis	Recirculation
Control	1.1303 ± 0.2239 n = 21	1.1303 ± 0.2239 n = 21	1.1303 ± 0.2239 n = 21
Shear	1.2535 ± 0.1572 n = 6	1.2064 ± 0.3654 n = 6	1.1279 ± 0.1160 n = 5
Stretch	1.6017 ± 0.4579 n = 6	0.7661 ± 0.1233 n = 6	1.6344 ± 0.5803 n = 6
Combined	2.0956 ± 0.2828 n = 6	0.7968 ± 0.0772 n = 6	1.7953 ± 0.6843 n = 4

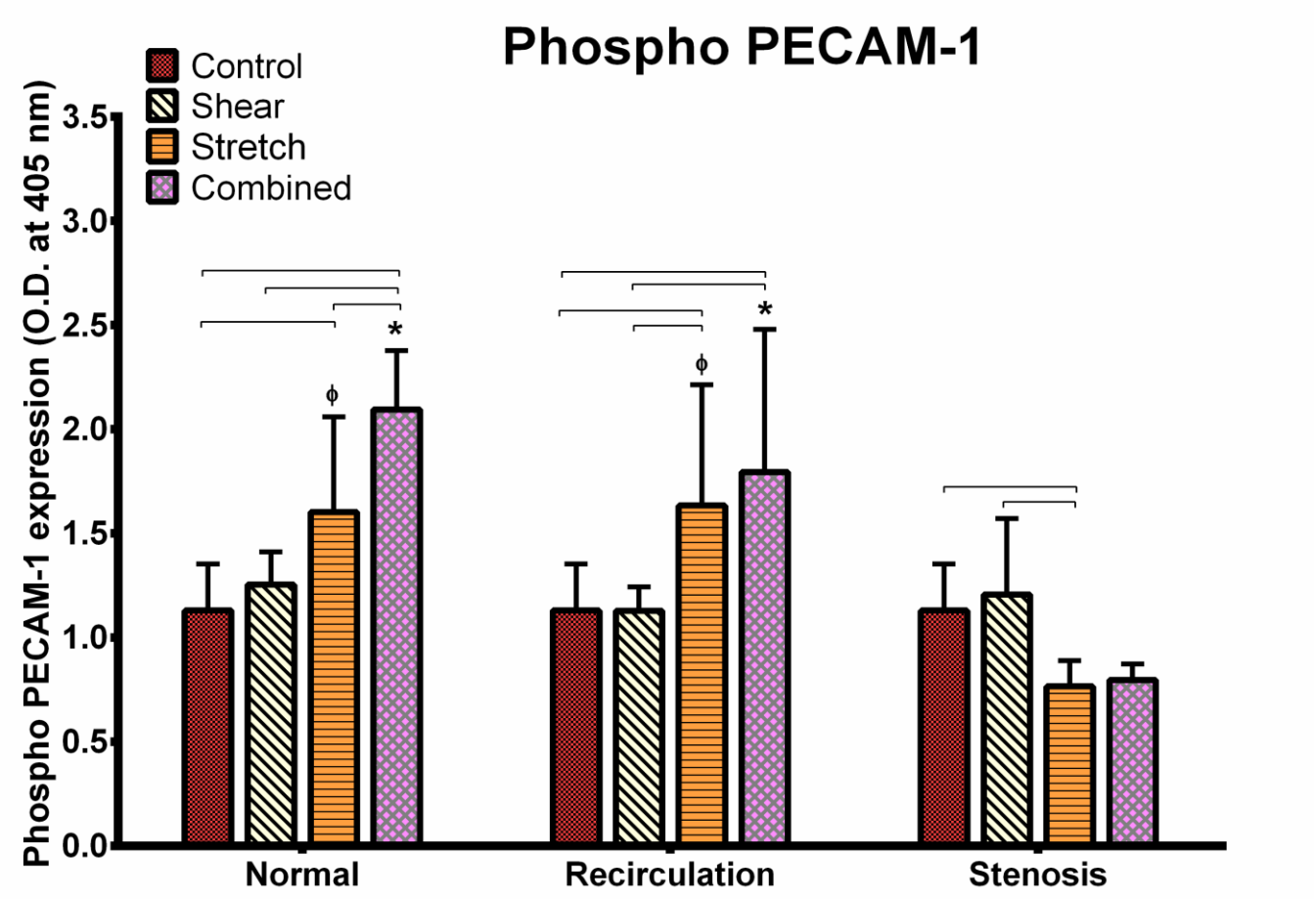

Figure 29. EC phospho-PECAM expression following single or combined mechanical stimulation under physiological and pathological conditions. When exposed to stretch magnitudes of 5% or higher, combined stimuli has an additive effect on EC phospho-PECAM expression. Data is presented as mean + standard deviation. *, denotes significant difference from stenosis combined treatment; ϕ, significantly different from stenosis low stretch (3%) treatment (Two-way ANOVA, *Tukey*, $P<0.05$).

As depicted in **Figure 29**, tensile stretch seemed to have a bigger effect on phospho-PECAM expression compared to shear stress. Phospho-PECAM expression under shear stress was similar under all conditions, while larger tensile stretch induced greater phospho-PECAM expression.

Shear stress and tensile strain seemed to have additive synergistic effect on PECAM phosphorylation, especially when to the strain was greater than 5%.

4.3.4.2 ERK 1/2

To check whether the MAPK pathway was activated due to mechanical stimulation, phosphorylated ERK 1/2 expression was measured. Two-way ANOVA indicated that neither physiological/pathological conditions (i.e., normal, stenosis, or recirculation) nor mechanical stimulation (i.e., fluid shear stress, cyclic tensile strain, or combined) had significant effects (P>0.12) on ERK 1/2 expression. The comparisons between different treatment groups are summarized in **Table 6**.

Table 6- Two-way ANOVA results indicate neither treatment (i.e., fluid shear stress, cyclic tensile strain, or combined) nor condition (i.e., normal, stenosis, or recirculation effects) have significant effects on phosphorylated ERK 1/2 expression. Data is presented as mean ± standard deviation. Adjusted P values accounting for multiple comparison are presented. P<0.05 is considered significant.

	Normal	Stenosis	Recirculation
Control	0.1358 ± 0.1594 n = 11	0.1358 ± 0.1594 n = 11	0.1358 ± 0.1594 n = 11
Shear	0.2859 ± 0.0350 n = 3	0.0176 ± 0.0051 n = 4	0.1228 ± 0.0945 n = 5
Stretch	0.2060 ± 0.0849 n = 6	0.0225 ± 0.0131 n = 6	0.0694 ± 0.1015 n = 8
Combined	0.3149 ± 0.1938 n = 6	0.0343 ± 0.0084 n = 5	0.0712 ± 0.1107 n = 10

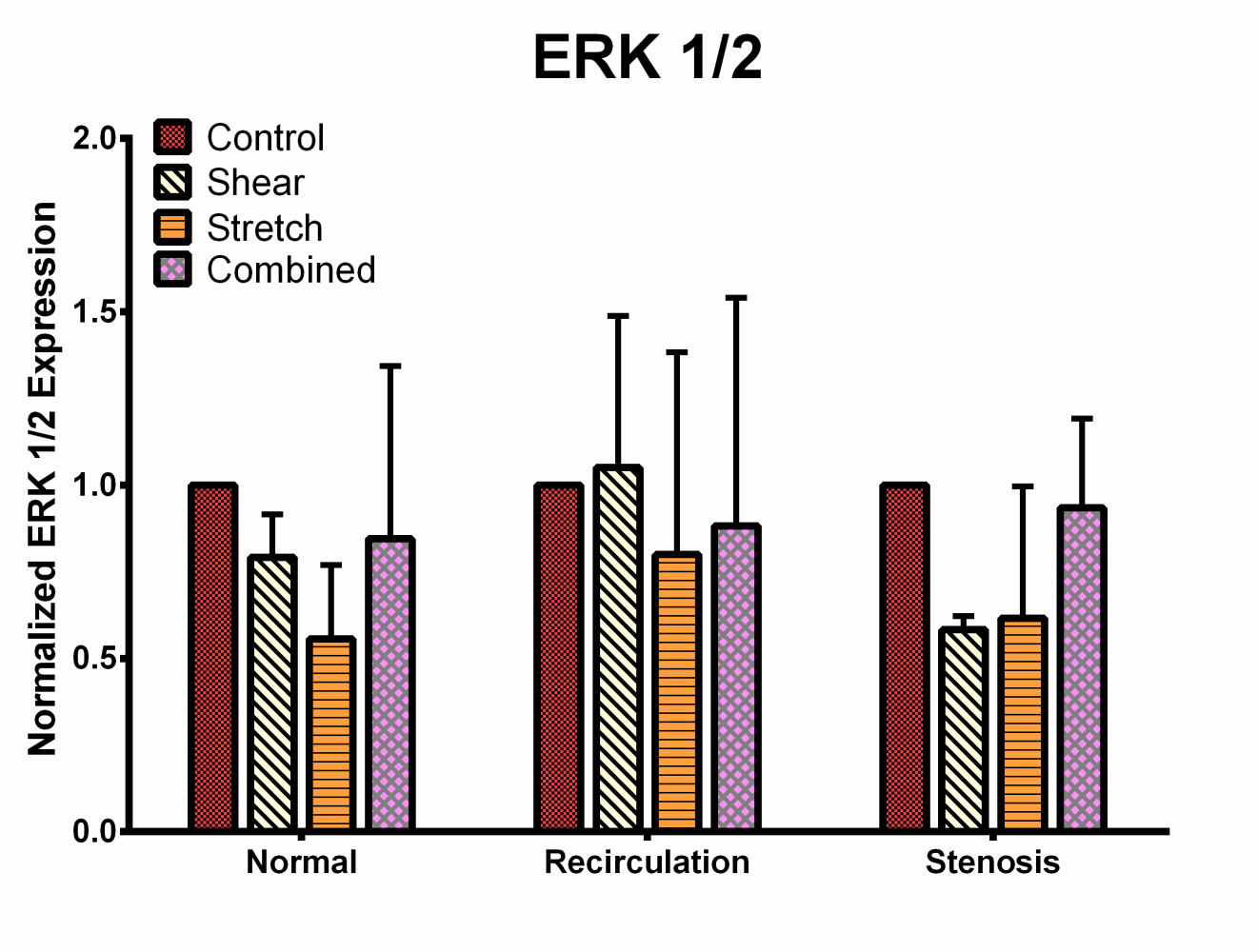

Figure 30. EC phosphorylated ERK 1/2 expression following mechanical stimulation, mimicking normal, recirculation and stenosis conditions. No significant differences (two-way ANOVA, $P>0.05$) in ERK1/2 expression were observed across treatments nor conditions. Data is presented as mean + standard deviation.

Phosphorylated ERK 1/2 expression in shear stress/tensile strain treated EC is shown in **Figure 30**. No significant difference was detected between different treatment groups or conditions. This could be due to the transient nature of ERK1/2 phosphorylation [158, 159].

4.3.4.3 NF-κB

Two-way ANOVA indicated that mechanical stimulation (i.e., fluid shear stress, cyclic tensile strain, or combined) but not physiological/pathological conditions (i.e., normal, stenosis, or recirculation) had significant effects on EC NF-κB activation. The comparisons between different treatment groups are summarized in **Table 7**.

Table 7- Two-way ANOVA results indicate treatment (i.e., fluid shear stress, cyclic tensile strain, or combined) as opposed to condition (i.e., normal, stenosis, or recirculation effects) had significant effects on EC NF-κB activation. Data is presented as mean ± standard deviation. Adjusted *P* values accounting for multiple comparison are presented. $p<0.05$ is considered significant.

0.0503
0.2453
0.6944

	Normal	Stenosis	Recirculation
Control	1.1252 ± 0.4014 n = 11	1.1252 ± 0.4014 n = 11	1.1252 ± 0.4014 n = 11
Shear	1.1451 ± 0.3506 n = 6	1.0935 ± 0.3466 n = 6	1.4168 ± 0.2221 n = 4
Tensile Stretch	0.8587 ± 0.2995 n = 6	1.0702 ± 0.0919 n = 5	1.3727 ± 0.2522 n = 3
Combined	0.9670 ± 0.1747 n = 5	1.6671 ± 0.1999 n = 4	1.4021 ± 0.1891 n = 5

0.2560
0.7163
0.8710
0.9060
0.6122
0.1308

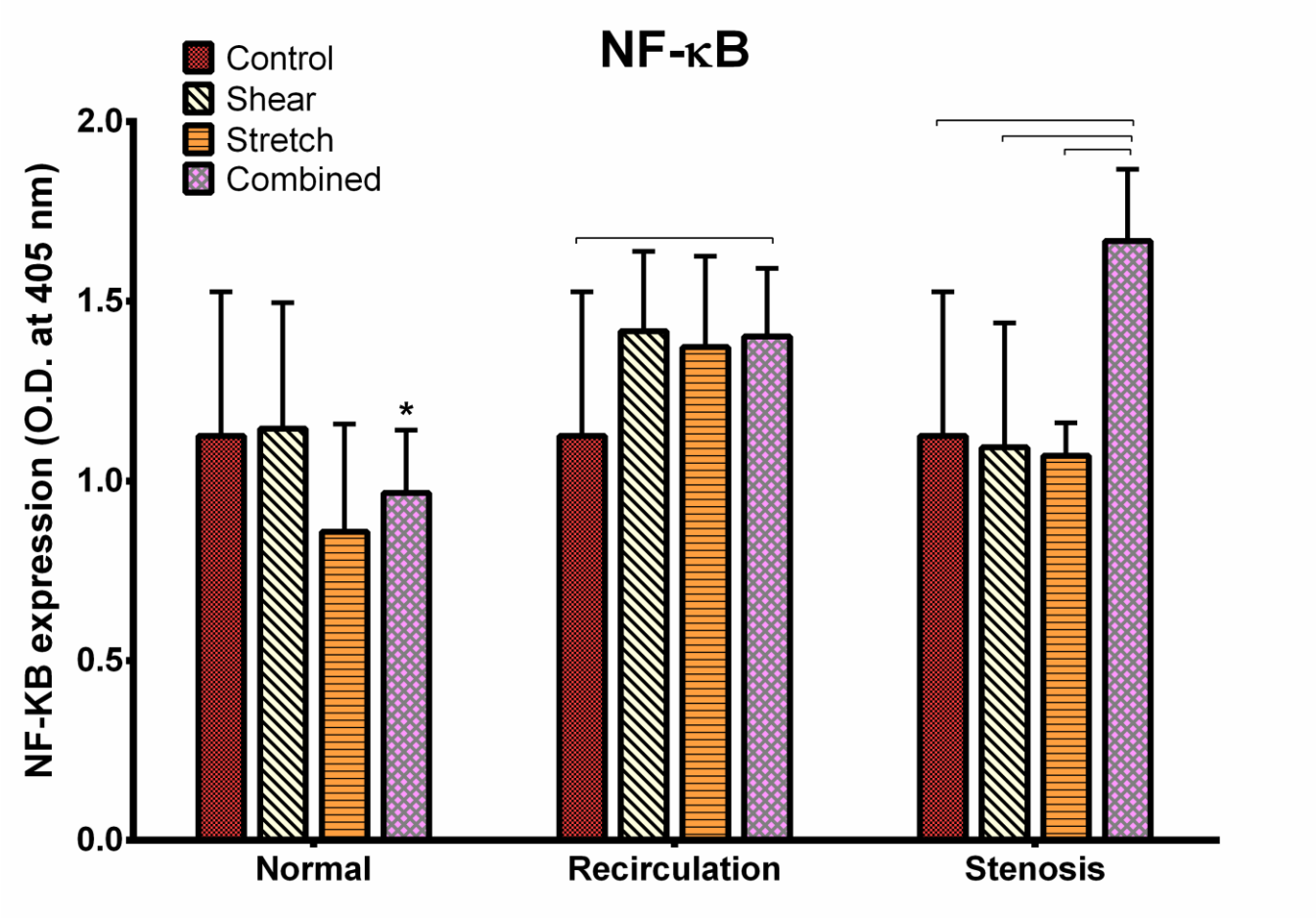

Figure 31. EC NF-κB expression following single or mechanical stimulation under physiological and pathological conditions. Combined shear stress and tensile strain stenosis conditions caused a significant increase in NF-kB expression as compared to combined normal conditions. Data is presented as mean + standard deviation. *, denotes significant difference from stenosis combined treatment (Two-way ANOVA, *Tukey*, $P<0.05$)

As shown in **Figure 31**, the greatest increase in NF-κB activation occurred under stenosis conditions when shear stress and tensile strain were applied simultaneously. Compared to untreated EC, combined shear stress and tensile strain also caused a significant increase in NF-κB activation under recirculation conditions.

4.3.4.4 ICAM-1

Two-way ANOVA indicated that both physiological/pathological conditions (i.e., normal, stenosis, or recirculation) and mechanical stimulation (i.e., fluid shear stress, cyclic tensile strain, or combined) had significant effects (P<0.001) on ICAM-1 expression. The comparisons between different treatment groups are summarized in **Table 8**.

Table 8- Two-way ANOVA results indicate treatment (i.e., fluid shear stress, cyclic tensile strain, or combined) and condition (i.e., normal, stenosis, or recirculation effects), both had significant effects on ICAM-1 expression. Data is presented as mean ± standard deviation. Adjusted P values accounting for multiple comparison are presented. P<0.05 is considered significant.

<.0001

<.0001 0.3762

0.0142 0.2291 0.6219 0.8666 0.9879 0.3591

	Normal	Stenosis	Recirculation
Control	0.4851 ± 0.1210 n = 17	0.4851 ± 0.1210 n = 17	0.4851 ± 0.1210 n = 17
Shear	0.4043 ± 0.1317 n = 6	0.5421 ± 0.0500 n = 5	0.5846 ± 0.1553 n = 6
Tensile Stretch	0.2902 ± 0.0230 n = 7	0.7167 ± 0.0710 n = 6	0.5919 ± 0.0739 n = 6
Combined	0.3643 ± 0.0915 n = 6	0.7766 ± 0.0694 n = 5	0.6431 ± 0.0678 n = 5

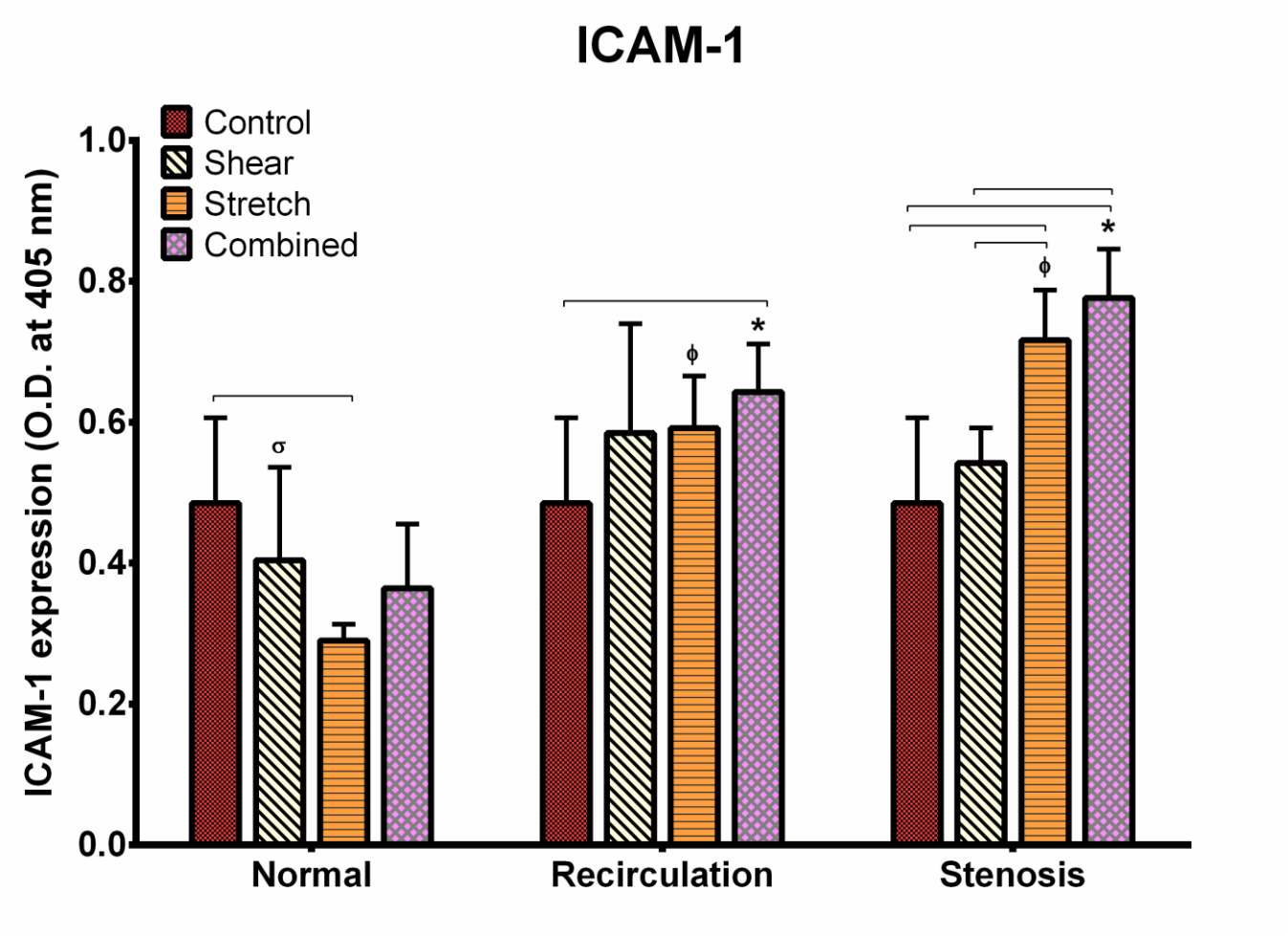

Figure 32. EC ICAM-1 surface protein expression following mechanical stimulation, mimicking normal, recirculation and stenosis conditions. ICAM-1 expression was significantly lower under normal physiological conditions than under diseased pathological conditions (recirculation and stenosis). Data is presented as mean + standard deviation. *, denotes significant difference from normal combined treatment; ϕ, significantly different from normal stretch treatment; σ, significantly different from recirculation low shear treatment. (Two-way ANOVA, *Tukey*, $P<0.05$)

Pathological low shear stress (recirculation shear) and reduced tensile stain (3% under stenosis conditions and 5% under recirculation conditions) induced significant increase in ICAM-1 expression. Overall, ICAM-1 expression was significantly lower under physiological conditions compared to that under pathological conditions (recirculation and stenosis). Moreover, shear stress and tensile strain seemed to have a synergistic effect on ICAM-1 expression, especially under pathological (stenosis and recirculation) conditions.

4.3 Discussion

ECs are sensitive to their mechanical environment. They can adjust their cytoskeleton, junctional proteins and cell-matrix interactions to maintain hemostasis when subject to mechanical loads. These structural responses are often accompanied by functional changes. In this chapter, EC response to physiological and pathological mechanical conditions, i.e., shear stress and tensile strain, was studied. The mechanical conditions used here mimicked that within coronary arteries under physiological and pathological conditions, as estimated by the FSI model developed in Chapter 2.

EC area and elongation in response to single and combined mechanical stimulation were characterized. Cell area significantly increased in response to combined shear stress and tensile strain compared to each single stimulation, suggesting cell area may respond to fluid shear stress and tensile strain in an additive manner. This observation agrees with a study reported by Zhao et al, in which fluid shear stress and cyclic circumferential strain had a synergistic effect on EC morphology[145]. Moreover, they suggested cyclic strain might increase EC sensitivity to shear stress, causing cell structural deformation at a lower shear stress. Our study demonstrated that elevated shear stress (3.7 Pa) significantly increased cell area compared to untreated cells, which was further increased (by 33%, $P<0.05$) when a 3% tensile strain was applied at the same time.

It's well established that EC can elongate in response to fluid shear stress [30] to decrease resistance to flow. When biaxial tensile strain was applied simultaneously with shear stress, the effect of shear on EC elongation was reduced. This somewhat differed from a previous report in which fluid shear stress and hoop stretch had synergistic effect on EC elongation. However, the stretch model used in that study was uniaxial, different from the biaxial strain used here. The opposing effect of shear stress and cyclic strain on EC elongation was also observed in Chapter 3 studies [66]. Under recirculation shear stress (0.7 Pa) and tensile strain (5%) conditions, equi-biaxial tensile strain significantly decreased cell

elongation compared to untreated cells, causing cells to look round. Such cobblestone morphology along recirculation regions has been reported by many studies [31].

PECAM-1, highly localized at EC junctions, plays important roles in endothelial cell mechanotransduction and many inflammatory responses [160]. PECAM-1 phosphorylates upon mechanical stimulation [161]. Our results suggested EC were more sensitive to tensile stretch than shear stress. Moreover, the synergistic effect of shear stress and tensile strain on EC PECAM-1 phosphorylation seemed to be dependent on the tensile strain magnitude. This could be explained by the fact that PECAM-1 is highly localized at cell junctions, and is directly pulled by forces resulted from tensile stretch. On the other hand, the effect from fluid shear stress on PECAM-1 phosphorylation might not be as strong, since shear stress is parallel to the cell surface. It has been reported that morphological responses of ECs induced by stretch were transmitted through intercellular junctions [141, 162]. Our results are in agreement with this conclusion. Tensile strain at 3, 5 and 7 % all caused higher phosphorylated PECAM-1 expression compared to fluid shear stress (0.7, 1 and 3.7 Pa). Furthermore, higher tensile strain, i.e., 5% and 7%, led to greater phosphorylated PECAM-1 expression compared to 3% strain.

This PECAM phosphorylation was hypothesized to lead the activation of the mitogen-activated protein kinase (MAPK) pathway [23, 24]. The MAPK cascade is a chain of serine/threonine protein kinases, which together act as an intracellular signal transduction pathway that responds to various extracellular stimuli such as physical and oxidative stress.

This cascade transduces the signal from a receptor on the surface of the cell to the DNA in the nucleus of the cell, causing transcriptional changes and differential expression of proteins, which determine cell function. MAPKs are known to regulate fundamental cellular processes including growth, proliferation, differentiation, motility, survival, apoptosis, stress response and inflammation [163]. The members of the mitogen-activated protein kinase (MAPK) family, including extracellular signal-regulated kinase (ERK1/2), N-terminal Jun kinase (JNK1/2) and p38 MAPK, have been shown to be involved in shear and cyclic stress induced EC inflammation [164-168]. Mechanical stress can induce the activation

of MAPKK kinases (Raf) via receptor-dependent and independent mechanisms which transduce the signal to small GTP-binding proteins (Ras, Rap1). MAPKKKs then phosphorylate and activate a downstream MAPK kinase, which in turn phosphorylates and activates MAPKs (ERK 1/2) [163].

However, no significant change in MAPK-ERK 1/2 expression was observed in our study following mechanical treatment (untreated, shear, stretch, combined) under physiological or pathological conditions (normal, recirculation, stenosis). This might be due to the time and force dependency of ERK 1/2 activation [158, 159]. Previous literature has shown disturbed flow enhances cell proliferation, an indicator of vascular dysfunction, via a sustained ERK activation; while laminar flow results in a low cell proliferation rate and a transient ERK activation [169]. ERK activation peaks at 10 and 15 min under 20% and 30 % cyclic stretch [170, 171] respectively, and at 30 min under shear stress[34]. In the present study, ERK1/2 activation was measured 1 hour following shear stress/tensile strain treatment, at which point, ECs might have adapted to the mechanical stimulation. In other words, we might have missed the transient change in ERK1/2 activation by conducting the measurements at 1 hour. In order to capture the transient changes in ERK1/2 activation, measured time-response may be needed. Furthermore, even though no significant difference in ERK 1/2 activation was observed, significant changes in the downstream transcription factor NF-κB activation occurred.

Activated ERK 1/2 can regulate targets in the cytosol and translocate to the nucleus where they phosphorylate pro-inflammatory transcription factors such as NF-kB, which regulate inflammatory gene and protein expression. NF-κB activation in endothelial cells mediates the expression of cytokines, chemokines and adhesion molecules, which recruit circulating leukocytes into the inflamed tissue.

Our study shows NF-κB activation significantly increased under stenosis conditions, when shear stress and tensile strain were applied to EC simultaneously (compared to single stimulation or untreated cells). However, neither shear stress nor tensile strain alone caused any significant change in NF-κB activation compared to untreated cells. Many previous studies have shown that varying levels of shear stress or cyclic strain can cause marked changes in NF-κB activation[172]; and physiological levels of

single stimulation could result in less NF-κB activation, compared to that at pathological levels. In the present study, no significant change in NF-κB activation was observed following shear stress (alone) or tensile strain (alone) stimulation. This could be due to the relatively short duration of mechanical stimulation (1 hr compared to 8, 12 or 24 hours). Interestingly, when shear stress and tensile strain were applied concurrently, a significant NF-κB increase was observed under pathological conditions (recirculation and stenosis) compared to normal conditions. These results agree with *in vivo* observations, where NF-κB signal transduction pathway in coronary artery endothelial cells is primed for activation in regions predisposed to atherosclerotic lesion formation[173]. These results also highlight the effect of concurrent stimulation from shear stress and tensile strain on NF-κB activation. Endothelium restricted inhibition of NF-κB activation has resulted in strongly reduced atherosclerotic plaque formation in mice [174]. Therefore, both shear stress and tensile strain need to be considered while investigating mechanical stress-induced atherosclerosis development.

NF-κB activation has been shown to induce cytokine and adhesion molecule expression, including ICAM-1[175]. ICAM-1, also known as CD54, is an immunoglobulin (Ig)-like cell adhesion molecule expressed on endothelial cells at low levels, yet upregulated following exposure to pro-inflammatory stimuli (low-shear stress for example). Our study shows low recirculation shear stress (0.7 Pa) as well as low stenotic (3%) and recirculation (5%) stretch significantly increased ICAM-1 expression compared to normal shear and stretch conditions alone. This agrees with previous literature, which shows altered shear stress or tensile strain alone stimulates the upregulation of ICAM-1 compared to physiological stress/strain [176] [177]. The combined effect of shear stress and tensile strain (pathological and physiological) on ICAM-1 expression was also studied by Liam T Breen et al.[156] They reported cyclic strain (4, 8, and 12%) downregulated ICAM-1 expression caused by physiological pulsatile fluid shear stress (4 Pa). However, under pathological oscillatory fluid shear stress (±0.5 Pa), cyclic strain upregulated ICAM-1 expression. Our study does not show a significant upregulation of ICAM-1 under fluid shear stress (0.7, 1, and 3.7 Pa) following 1 hr stimulation. The disagreement in results is probably due to the

the difference in mechanical stimulation duration (their study applied stimuli for 12 h). Overall, ICAM-1 expression was significantly lower under physiological conditions compared to that under pathological conditions (recirculation and stenosis). Moreover, combined stimulation had an additive effect in ICAM-1 expression under pathological conditions, but not under normal conditions.

Interestingly, enhanced phosphorylated PECAM-1 expression did not result in higher ICAM-1 expression, as commonly suggested [178, 179]. On the contrary, our results suggest an increase in phosphorylated PECAM-1 expression might help modulate and decrease inflammatory responses. Phosphorylated PECAM-1 expression was significantly lower under stenosis conditions compared to normal conditions. Yet, downstream NF-κB activation and ICAM-1 expression were significantly higher under stenosis conditions compared to normal conditions. This suggests that the EC MAPK pathway activation observed here may not have resulted from PECAM-1 phosphorylation. It is likely that other EC mechanoreceptors are involved in EC response to shear stress and/or cyclic strain signals[24].

Overall, our results demonstrated that EC respond to combined shear stress and tensile strain differently than to each single simulation. The study also showed that EC responded to varying mechanical combinations differently. Physiological conditions (1 Pa shear stress with 7% cyclic strain) resulted in less inflammatory protein production than pathological conditions (stenosis: 3.7 Pa with 3% cyclic strain; recirculation region: 0.7 Pa with 5% cyclic strain).

4.4 Limitations

The shearing-stretching experiments to study the effect of both fluid shear stress and tensile strain on EC activation had the following limitations:

1. The MAPK-ERK 1/2 expression has been reported to be transient in nature. Therefore, to be able to better monitor any changes in this pathway, measurements will need to done at various time points, as opposed to one sole 1-hour measurement.
2. The Young's modulus of the flexible-membrane substrate on which cells were grown is much lower than typical glass substrates. Hence, previous literature data on fluid shear stress impact on EC activation cannot be directly compared to our results, since the substrate property may have an additional effect on EC's response[38].

Chapter V

DISCUSSION, CONCLUSIONS AND FUTURE DIRECTIONS

5.1 Discussion

The FSI model was validated to some extent by the results obtain in the experimental section of the dissertation. (last aim) The pathological waveforms generated elevated levels of inflammatory responses, ie. ICAM-1, compared to the physiological waveforms, in both single and combined mechanical stimuli combinations.

These results also support our hypothesis. Altered shear stress and tensile strain lead to significant changes in EC morphology and function, accelerating local inflammatory responses.

Unexpectedly, phosphorylated PECAM-1's role in activating the MAPK pathway towards an increased inflammatory or atherogenic response was not seen. On the contrary, based on the results, it can be speculated phosphorylated PECAM-1 may be responsible for activating or mediating atheroprotective responses. A higher PECAM-1 phosphorylation in response to shear stress alone was not produced. This was contrary to other *in vitro* studies, which have seen an increase in phosphorylated PECAM in response to mechanical stimuli[161]. This difference might have arose as an effect of the substrates used. Chiu et al [161], utilized glass substrates in their studies, which have a much higher Young's Modulus (YM) compared to the flexible silicon substrate used in ours. (10^3 difference). The flexible substrate has a much similar YM to the human coronary artery, which increases the physiological relevance of the *in vitro* setup.

Tensile strain, on the other hand, did cause a noticeable increase in PECAM-1 phosphorylation in our studies. Results suggested tensile strain might have a dominant effect on PECAM-1 phosphorylation

as compared to shear stress *in vivo*. As tensile strain is increased, atheroprotective effects are improved (for 3%, 5% and 7% tensile strain magnitudes)

The increase in cell inflammatory response is speculated to be possibly correlated with cell increase in cell area. The highest cell area (resulting from the combined stenosis conditions), produced the lowest levels of PECAM phosphorylation, yet the highest levels of NF-κB activation and ICAM-1. More experiments need to be done to increase power.

Overall, a deeper understanding on EC mechanotransduction was gained, along with a delineation between normal and pathological mimicking waveforms. The normal and pathological waveforms obtained can be used in more *in vitro* studies to further investigate EC mechanotransductory responses.

5.1 Conclusions

A fluid-structure interaction (FSI) model of the left anterior descending (LAD) coronary artery was developed under physiological and pathological conditions. The model estimated the dynamic fluid shear stress and cyclic tensile strain distribution/history on the moving coronary artery wall. Patient-specific geometry, transient blood flow, blood vessel wall viscoelasticity, blood vessel cyclic bending, and myocardium contraction were incorporated into the FSI model to increase its physiological relevance. This is the first large LAD FSI simulation model (>3mm) that included the effect of myocardium contraction. The results indicated that along with LAD cyclic stretching and bending motion, myocardial contraction exerted a substantial mechanical stress/strain on the artery and had a significant effect on coronary hemodynamics/mechanics. Values estimated using this model agreed well with that reported in literature (numerical simulation or *in vivo* measurement), validating the improved physiological relevance and accuracy of the model.

A programmable shearing-stretching device that is capable of applying physiologically relevant dynamic fluid shear stress (FSS) and cyclic tensile strain (CS) simultaneously to endothelial cells (EC) was designed, fabricated, characterized and validated. The system integrated a programmable vacuum-driven strain device with a programmable cone-and-plate shearing device, to allow concurrent application of pulsatile shear stress and cyclic strain to cultured ECs. Its main advantage over previous systems was its ease of use and precise control of shear stress and strain. The device allows for equal-biaxial, uni-axial and other combinations of biaxial strain by modifying the supporting plate. By adjusting the motor speed and the cyclic vacuum pressure, this shearing-stretching device can generate various combinations of fluid shear stress and tensile strain, providing an easy solution to establish physiologically relevant mechanical environment. Stress/strain conditions generated by the device were validated experimentally, and the effectiveness of the device was evaluated through EC morphology changes under various mechanical loading conditions.

Physiological and pathological shear stress and/or tensile strain (derived from the FSI model) were applied to cultured human coronary artery endothelial cells (HCAEC), using the shearing-stretching device developed. EC morphological and functional responses to single and combined stimulation were characterized. Changes in cell morphology were evaluated by cell area and elongation. Changes in EC inflammatory responses were evaluated by characterizing EC activation, i.e., cell surface ICAM-1 expression, PECAM-1 tyrosine phosphorylation, associated mechanotransduction pathway activation, i.e. MAPK (ERK1/2) pathway and associated transcription factor NF-κB activation.

Results obtained from these experiments support our hypothesis that combined stimulation from altered shear stress and tensile strain (stenosis and recirculation conditions) can lead to significant changes in EC morphology and function, which may accelerate local inflammatory responses.

The results obtained from this study help us better understand how different mechanical stress/strain conditions interact to regulate EC function and disease initiation. New insight in EC mechanotransduction under physiological and pathological mechanical conditions help to identify factors that are responsible for EC dysfunction, and lead to preventive and therapeutic solutions for cardiovascular diseases .

5.2 Future Directions

1. More in depth studies altering fluid shear stress and tensile strain magnitudes and frequencies, resulting in more condition combinations, can help us better understand the complex interplay among mechanical forces, and possibly identify mechanical forces which dominate different inflammatory protein responses.

2. Moreover, studying the impact of an additional mechanical force – uniaxial strain, might lead us to even more physiologically relevant EC characterization due to different mechanical environments.

3. Furthermore, the development of a more discrete characterization of fluid shear stress and tensile strain will allow us to better estimate the actual shear stress and strain values ECs are undergoing. To do this, a micrometer area of the macroscopic coronary artery can be modeled. This improved FSI model would use as input the output of the FSI model developed in this dissertation. From thereon, the mesh resolution will be decreased to 10μm to approach EC size.

4. The addition of relevant cell layers, through a co-culture cells, or the addition of platelets into the shearing solution, will allow us to study EC response when together with smooth muscle cells for example, or in the presence of platelets. Both situations will further improve the physiological relevance for experimentation. Recent lab data shows platelet modulate endothelial cell response to EC activation[180], so it would be interesting to see how platelets modulate this response, in a more physiologically relevant mechanical environment.

Supplementary Information

Device characterization using vacuum controller

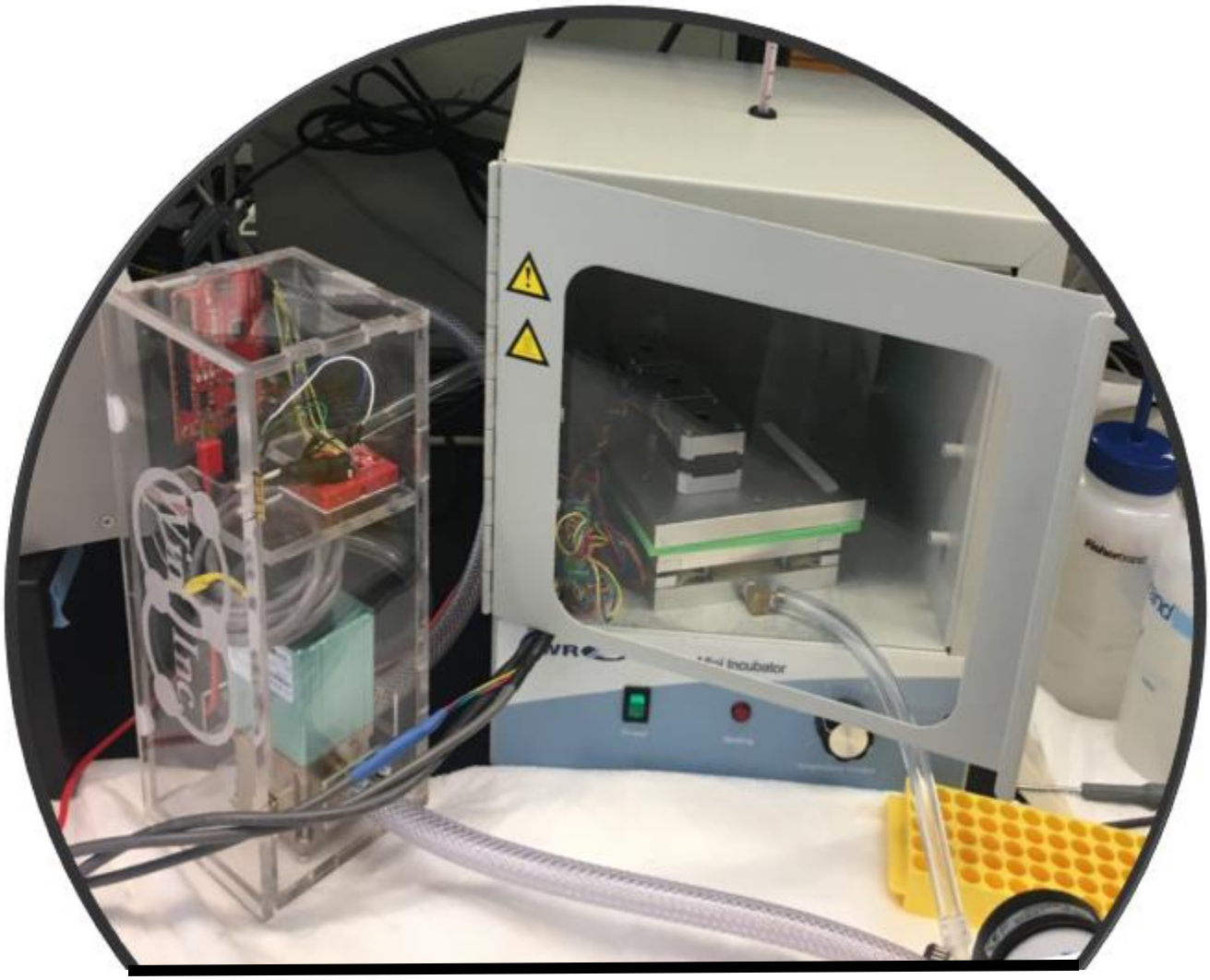

Figure 33. Shearing-stretching device setup using a vacuum controller instead of the piston pump from Chapter 3 to regulate vacuum pressures.

An Ashcroft pressure gauge, code # 25D1005PS02L60# - BL was used to measure vacuum output by pressure controller. The average strain or deformation applied to the Flexcell elastic membrane was

computed by tracking marker motion on the elastic membrane through a MATLAB code attached in the section below.

The average strain produced at different vacuum pressures was calculated and recorded. The calibration **Figure 34** shows the linear relationship between voltage and strain produced using the vacuum controller. The vacuum controller was regulated through an Arduino. The Arduino code input used for strain was a square wave (attached below), and the output, due to the delay in response time, imposed in the elastic membrane was a sinusoidal wave.

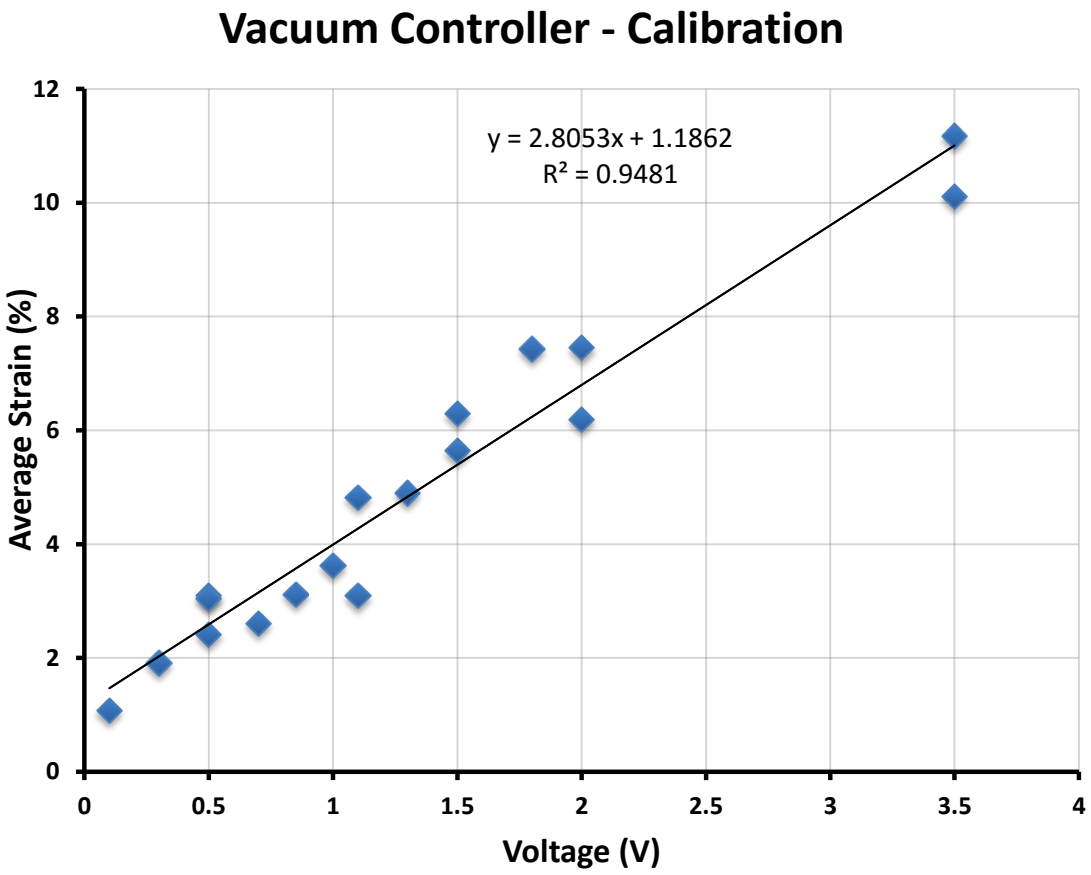

Figure 34. Vacuum controller calibration depicting a linear relationship between input voltage and average elastic membrane strain produced.

Code for Marker Tracking

Once a video has been recorded of the elastic membrane (with the markers) in motion, processing follows:

1. Convert video file into the desired frame/second. The higher the frame/second, the better the time resolution you would have as output.

   An open source algorithm was used for this purpose[168]:

```
function imgs = getVideoFrames(vid, startt, endt, step, savetodir)
% extracts frames from a video and saves them as image files in a given folder.
%
% create: 5/9/2014 (earliest known)
% modified: 12/10/2014 [fix a bug for output directory]
% author(s): Dongxi Zheng
%
% description:
%   This function generates a series of images corresponding to specified
%   frames of a given video file. Users can specify the time in second of
%   the starting frame and the time in second of the ending frame as well
%   as the time lap in second between two successive frames. Users can also
%   specify in which folder to store these images.
%
%   inputs:
%   vid - a VideoReader object or a path to a video file
%   from - the starting second of the extracted frames (default 0)
%   to - the ending second of the extracted frames (default end time of video)
%   step - the interval in seconds between frames (default 5)
%   savetodir - (optional) the output directory (default a
%               "tmp-extracted-frames" subfolder of the video file's
%               directory or of the current execution directory)
% outputs:
%   imgs - heigth X width X colors X frames arrays representing the
%          extracted frames.

    % limit input from 0 to 5 arguments
    narginchk(0, 5);

    % constants for default values
    DEFAULTSTARTT = 0; % default start time = 1 seconds
    DEFAULTSTEP = 5; % default step = 5 seconds
    MINSTEP = 10^(-9); % minimum step = 1 nanosecond
    DEFAUTOUTDIRNAME = 'tmp-extracted-frames'; % default output dir name
```

```
% read the video file and its properties
if nargin < 1
    [fn, fp, ~] = ...
        uigetfile('*','Please choose the video file to be processed.');
    vid = [fp, fn];
end
if isa(vid, 'VideoReader')
    vidObj = vid;
else
    vidObj = VideoReader(vid);
end
frameRate = vidObj.FrameRate;
duration = vidObj.Duration;
% nFrames = vidObj.NumberOfFrames;
[nrow, ncol, nclr] = size(read(vidObj, 1));
% vidHeight = xyloObj.Height;
% vidWidth = xyloObj.Width;

% set default values to the rest arguments when no specified
% set default start frame time
if nargin < 2
    startt = DEFAULTSTARTT;
    userinput = input(['Type in the time in seconds of the starting ', ...
                       'frame, \nor simply enter to accept ', ...
                       'default (', num2str(startt), ' seconds): '],'s');
    tmpstartt = str2double(userinput);
    if (~isnan(tmpstartt))
        startt = min(max(0,tmpstartt),duration);
    end
end
% set default end frame time
if nargin < 3
    endt = duration;
    userinput = input(['Type in the time in seconds of the stopping', ...
                       'frame, \nor simply enter to accept ', ...
                       'default (', num2str(endt), ' seconds): '],'s');
    tmpendt = str2double(userinput);
    if (~isnan(tmpendt))
        endt = min(max(startt,tmpendt),duration);
    end
end
% set default frame interval (step)
if nargin < 4
    step = DEFAULTSTEP;
    userinput = input(['Type in the time in seconds between two ', ...
                       'extracted frames, \nor simply enter to accept ', ...
                       'default (', num2str(step), ' seconds): '],'s');
    tmpstep = str2double(userinput);
    if (~isnan(tmpstep))
        step = min(max(MINSTEP,tmpstep),endt-startt);
    end
end
% set default savetodir value
if nargin < 5
    videopath = './';
    if (isa(vid, 'char'))
        [videopath,~,~] = fileparts(vid);
    end
```

```
        savetodir = fullfile(videopath,DEFAUTOUTDIRNAME);
        userinput = input(['Do you want to set the output directory?\n', ...
                           '(The default is: "', strrep(savetodir,'\','/'), ...
                           '")\n', '(y/n): '],'s');
        if strcmp(userinput, 'y')
            savetodir = uigetdir;
        end
    end

    % calculate the start and end frame indices and the number of frames to
    % skip each time
    startF = round(frameRate*startt)+1;
    endF = round(frameRate*endt);
    stepF = round(frameRate*step)+1;
    disp(['Extracting frames from ',vidObj.Name]);
    disp(['starting at frame no.', num2str(startF), ...
          ' (at second ', num2str(startt), '),']);
    disp(['stopping at frame no.', num2str(endF), ...
          ' (at second ', num2str(endt), '),']);
    disp(['and by every other ', num2str(stepF), ' frames (', ...
          num2str(step), ' seconds).']);
    disp(['Output folder: "', savetodir, '"']);

    % allocate the memory for storing the frames
    imgs = uint8(zeros(nrow, ncol, nclr, floor((endF-startF)/stepF)+1));

    % read one frame at a time.
    count = 0;
    for k = startF:stepF:endF
        count = count+1;
        imgs(:,:,:,count) = read(vidObj, k);
    end

    % write images to files
    if exist('savetodir','var')
        if (~exist(savetodir,'dir'))
            mkdir(savetodir);
        end
        count = 0;
        padding = power(10,size(num2str(max(startF, endF)),2));
        for k = startF:stepF:endF
            count = count+1;
            padded_k = num2str(padding+k);
            img = imgs(:,:,:,count);
            imwrite(img, [savetodir,'\frame',padded_k(2:end),'.jpg'], 'JPG');
        end
    end
end
```

2. Find the markers in one frame. To do that, first convert the frames to grayscale, then threshold the image to only see the markers. To set the threshold, the code utilizes an open-source code which needs to be attached to file for it to run [169].

Threshold code:

```
function [level,bw] = thresh_tool(im,cmap,defaultLevel) %mainfunction
%THRESH_TOOL  Interactively select intensity level for image thresholding.
%   THRESH_TOOL launches a GUI (graphical user interface) for thresholding
%   an intensity input image, IM. IM is displayed in the top left corner. A
%   colorbar and IM's histogram are displayed on the bottom. A line on the
%   histogram indicates the current threshold level. A binary image is
%   displayed in the top right based on the selected level.  To change the
%   level, click and drag the line. The output image updates automatically.
%
%   There are two ways to use this tool.
%
%Mode 1 - nonblocking behavior:
%   THRESH_TOOL(IM) launches GUI tool.  You can continue using the MATLAB
%   Desktop.  Since no results are needed, the function does not block
%   execution of other commands.
%
%   THRESH_TOOL(IM,CMAP) allows the user to specify the colormap, CMAP.  If
%   not specified, the default colormap is used.
%
%   THRESH_TOOL(IM,CMAP,DEFAULTLEVEL) allows the user to specify the
%   default threshold level. If not specified, DEFAULTLEVEL is determined
%   by GRAYTHRESH. Valid values for DEFAULTLEVEL must be consistent with
%   the data type of IM for integer intensity images: uint8 [0,255], uint16
%   [0,65535], int16 [-32768,32767].
%
%   Example
%       x = imread('rice.png');
%       thresh_tool(x)          %no return value, so MATLAB keeps running
%
%Mode 2 - blocking behavior:
%   LEVEL = THRESH_TOOL(...) returns the user selected level, LEVEL, and
%   MATLAB waits for the result before proceeding.  This blocking behavior
%   mode allows the tool to be inserted into an image processing algorithm
%   to support an automated workflow.
%
%   [LEVEL,BW] = THRESH_TOOL(...) also returns the thresholded binary
%   output image, BW.
%
%   Example
%       x = imread('rice.png');
%       lev = thresh_tool(x)    %MATLAB waits for GUI tool to finish
%
%See also COLORMAP, GRAYTHRESH, IM2BW.

%defensive programming
error(nargchk(1,3,nargin))
error(nargoutchk(0,2,nargout))
```

```
%validate defaultLevel within range
if nargin>2 %uer specified DEFAULTLEVEL
  dataType = class(im);
  switch dataType
    case 'uint8','uint16','int16'
      if defaultLevel<intmin(dataType) | defaultLevel>intmax(dataType)
        error(['Specified DEFAULTLEVEL outside class range for ' dataType])
      elseif defaultLevel<min(im(:)) | defaultLevel>max(im(:))
        error('Specified DEFAULTLEVEL outside data range for IM')
      end
    case 'double','single'
      %okay, do nothing
    otherwise
      error(['Unsupport image type ' dataType])
  end %switch
end

max_colors=1000;    %practical limit

%calculate bins centers
color_range = double(limits(im));
if isa(im,'uint8') %special case [0 255]
  color_range = [0 255];
  num_colors = 256;
  di = 1;
elseif isinteger(im)
  %try direct indices first
  num_colors = diff(color_range)+1;
  if num_colors<max_colors %okay
    di = 1;                                 %inherent bins
  else %too many levels
    num_colors = max_colors;                %practical limit
    di = diff(color_range)/(num_colors-1);
  end
else %noninteger
  %try infering discrete resolution first (intensities often quantized)
  di = min(diff(sort(unique(im(:)))));
  num_colors = round(diff(color_range)/di)+1;
  if num_colors>max_colors %too many levels
    num_colors = max_colors;                %practical limit
    di = diff(color_range)/(num_colors-1);
  end
end
bin_ctrs = [color_range(1):di:color_range(2)];
FmtSpec = ['%.' num2str(ceil(-log10(di))) 'f'];

%new figure - interactive GUI tool for level segmenting
h_fig = figure;
set(h_fig,'ToolBar','Figure')
if nargin>1 && isstr(cmap) && strmatch(lower(cmap),'gray')
  full_map = gray(num_colors);
elseif nargin>1 && isnumeric(cmap) && length(size(cmap))==2 && size(cmap,2)==3
  full_map = cmap;
else
  full_map = jet(num_colors);
end
setappdata(h_fig,'im',im)
setappdata(h_fig,'FmtSpec',FmtSpec)
```

```
%top left - input image
h_ax1 = axes('unit','norm','pos',[0.05 0.35 0.4 0.60]);
rgb = im2rgb(im,full_map);
  function rgb = im2rgb(im,full_map); %nested
    %coerce intensities into gray range [0,1]
    gray = imadjust(im,[],[0 1]);
    %generate indexed image
    num_colors = size(full_map,1);
    ind = gray2ind(gray,num_colors);
    %convert indexed image to RGB
    rgb = ind2rgb(ind,full_map);
  end %im2rgb

image(rgb), axis image
%subimage(im,full_map)
axis off, title('Input Image')

%top right - segmented (eventually)
h_ax2 = axes('unit','norm','pos',[0.55 0.35 0.4 0.60]);
axis off
setappdata(h_fig,'h_ax2',h_ax2)

%next to bottom - intensity distribution
h_hist = axes('unit','norm','pos',[0.05 0.1 0.9 0.2]);
n = hist(double(im(:)),bin_ctrs);
bar(bin_ctrs,n)
axis([color_range limits(n(2:end-1))]) %ignore saturated end scaling
set(h_hist,'xtick',[],'ytick',[])
title('Intensity Distribution')

%very bottom - colorbar
h_cbar = axes('unit','norm','pos',[0.05 0.05 0.9 0.05],'tag','thresh_tool_cbar');
subimage(color_range,[0.5 1.5],1:num_colors,full_map)
set(h_cbar,'ytick',[],'xlim',color_range)
axis normal

v=version;
if str2num(v(1:3))>=7
  %link top axes (pan & zoom)
  linkaxes([h_ax1 h_ax2])
  %link bottom axes (X only - pan & zoom)
  linkaxes([h_hist h_cbar],'x')
end

%colorbar tick locations
set(h_cbar,'xtick',color_range)

%threshold level - initial guess (graythresh)
if nargin>2 %user specified default level
  my_level = defaultLevel;
else %graythresh default
  lo = double(color_range(1));
  hi = double(color_range(2));
  norm_im = (double(im)-lo)/(hi-lo);
  norm_level = graythresh(norm_im); %GRAYTHRESH assumes DOUBLE range [0,1]
  my_level = norm_level*(hi-lo)+lo;
end
```

```
%display level as vertical line
axes(h_hist)
h_lev = vline(my_level,'-');
set(h_lev,'LineWidth',2,'color',0.5*[1 1 1],'UserData',my_level)
setappdata(h_fig,'h_lev',h_lev)

%attach draggable behavior for user to change level
move_vline(h_lev,@update_plot);

axes(h_cbar)
y_lim = get(h_cbar,'ylim');

% PLACE TEXT LOCATION ON COLORBAR (Laurens)
%h_text = text(my_level,mean(y_lim),num2str(round(my_level)));
h_text = text(my_level,mean(y_lim),'dummy','HorizontalAlignment','Center');
if nargin<2
  text_color = 0.5*[1 1 1];
else
  text_color = 'm';
end
set(h_text,'FontWeight','Bold','color',text_color,'Tag','cbar_text')
movex_text(h_text,my_level)
%%%%%%%%%%%%%%%%%%%%%%%%

%segmented image
bw = im>my_level;
axes(h_ax2)
hold on
subimage(bw), axis off, axis ij
hold off
title('Segmented')

update_plot

%add reset button (resort to initial guess)
h_reset = uicontrol('unit','norm','pos',[0.0 0.95 .1 .05]);
set(h_reset,'string','Reset','callback',@ResetOriginalLevel)

if nargout>0 %return result(s)
  h_done = uicontrol('unit','norm','pos',[0.9 0.95 0.1 0.05]);
  set(h_done,'string','Done','callback','delete(gcbo)') %better
  %inspect(h_fig)
  set(h_fig,'WindowStyle','modal')
  waitfor(h_done)
  if ishandle(h_fig)
    h_lev = getappdata(gcf,'h_lev');
    level = mean(get(h_lev,'xdata'));
    if nargout>1
      h_im2 = findobj(h_ax2,'type','image');
      bw = logical(rgb2gray(get(h_im2,'cdata')));
    end
    delete(h_fig)
  else
    warning('THRESHTOOL:UserAborted','User Aborted - no return value')
    level = [];
  end
end
```

```
end %thresh_tool (mainfunction)


function ResetOriginalLevel(hObject,varargin) %subfunction
h_lev = getappdata(gcf,'h_lev');
init_level = get(h_lev,'UserData');
set(h_lev,'XData',init_level*[1 1])
text_obj = findobj('Type','Text','Tag','cbar_text');
movex_text(text_obj,init_level)
update_plot
end %ResetOriginalLevel (subfunction)


function update_plot %subfunction
im = getappdata(gcf,'im');
h_lev = getappdata(gcf,'h_lev');
my_level = mean(get(h_lev,'xdata'));
h_ax2 = getappdata(gcf,'h_ax2');
h_im2 = findobj(h_ax2,'type','image');
%segmented image
bw = (im>my_level);
rgb_version = repmat(double(bw),[1 1 3]);
set(h_im2,'cdata',rgb_version)
end %update_plot (subfunction)


%function rgbsubimage(im,map), error('DISABLED')


%--------------------------------------------------------------------
function move_vline(handle,DoneFcn) %subfunction
%MOVE_VLINE implements horizontal movement of line.
%
%  Example:
%    plot(sin(0:0.1:pi))
%    h=vline(1);
%    move_vline(h)
%
%Note: This tools strictly requires MOVEX_TEXT, and isn't much good
%      without VLINE by Brandon Kuczenski, available at MATLAB Central.
%<http://www.mathworks.com/matlabcentral/fileexchange/loadFile.do?objectId=1039&obj
ectType=file>

% This seems to lock the axes position
set(gcf,'Nextplot','Replace')
set(gcf,'DoubleBuffer','on')

h_ax=get(handle,'parent');
h_fig=get(h_ax,'parent');
setappdata(h_fig,'h_vline',handle)
if nargin<2, DoneFcn=[]; end
setappdata(h_fig,'DoneFcn',DoneFcn)
set(handle,'ButtonDownFcn',@DownFcn)

  function DownFcn(hObject,eventdata,varargin) %Nested--%
    set(gcf,'WindowButtonMotionFcn',@MoveFcn)           %
```

```
    set(gcf,'WindowButtonUpFcn',@UpFcn)                  %
  end %DownFcn-----------------------------------------%

  function UpFcn(hObject,eventdata,varargin) %Nested----%
    set(gcf,'WindowButtonMotionFcn',[])                  %
    DoneFcn=getappdata(hObject,'DoneFcn');               %
    if isstr(DoneFcn)                                    %
      eval(DoneFcn)                                      %
    elseif isa(DoneFcn,'function_handle')                %
      feval(DoneFcn)                                     %
    end                                                  %
  end %UpFcn-------------------------------------------%

  function MoveFcn(hObject,eventdata,varargin) %Nested------%
    h_vline=getappdata(hObject,'h_vline');                 %
    h_ax=get(h_vline,'parent');                            %
    cp = get(h_ax,'CurrentPoint');                         %
    xpos = cp(1);                                          %
    x_range=get(h_ax,'xlim');                              %
    if xpos<x_range(1), xpos=x_range(1); end               %
    if xpos>x_range(2), xpos=x_range(2); end               %
    XData = get(h_vline,'XData');                          %
    XData(:)=xpos;                                         %
    set(h_vline,'xdata',XData)                             %
    %update text                                           %
    text_obj = findobj('Type','Text','Tag','cbar_text');   %
    movex_text(text_obj,xpos)                              %
  end %MoveFcn-----------------------------------------%

end %move_vline(subfunction)


%--------------------------------------------------------------------------
function [x,y] = limits(a) %subfunction
% LIMITS returns min & max values of matrix; else scalar value.
%
%   [lo,hi]=LIMITS(a) returns LOw and HIgh values respectively.
%
%   lim=LIMITS(a) returns 1x2 result, where lim = [lo hi] values

if nargin~=1 | nargout>2 %bogus syntax
  error('usage: [lo,hi]=limits(a)')
end

siz=size(a);

if prod(siz)==1 %scalar
  result=a;                         % value
else %matrix
  result=[min(a(:)) max(a(:))];     % limits
end

if nargout==1 %composite result
  x=result;                         % 1x2 vector
elseif nargout==2 %separate results
  x=result(1);                      % two scalars
  y=result(2);
else %no result
```

```
  ans=result                          % display answer
end

end %limits (subfunction)


%-----------------------------------------------------------------------
function movex_text(h_txt,x_pos) %subfunction
FmtSpec=getappdata(get(get(h_txt,'parent'),'parent'),'FmtSpec');
msg=sprintf(FmtSpec,x_pos);
pos=get(h_txt,'position');
pos(1)=x_pos;
set(h_txt,'Position',pos,'String',msg)
end %movex_text


%-------------------------------------------------------------------------------
----------------------------
function hhh=vline(x,in1,in2) %subfunction
% function h=vline(x, linetype, label)
%
% Draws a vertical line on the current axes at the location specified by 'x'.
Optional arguments are
% 'linetype' (default is 'r:') and 'label', which applies a text label to the graph
near the line.  The
% label appears in the same color as the line.
%
% The line is held on the current axes, and after plotting the line, the function
returns the axes to
% its prior hold state.
%
% The HandleVisibility property of the line object is set to "off", so not only
does it not appear on
% legends, but it is not findable by using findobj.  Specifying an output argument
causes the function to
% return a handle to the line, so it can be manipulated or deleted.  Also, the
HandleVisibility can be
% overridden by setting the root's ShowHiddenHandles property to on.
%
% h = vline(42,'g','The Answer')
%
% returns a handle to a green vertical line on the current axes at x=42, and
creates a text object on
% the current axes, close to the line, which reads "The Answer".
%
% vline also supports vector inputs to draw multiple lines at once.  For example,
%
% vline([4 8 12],{'g','r','b'},{'l1','lab2','LABELC'})
%
% draws three lines with the appropriate labels and colors.
%
% By Brandon Kuczenski for Kensington Labs.
% brandon_kuczenski@kensingtonlabs.com
% 8 November 2001

% Downloaded 8/7/03 from MATLAB Central
%
http://www.mathworks.com/matlabcentral/fileexchange/loadFile.do?objectId=1039&objec
tType=file
```

```
if length(x)>1  % vector input
    for I=1:length(x)
        switch nargin
        case 1
            linetype='r:';
            label='';
        case 2
            if ~iscell(in1)
                in1={in1};
            end
            if I>length(in1)
                linetype=in1{end};
            else
                linetype=in1{I};
            end
            label='';
        case 3
            if ~iscell(in1)
                in1={in1};
            end
            if ~iscell(in2)
                in2={in2};
            end
            if I>length(in1)
                linetype=in1{end};
            else
                linetype=in1{I};
            end
            if I>length(in2)
                label=in2{end};
            else
                label=in2{I};
            end
        end
        h(I)=vline(x(I),linetype,label);
    end
else
    switch nargin
    case 1
        linetype='r:';
        label='';
    case 2
        linetype=in1;
        label='';
    case 3
        linetype=in1;
        label=in2;
    end




    g=ishold(gca);
    hold on

    y=get(gca,'ylim');
    h=plot([x x],y,linetype);
    if length(label)
```

```
        xx=get(gca,'xlim');
        xrange=xx(2)-xx(1);
        xunit=(x-xx(1))/xrange;
        if xunit<0.8
            text(x+0.01*xrange,y(1)+0.1*(y(2)-y(1)),label,'color',get(h,'color'))
        else
            text(x-.05*xrange,y(1)+0.1*(y(2)-y(1)),label,'color',get(h,'color'))
        end
    end

    if g==0
    hold off
    end
    set(h,'tag','vline','handlevisibility','off')
end % else

if nargout
    hhh=h;
end

end %vline (subfunction)
```

Actual step code:

```
%readimages%converttotiff%converttograyscale%cropdesireare%threshold/convertobw%
in_dir = 'C:\Users\Student\Documents\Lab 2014\Matlab Codes\images2\images\images';
out_dir = 'C:\Users\Student\Documents\Lab 2014\Matlab Codes\images2\images\images';


for px = 1: 1; %change this number second time, do first time with one only

      fname = sprintf('frame (%d).jpg', px);  %reads jpg, can modify%change name of
file here accordingly %d is for numbr, the other is read as string
      fname2 = sprintf('thresholdedandcroppedframe44%d.tiff', px);

    %read file
I = imread(fullfile(out_dir, fname));
    %rgb to grayscale
    out_image = rgb2gray(I);
    %crop image
    imshow(out_image);
h = imrect(gca, [50 50 900 900]);
setResizable(h,0)
position = wait(h);
I_cropped = imcrop(out_image,position);
figure();
imshow(I_cropped);
    [I_cropped rect] = imcrop(out_image);
    %threshold image
    level=thresh_tool(I_cropped);
    level2= level/255;
    %apply threshold to image
    BW=im2bw(I_cropped,level2);
    BW2=imcomplement(BW)
    BW3=bwareaopen(BW,30); %this can be changed
    %save image
    imwrite(BW3, fullfile(out_dir, fname2));
     L=bwlabel(BW3);
     STATS = regionprops(L,
'Centroid','MajorAxisLength','MinorAxisLength','Orientation','PixelIdxList');
   centroids = cat(1, STATS.Centroid);
   imshow(BW3)
   hold on
   plot(centroids(:,1), centroids(:,2), 'b*')
   hold off
end
% First, make an image with a light gray background instead
% of a black background, so that the numbers will be visible
% on top of it.
I3 = im2uint8(BW3);
I3(~BW3) = 100;
I3(BW3) = 240;
imshow(I3, 'InitialMagnification', 'fit')

% Now plot the number of each sorted object at the corresponding
% centroid:
```

```
hold on
for k = 1:numel(STATS)
   centroid = STATS(k).Centroid;
   text(centroid(1), centroid(2), sprintf('%d', k));
end
hold off
```

3. Once the threshold has been set, run the program through all the frames available. The program stores the centroid information for each marker over all the frames.

```
%readimages%converttotiff%converttograyscale%cropdesireare%threshold/convertobw%
in_dir = 'C:\Users\Student\Documents\Lab 2014\Matlab Codes\images2\images\images';
out_dir = 'C:\Users\Student\Documents\Lab 2014\Matlab Codes\images2\images\images';

M= zeros (1300,1300); %prealloction

for px = 1: 540; %change this number second time, do first time with one only

      fname = sprintf('frame (%d).jpg', px);  %reads jpg, can modify%change name of
file here accordingly %d is for numbr, the other is read as string
      fname2 = sprintf('thresholdedandcroppedframe44%d.tiff', px);
    %read file
I = imread(fullfile(out_dir, fname));
    %rgb to grayscale
    out_image = rgb2gray(I);
    %crop image
    I_cropped2 = imcrop(out_image, rect);
    %apply threshold to image
    BW=im2bw(I_cropped2,level2);
    BW2=imcomplement(BW)
    BW3=bwareaopen(BW2,30); %this can be changed
    %save image
    imwrite(BW3, fullfile(out_dir, fname2));

     L=bwlabel(BW3);
     s = regionprops(L, 'Centroid');
     STATS = regionprops(L,'centroid');
     STATS2 = struct2cell(STATS);
     STATS3 = cell2mat(STATS2)
     size(M)
size(STATS3)
size(px)
M(px,1:size(STATS3,2)) = STATS3;
%M (px,:)= STATS3;
end
```

```
fname3=sprintf('centroid_distances 0.2 atm.xls');  %change this
%xlswrite(fname3, M);
xlswrite(fullfile(out_dir,fname3), M);

%works for plotting
%figure;
%for ii = 1:2
 % subplot(1,2,ii)
  %hold on
  %plot(M(:,ii));
  %caption = sprintf('This is plot #%d', ii);
%title(caption, 'FontSize', 12);
%end
```

MATLAB codes for morphology characterization

Cell Elongation

Cell elongation was quantified through the Nikon Image Analysis Software, where a user would draw an ellipse around 4 cells/image. The software would then measure the ratio of long/short axis.

Nucleus Elongation

1. Code opens the image, converts it to grayscale, then user manually thresholds it and selects various nuclei. Program then ouputs nuclei area, orientation, and major/minor axis length (elongation)

```
%readimages%converttotiff%converttograyscale%cropdesireare%threshold/convertobw%
in_dir = 'C:\Users\Daphne\Documents\Lab 2014\Fluorescence Images PECAM, VECAD,
phalloidin, CD41\10-06-14-Flexcell stretch and shear\dapi fixed';
out_dir = 'C:\Users\Daphne\Documents\Lab 2014\Fluorescence Images PECAM, VECAD,
phalloidin, CD41\10-06-14-Flexcell stretch and shear\dapi fixed';

%M= zeros (20,20)
for px = 1: 1; %change this number second time, do first time with one only

      fname = sprintf('10_06_14_30085.jpg', px);  %reads jpg, can modify%change
name of file here accordingly %d is for numbr, the other is read as string
      fname2 = sprintf('thresholdedandcroppedframe%d.tiff', px);
    %read file
I = imread(fullfile(out_dir, fname));
    %rgb to grayscale
    out_image = rgb2gray(I);
    %crop image
    imshow(out_image);
h = imrect(gca, [75 68 2000 2000]);
setResizable(h,0)
position = wait(h);
I_cropped = imcrop(out_image,position);
figure();
imshow(I_cropped);
    %[I_cropped rect] = imcrop(out_image);
    %threshold image
    level=thresh_tool(I_cropped);
    level2= level/255;
    %apply threshold to image
    BW=im2bw(I_cropped,level2);
```

```
    %BW2=imcomplement(BW)
    BW3=bwareaopen(BW,30); %this can be changed
    %save image
    imwrite(BW3, fullfile(out_dir, fname2));
     L=bwlabel(BW3);
     D=bwselect(L);
     STATS = regionprops(D,
'Centroid','MajorAxisLength','MinorAxisLength','Orientation','PixelIdxList');

   centroids = cat(1, STATS.Centroid);
   imshow(BW3)
   hold on
   plot(centroids(:,1), centroids(:,2), 'b*')
   hold off

end
% First, make an image with a light gray background instead
% of a black background, so that the numbers will be visible
% on top of it.
I3 = im2uint8(BW3);
I3(~BW3) = 100;
I3(BW3) = 240;
imshow(I3, 'InitialMagnification', 'fit')

% Now plot the number of each sorted object at the corresponding
% centroid:


hold on
for k = 1:numel(STATS)
   centroid = STATS(k).Centroid;
   text(centroid(1), centroid(2), sprintf('%d', k));
end
hold off
```

Cell Junctional Actin Accumulation

1. Read images, convert to grayscale, and draw multiple lines **from the inside to the outside of the cell** (direction is important, over the junctional actin accumulation)

```
%readimages%converttotiff%converttograyscale%

clear('all');

in_dir = 'E:\Lab 2014\Fluorescence Images\Flexcell\091914 - Flexcell\Actin';

in_dir_points = 'E:\Lab 2014\Fluorescence Images\Flexcell\091914 -
Flexcell\Actin_points';

all_file_names = dir(in_dir_points);
```

```
in_dir = 'E:\Lab 2014\Fluorescence Images\Flexcell\091914 - Flexcell\Actin';

out_dir = 'E:\Lab 2014\Fluorescence Images\Flexcell\091914 - Flexcell\Actin';

results_name = 'E:\Lab 2014\Fluorescence Images\Flexcell\091914 -
Flexcell\output.txt';

diary off

diary(results_name);

diary on

%for px = 1: 1; %change this number second time, do first time with one only

points_ignored = 0;

for index = 1:size(all_file_names,1),

  if all_file_names(index).isdir

    continue;

  end

  current_name = all_file_names(index).name;

 fname = sprintf(current_name);  %reads jpg, can modify%change name of file here
accordingly %d is for numbr, the other is read as string


  %read file

  I = imread(fullfile(out_dir, fname));

  out_image = rgb2gray(I);

  %read los puntos

points = csvread (fullfile(in_dir_points, fname));


  average = 0;

  p_points = 0;

  for index_point = 1:size(points,1)


    temp = points(index_point,:);

    xf = temp(1);

    yf = temp(2);

    xi = temp(3);

    yi = temp(4);


    n = max(abs(yf - yi), abs(xf - xi));

    dx = (xf - xi) / n;
```

```
dy = (yf - yi) / n;

vx = xi:dx:xf;
vy = yi:dy:yf;

if xi == xf,
  vx = ones(size(vy)) * xi;
end
if yi == yf,
  vy = ones(size(vx)) * yi;
end



data_profile=improfile (out_image,vx,vy);
%plot(data_profile)
%[xi, yi, xf, yf]
%pause
% size(data_profile)
% data_profile (1:5,1)
%hist(data_profile);

[maximum, index_max] = max (data_profile);

m= mean (data_profile);
sd= std (data_profile);

i = find(data_profile <(m+0*sd));
i_final = i(i > index_max);

% index_max
% m+0*sd
minimum = mean (data_profile (i_final));
```

```
    ratio = maximum / minimum;
    %[xf, yf, xi, yi]
    %plot(data_profile)
    %pause

    if isnan(ratio),
      index;
      points_ignored = points_ignored + 1;
      continue
      m
      index_max
      i_final

      size(i_final)

    end
    average = average + ratio;
    p_points = p_points + 1;

  end

  average =  average / p_points;
  if isnan(average)
    p_points
    pause
  end
  %disp(sprintf('For filename %s, line #  %d: %f', current_name, p_points,
average));
  disp(sprintf('%s\t%d\t%f', current_name, p_points, average));
  %points



  % imwrite(BW3, fullfile(out_dir, fname2));


end
```

```
%       L=bwlabel(BW3);

%       s = regionprops(L, 'Centroid');

%       STATS = regionprops(L,'Centroid') ;


% end


diary off
```

2. Archive all data

```
clear('all');

in_dir = 'C:\Users\Student\Documents\Lab 2014\Fluorescence Images\Flexcell\091914 -
Flexcell\Actin';

in_dir_points = 'C:\Users\Student\Documents\Lab 2014\Fluorescence
Images\Flexcell\091914 - Flexcell\Actin_points';
```

```
in_dir_figures = 'C:\Users\Student\Documents\Lab 2014\Fluorescence
Images\Flexcell\091914 - Flexcell\Actin_figures';


all_file_names = dir(in_dir);




in_dir = 'C:\Users\Student\Documents\Lab 2014\Fluorescence Images\Flexcell\091914 -
Flexcell\Actin';

out_dir = 'C:\Users\Student\Documents\Lab 2014\Fluorescence Images\Flexcell\091914 -
Flexcell\Actin';


%for px = 1: 1; %change this number second time, do first time with one only


for index = 1:size(all_file_names,1),

  if all_file_names(index).isdir

    continue;

  end


  fname = all_file_names(index).name


  if exist(fullfile(in_dir_figures, fname), 'file') == 2,

    continue

  end


  %read file

  I = imread(fullfile(out_dir, fname));


  cursor_info = zeros(1,1);


  h = figure;

  imshow(I);

  pause;


  saveas(h,fullfile(in_dir_figures, fname));

  close(h);
```

```
  n_points = size(cursor_info,2)
  if n_points <= 1,
    continue
  end
  points = zeros(n_points/2,4);
  index_point = 1;
  for j = 1: n_points,
    if mod(j,2) == 1,
      points(index_point,1:2) = cursor_info (j).Position;
    else
      points(index_point,3:4) = cursor_info (j).Position;
      index_point = index_point + 1;
    end
  end
  csvwrite(fullfile(in_dir_points, fname),points);
end
```

EC-platelet interaction manuscript

Thrombosis Research 150 (2017) 44–50

Contents lists available at ScienceDirect

Thrombosis Research

journal homepage: www.elsevier.com/locate/thromres

Full Length Article

Platelets modulate endothelial cell response to dynamic shear stress through PECAM-1

Daphne Meza [a], Saravan K. Shanmugavelayudam [b], Arielys Mendoza [a], Coralys Sanchez [a], David A. Rubenstein [a], Wei Yin [a,b,*]

[a] Department of Biomedical Engineering, Stony Brook University, Stony Brook, NY 11794, United States
[b] School of Mechanical and Aerospace Engineering, Oklahoma State University, Stillwater, OK 74074, United States

GPIIb/IIIa [16]. Proteins that are essential for platelet adhesion include P-selectin, von Willebrand factor (vWF), and ICAM-1. P-selectin mediates platelet rolling on EC [17], vWF is required for platelet adhesion through GPIbα, and ICAM-1 has been reported to mediate GPIIb/IIIa-dependent bridging mechanism through fibrinogen [15]. Rosenblum et al. suggested that EC surface PECAM-1 may also contribute to platelet adhesion and aggregation at injury sites [18]. However, the role of PECAM-1 in platelet adhesion to EC has not been thoroughly investigated. We recently reported that platelet-EC interaction could greatly affect platelet activation state and platelet surface adhesion protein (GPIb and GPIIb) expression under shear flow [19]. However, how platelets affect EC responses to physiological or pathological flow remains unclear.

In the present study, human coronary artery EC were exposed to various physiologically relevant dynamic shear stress waveforms in a programmable cone and plate shearing device, in the presence of platelets. Platelet adhesion to EC monolayer was quantified, the effect of platelets on EC surface ICAM-1 expression was measured, and the role of PECAM-1 in platelet-EC interaction was evaluated.

2. Materials and methods

2.1. Endothelial cell culture

Human coronary artery endothelial cells (HCAEC) were purchased

expression, followed by an alkaline phosphatase conjugated goat anti-mouse secondary antibody (Sigma-Aldrich, St. Louis, MO). Antibody binding was detected using a P-nitrophenyl phosphate substrate (pNPP at 1 mg/mL, from Life Technologies, Carlsbad, CA) at 405 nm. Untreated EC (no shear, no platelets) were used as the negative experimental control.

EC total ICAM-1 expression was measured using Western blot. Following shear exposure (37 °C, 1 h), EC were washed and trypsinized. Collected cells were centrifuged at 1000 × *g* for 5 min. Cell pellet was then re-suspended in lysis buffer containing Triton X-100, protease inhibitors and phosphatase inhibitors (Life Technologies), and incubated at 4 °C for 1 h. After standard Western blot procedures, EC total ICAM-1 expression was analyzed using a C-digit blot scanner (LI-COR Biotechnology, Lincoln, NE). EC β-actin was used as a protein loading control.

Shear stress induced changes in ICAM-1 mRNA expression was measured using RT-PCR. Following shear exposure (60 min, 37 °C), EC were washed and collected in Trizol reagent (Invitrogen). RNA was isolated and then reverse transcribed using the cDNA synthesis kit from Quanta Biosciences (Gaithersburg, MD), following the manufacturer's instruction. The forward and reverse primers for ICAM-1 were designed using the Primer Express Software (Applied Biosystems). The forward primer for ICAM-1 was 5′-AGACAGTGACCATCTACAGCTTTCC-3′, and the reverse primer was 5′-CACCTCGGTCCCTTCTGAGA-3′. β-actin was used as the housekeeping gene control. The forward and reverse primer

serum or antibiotics. PECAM-1 siRNA was then introduced and incubated with EC monolayer for 6 h. Following transfection, EC were allowed to grow in normal culture medium for an additional 18–24 h before shear stress exposure with platelets. Western blot was performed to determine transfection efficiency in total cellular PECAM-1. The number of platelets adhered to transfected EC was quantified as described before.

2.9. Statistics

Statistical analysis of the data obtained from all experiments was carried out using ANOVA (ICAM-1 expression with or without siRNA treatment, NO release, platelet adhesion to EC, EC surface PECAM-1 expression/phosphorylation) or student's *t*-test (EC PECAM-1 expression following siRNA treatment). If significant difference ($P < 0.05$) was detected by ANOVA, Student-Newman-Keuls post-hoc test was used to conduct further comparisons between different treatment groups. All statistical analysis was conducted using Microsoft Excel or SAS 9.3.

3. Results

3.1. Endothelial cell ICAM-1 expression

EC were exposed to normal or low pulsatile shear stress in the presence or absence of platelets. Following shear exposure, EC were washed

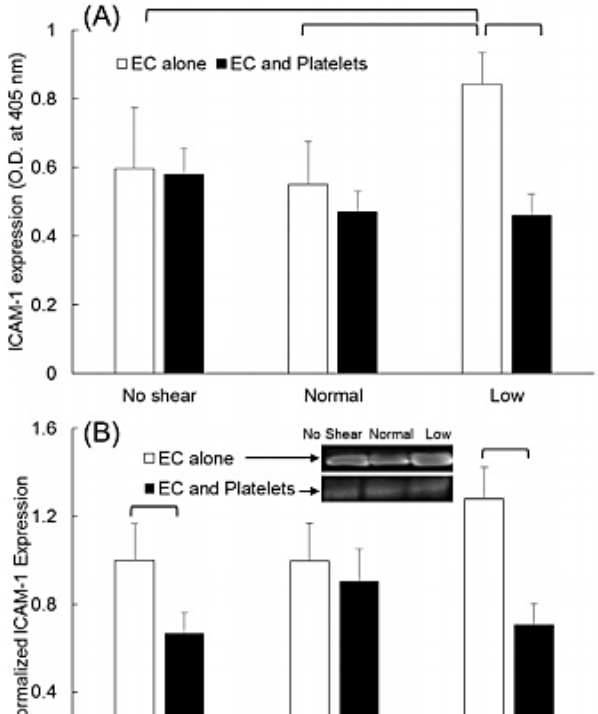

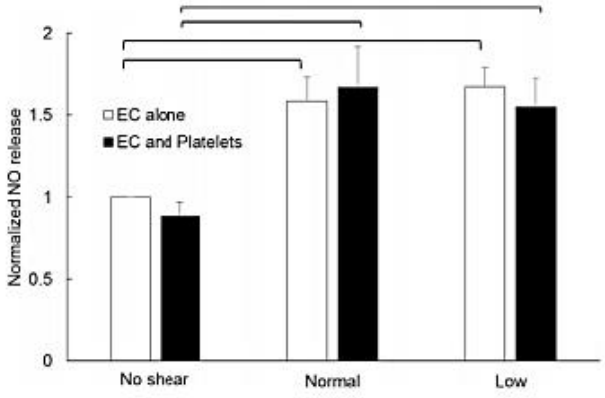

Fig. 2. Normalized NO release in EC culture medium following shear stress treatment, with or without the presence of platelets. Data is presented as mean + standard error. All significant differences ($P < 0.05$) are marked.

large number of platelets adhered to EC junctions, co-localized with highly expressed PECAM-1.

The number of platelets adhered to EC monolayer following shear stress exposure was qualified using an in-house MATLAB program (results from the program were confirmed by different individuals' counting by eyes). As shown in Table 1 (row 1), the number of adhered platelets increased significantly under low pulsatile shear stress ($P < 0.05$, n = 4, ANOVA), compared to normal pulsatile shear stress or static (no shear) conditions.

3.4. EC surface PECAM-1 expression and phosphorylation

EC surface PECAM-1 expression and PECAM-1 phosphorylation was measured using a murine monoclonal PECAM-1 antibody and a rabbit

3.5. PECAM-1 siRNA transfection

To determine if PECAM-1 mediated platelet adhesion to EC and contributed to the above observed EC responses, EC surface PECAM-1 expression was suppressed using siRNA. Results obtained from Western blot experiments indicated that siRNA transfection significantly ($P < 0.05$, student's *t*-test) reduced HCAEC PECAM-1 expression (Supplementary Fig. 1).

Following successful transfection, EC were exposed to normal or low pulsatile shear stress as described before in a cone and plate shearing device, in the presence of platelets. Platelet adhesion to EC was visualized using immunofluorescence microscopy. The numbers of platelets adhered to EC monolayers after EC were treated with a control non-specific siRNA and PECAM-1 siRNA were summarized in Table 1 (row 2 and 3). The results demonstrated that the absence of PECAM-1 affected platelet adhesion significantly ($P < 0.05$, ANOVA). When EC surface PECAM-1 was mostly diminished, shear stress-induced platelet adhesion to EC surface was significantly reduced, regardless of the shear stress magnitude ($P < 0.05$ for both normal and low shear stress, when control-siRNA- and PECAM-siRNA-treated EC were compared).

In parallel, after PECAM siRNA-transfected EC were exposed to normal and low pulsatile shear stress in the presence of platelets, EC surface ICAM-1 expression was measured using ELISA. The results (Fig. 5) demonstrated that when PECAM-1 was absent, EC did not respond to pathological low shear stress by enhancing cell surface ICAM-1 expression (i.e., cell activation), and the presence of platelets did not reduce EC surface ICAM-1 expression.

4. Discussion

Shear stress plays important roles in endothelial cell and platelet

Table 1
Number of adhered platelets to EC following shear stress exposure.

	No shear	Normal shear	Low shear
Untreated EC and platelets	187.6 ± 44.5	630.2 ± 308.7	1364.3 ± 494.9
EC were treated with nor-specific siRNA		732.0 ± 239.0	1826.8 ± 192.8
EC were treated with PECAM-1 siRNA		173.7 ± 115.8	258.3 ± 142.3
Platelets were treated with PECAM-1 antibody		53.0 ± 64.8	238.8 ± 196.2

It is well established that endothelial cells and platelets interact with each other. However, how such interaction affects each cell type's response to altered shear stress is under investigated. Recently, we reported that endothelial cells can enhance platelet sensitivity (i.e., activity, aggregation and adhesion potential, etc.) to dynamic shear stress [19]. In the present study, the effect of platelets on EC response to shear flow was investigated. The nitric oxide measurement indicated that EC NO release increased significantly following shear exposure, but was not affected by the presence of platelets (Fig. 2). These results suggested that platelets did not affect EC normal response to flow. It was rather surprising that the presence of platelets counteracted the effects of pathological low shear stress, and inhibited EC ICAM-1 expression at both protein and mRNA levels. Many proteins released from platelet α-granules and dense bodies are known to promote platelet activation, aggregation (such as ADP, platelet factor 4 and P-selectin), and EC inflammatory responses (such as CD40L) [26,27]. Only a handful of platelet-released proteins (such as α2-plasmin inhibitor, tissue factor pathway inhibitor, α1-protease inhibitor, C1-inhibitor and plasminogen activator inhibitor-1) have inhibitory functions [28]. But none of those proteins have been reported to directly regulate EC ICAM-1 expression. monolayer under shear stress decreased dramatically, and the presence of platelets did not affect EC surface ICAM-1 expression at all (Fig. 5).

It has been reported that the onset of shear stress can activate NF-κB, an important transcription factor for many inflammatory proteins including ICAM-1. However, this response is usually transient. Under physiological conditions, as EC adapt to their mechanical environment, NF-κB activation would decrease, leading to reduced EC activation. Some studies reported that EC could adapt to flow rather quickly with significant changes in NF-κB activation/deactivation occurring within 1 h [30–33], while others have shown that this process could take 15–20 h [34]. Tzima et al. demonstrated that under pathological flow/shear, PECAM-1 knockout mice failed to activate NF-κB and upregulate associated inflammatory gene expression, suggesting PECAM-1 mechanotransduction pathway was required during atherogenesis [35]. In the present study, EC were exposed to shear stress for 1 h, it is possible that platelets affected EC adaptation towards the changed shear stress environment by blocking PECAM-1, thus affecting NF-κB activation and subsequent ICAM-1 expression. To elucidate how platelets interfere with EC mechanotransduction under shear stress, and how PECAM-1 is involved, the transient activation state of NF-κB needs to be investigated.

PECAM-1 has been studied extensively as a vascular barrier and mechanotransducer [36–38], but its role in platelet-EC interaction and adhesion has not been well characterized. The well-studied GPIbα and GPIIb/IIIa are abundant on platelet surface, and our previous study has shown that the presence of platelets did not affect EC surface vWF expression under pathological low shear stress [19]. Therefore, the observed changes in platelet adhesion to EC monolayer are not likely mediated only by GPIbα, GPIIb and/or vWF. Many studies have demonstrated homophilic interactions of PECAM-1 can form between leukocytes and EC [39,40], but there is no direct evidence showing that platelets can bind to EC through homophilic interactions between plate-

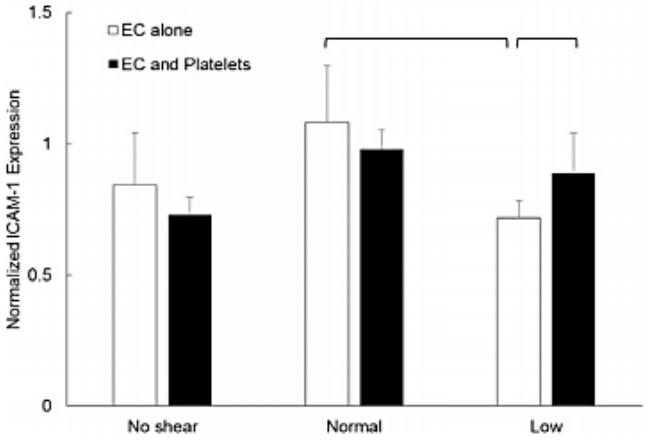

Fig. 5. Normalized ICAM-1 expression on PECAM siRNA treated HCAEC surface, measured by ELISA. The presence of platelets did not affect ICAM-1 expression. Data is presented as mean + standard error. All significant differences ($P < 0.05$) are marked.

decreased, it was still sufficient to block EC surface PECAM-1 mechanosensing and mechanotransduction, and thus inhibiting EC ICAM-1 expression; 2) through a different mechanism, platelets inhibited EC surface ICAM-1 upregulation under low shear stress, and PECAM-1 was not the major mediator. Better blocking experiments will be needed to completely block platelet adhesion to EC, to elucidate how platelet-EC physical contact affects EC activation under pathological shear stress. Antibodies against GPIb and GPIIb will be needed. However, it could be extremely challenging to completely block platelet adhesion to EC under shear stress.

Our results here demonstrated that PECAM-1 plays an important role in platelet adhesion to EC under pathological flow. Our results also indicated that EC responded to pathological low shear stress by PECAM-1 phosphorylation, but not by the amount of PECAM-1 expressed (Fig. 4). In the present study, an antibody specific to PECAM-1 tyrosine 713 phosphorylation was used to determine the activation state of EC surface PECAM-1, as tyrosine 713 phosphorylation can occur following EC exposure to shear stress, and lead to downstream mechanotransduction pathway (such as MAPK pathway) activation [41,42]. However, upon shear stress stimulation, other tyrosine sites of PECAM-1 could also get phosphorylated. For example, tyrosine site 686 plays critical roles in PECAM-Src interaction [43], as well as $\alpha_{IIb}\beta_{III}$-mediated platelet aggregation [44]. To fully understand the phosphorylation state of PECAM-1 under shear flow, various phosphorylation sites within PECAM-1 may need to be further examined. It is possible that platelets interfered with EC response to pathological flow by binding to PECAM-1, which prevented EC surface PECAM-1 phosphorylation and the subsequent EC activation.

Overall, this study explored the role of PECAM-1 in platelet-EC interaction and adhesion under pathological shear stress. Our results suggested that PECAM-1 could mediate platelet adhesion to EC at cell junctions, which could result in dampened mechanical signal and inhibited EC activation under pathological flow conditions. Therefore, in addition to anti-platelet activation therapy, preventing EC from reacting to altered pathological flow by inhibiting PECAM-1 activation may be an effective way to impede atherosclerosis initiation and progression.

Supplementary data to this article can be found online at http://dx.doi.org/10.1016/j.thromres.2016.12.003.

Conflict of interest statement

None.

References

[1] J. Partridge, H. Carlsen, K. Enesa, H. Chaudhury, M. Zakkar, L. Luong, A. Kinderlerer, M. Johns, R. Blomhoff, J.C. Mason, D.O. Haskard, P.C. Evans, Laminar shear stress acts as a switch to regulate divergent functions of nf-kappab in endothelial cells, FASEB J. 21 (2007) 3553–3561.
[2] C.F. Dewey Jr., S.R. Bussolari, M.A. Gimbrone Jr., P.F. Davies, The dynamic response of vascular endothelial cells to fluid shear stress, J. Biomech. Eng. 103 (1981) 177–185.
[3] B.J. Hunt, K.M. Jurd, Endothelial cell activation. A central pathophysiological process, BMJ 316 (1998) 1328–1329.
[4] C.M. Gibson, L. Diaz, K. Kandarpa, F.M. Sacks, R.C. Pasternak, T. Sandor, C. Feldman, P.H. Stone, Relation of vessel wall shear stress to atherosclerosis progression in human coronary arteries, Arterioscler. Thromb. 13 (1993) 310–315.
[5] D.N. Ku, D.P. Giddens, C.K. Zarins, S. Glagov, Pulsatile flow and atherosclerosis in the human carotid bifurcation. Positive correlation between plaque location and low oscillating shear stress, Arteriosclerosis 5 (1985) 293–302.
[6] L. Yang, R.M. Froio, T.E. Sciuto, A.M. Dvorak, R. Alon, F.W. Luscinskas, Icam-1 regulates neutrophil adhesion and transcellular migration of tnf-alpha-activated vascular endothelium under flow, Blood 106 (2005) 584–592.
[7] J.J. Chiu, P.L. Lee, C.N. Chen, C.I. Lee, S.F. Chang, L.J. Chen, S.C. Lien, Y.C. Ko, S. Usami, S. Chien, Shear stress increases icam-1 and decreases vcam-1 and e-selectin expressions induced by tumor necrosis factor-[alpha] in endothelial cells, Arterioscler. Thromb. Vasc. Biol. 24 (2004) 73–79.
[8] C. Lawson, S. Wolf, Icam-1 signaling in endothelial cells, Pharmacol. Rep. 61 (2009) 22–32.
[9] M.J. Davies, J.L. Gordon, A.J. Gearing, R. Pigott, N. Woolf, D. Katz, A. Kyriakopoulos, The expression of the adhesion molecules icam-1, vcam-1, pecam, and e-selectin in human atherosclerosis, J. Pathol. 171 (1993) 223–229.
[10] Y. Nakashima, E.W. Raines, A.S. Plump, J.L. Breslow, R. Ross, Upregulation of vcam-1 and icam-1 at atherosclerosis-prone sites on the endothelium in the apoe-deficient mouse, Arterioscler. Thromb. Vasc. Biol. 18 (1998) 842–851.
[11] T. Nagel, N. Resnick, W.J. Atkinson, C.F. Dewey Jr., M.A. Gimbrone Jr., Shear stress selectively upregulates intercellular adhesion molecule-1 expression in cultured human vascular endothelial cells, J. Clin. Invest. 94 (1994) 885–891.
[12] D.C. Chappell, S.E. Varner, R.M. Nerem, R.M. Medford, R.W. Alexander, Oscillatory shear stress stimulates adhesion molecule expression in cultured human endothelium, Circ. Res. 82 (1998) 532–539.
[13] M. Morigi, C. Zoja, M. Figliuzzi, M. Foppolo, G. Micheletti, M. Bontempelli, M. Saronni, G. Remuzzi, A. Remuzzi, Fluid shear stress modulates surface expression of adhesion molecules by endothelial cells, Blood 85 (1995) 1696–1703.
[14] H. Tsuboi, J. Ando, R. Korenaga, Y. Takada, A. Kamiya, Flow stimulates icam-1 expression time and shear stress dependently in cultured human endothelial cells, Biochem. Biophys. Res. Commun. 206 (1995) 988–996.
[15] T. Bombeli, B.R. Schwartz, J.M. Harlan, Adhesion of activated platelets to endothelial cells: evidence for a gpiibiiia-dependent bridging mechanism and novel roles for endothelial intercellular adhesion molecule 1 (icam-1), alphavbeta3 integrin, and gpibalpha, J. Exp. Med. 187 (1998) 329–339.
[16] J.M. Li, R.S. Podolsky, M.J. Rohrer, B.S. Cutler, M.T. Massie, M.R. Barnard, A.D. Michelson, Adhesion of activated platelets to venous endothelial cells is mediated via gpiib/iiia, J. Surg. Res. 61 (1996) 543–548.
[17] T.G. Diacovo, K.D. Puri, R.A. Warnock, T.A. Springer, U.H. von Andrian, Platelet-mediated lymphocyte delivery to high endothelial venules, Science 273 (1996) 252–255.
[18] W.L. Rosenblum, G.H. Nelson, B. Wormley, P. Werner, J. Wang, C.C. Shih, Role of platelet-endothelial cell adhesion molecule (pecam) in platelet adhesion/aggregation over injured but not denuded endothelium in vivo and ex vivo, Stroke 27 (1996) 709–711.
[19] W. Yin, F. Rouf, S. Shanmugavelayudam, D. Rubenstein, Endothelial cells modulate platelet response to dynamic shear stress, Cardiovasc. Eng. Technol. 5 (2014) 145–153.
[20] S.K. Shanmugavelayudam, D.A. Rubenstein, W. Yin, Effect of geometrical assumptions on numerical modeling of coronary blood flow under normal and disease conditions, J. Biomech. Eng. 132 (2010) 061004.
[21] M. Hasan, D.A. Rubenstein, W. Yin, Effects of cyclic motion on coronary blood flow, J. Biomech. Eng-T Asme. (2013) 135.
[22] W. Yin, D. Rubenstein, Dose effect of shear stress in platelet complement activation in a cone and plate shearing device, Cell. Mol. Bioeng. 2 (2009) 274–280.
[23] W. Yin, S.K. Shanmugavelayudam, D.A. Rubenstein, The effect of physiologically relevant dynamic shear stress on platelet and endothelial cell activation, Thromb. Res. 127 (2011) 235–241.
[24] J. Sun, C. Paddock, J. Shubert, H.B. Zhang, K. Amin, P.J. Newman, S.M. Albelda, Contributions of the extracellular and cytoplasmic domains of platelet-endothelial cell adhesion molecule-1 (pecam-1/cd31) in regulating cell-cell localization, J. Cell Sci. 113 (2000) 1459–1469.
[25] Y.S. Chatzizisis, A.U. Coskun, M. Jonas, E.R. Edelman, C.L. Feldman, P.H. Stone, Role of endothelial shear stress in the natural history of coronary atherosclerosis and vascular remodeling: molecular, cellular, and vascular behavior, J. Am. Coll. Cardiol. 49 (2007) 2379–2393.
[26] I.S. Grewal, R.A. Flavell, Cd40 and cd154 in cell-mediated immunity, Annu. Rev. Immunol. 16 (1998) 111–135.
[27] V. Henn, J.R. Slupsky, M. Grafe, I. Anagnostopoulos, R. Forster, G. Muller-Berghaus, R.A. Kroczek, Cd40 ligand on activated platelets triggers an inflammatory reaction of endothelial cells, Nature 391 (1998) 591–594.
[28] J.A. Ware, B.S. Coller, Platelet morphology, biochemistry, and function, in: E. Beutler, M.A. Lichtman, B.S. Coller, T.J. Kipps (Eds.), Williams Hematology, McGraw-Hill, Inc., New York 1995, pp. 1161–1201.

[29] O. Gidlof, M. van der Brug, J. Ohman, P. Gilje, B. Olde, C. Wahlestedt, D. Erlinge, Platelets activated during myocardial infarction release functional mirna, which can be taken up by endothelial cells and regulate icam1 expression, Blood 121 (2013) 3908–3917 (S3901-3926).
[30] D.C. Hay, C. Beers, V. Cameron, L. Thomson, F.W. Flitney, R.T. Hay, Activation of nf-κb nuclear transcription factor by flow in human endothelial cells, Biochim. Biophys. Acta, Mol. Cell Res. 1642 (2003) 33–44.
[31] H. Jo, K. Sipos, Y.M. Go, R. Law, J. Rong, J.M. McDonald, Differential effect of shear stress on extracellular signal-regulated kinase and n-terminal jun kinase in endothelial cells. Gi2- and gbeta/gamma-dependent signaling pathways, J. Biol. Chem. 272 (1997) 1395–1401.
[32] S. Mohan, N. Mohan, E.A. Sprague, Differential activation of nf-kappa b in human aortic endothelial cells conditioned to specific flow environments, Am. J. Phys. 273 (1997) C572–C578.
[33] J. Chen, J. Green, A. Yurdagul Jr., P. Albert, M.C. McInnis, A.W. Orr, Avβ3 integrins mediate flow-induced nf-κb activation, proinflammatory gene expression, and early atherogenic inflammation, Am. J. Pathol. 185 (2015) 2575–2589.
[34] Y. Castier, B. Ramkhelawon, S. Riou, A. Tedgui, S. Lehoux, Role of nf-kappab in flow-induced vascular remodeling, Antioxid. Redox Signal. 11 (2009) 1641–1649.
[35] E. Tzima, M. Irani-Tehrani, W.B. Kiosses, E. Dejana, D.A. Schultz, B. Engelhardt, G. Cao, H. DeLisser, M.A. Schwartz, A mechanosensory complex that mediates the endothelial cell response to fluid shear stress, Nature 437 (2005) 426–431.
[36] E. Dejana, R. Spagnuolo, G. Bazzoni, Interendothelial junctions and their role in the control of angiogenesis, vascular permeability and leukocyte transmigration, Thromb. Haemost. 86 (2001) 308–315.
[37] K. Hashimoto, N. Kataoka, E. Nakamura, K. Hagihara, M. Hatano, T. Okamoto, H. Kanouchi, Y. Minatogawa, S. Mohri, K. Tsujioka, F. Kajiya, Monocyte transendothelial migration augments subsequent transmigratory activity with increased pecam-1 and decreased ve-cadherin at endothelial junctions, Int. J. Cardiol. 149 (2011) 232–239.
[38] S.K. Shaw, B.N. Perkins, Y.C. Lim, Y. Liu, A. Nusrat, F.J. Schnell, C.A. Parkos, F.W. Luscinskas, Reduced expression of junctional adhesion molecule and platelet/endothelial cell adhesion molecule-1 (cd31) at human vascular endothelial junctions by cytokines tumor necrosis factor-alpha plus interferon-gamma does not reduce leukocyte transmigration under flow, Am. J. Pathol. 159 (2001) 2281–2291.
[39] J.R. Privratsky, P.J. Newman, Pecam-1: regulator of endothelial junctional integrity, Cell Tissue Res. 355 (2014) 607–619.
[40] V. Rathore, M.A. Stapleton, C.A. Hillery, R.R. Montgomery, T.C. Nichols, E.P. Merricks, D.K. Newman, P.J. Newman, Pecam-1 negatively regulates gpib/v/ix signaling in murine platelets, Blood 102 (2003) 3658–3664.
[41] K.S. Heo, K. Fujiwara, J. Abe, Shear stress and atherosclerosis, Mol. Cell 37 (2014) 435–440.
[42] M. Osawa, M. Masuda, N. Harada, R.B. Lopes, K. Fujiwara, Tyrosine phosphorylation of platelet endothelial cell adhesion molecule-1 (pecam-1, cd31) in mechanically stimulated vascular endothelial cells, Eur. J. Cell Biol. 72 (1997) 229–237.
[43] D.E. Jackson, K.R. Kupcho, P.J. Newman, Characterization of phosphotyrosine binding motifs in the cytoplasmic domain of platelet/endothelial cell adhesion molecule-1 (pecam-1) that are required for the cellular association and activation of the protein-tyrosine phosphatase, shp-2, J. Biol. Chem. 272 (1997) 24868–24875.
[44] C.T. Hua, J.R. Gamble, M.A. Vadas, D.E. Jackson, Recruitment and activation of shp-1 protein-tyrosine phosphatase by human platelet endothelial cell adhesion molecule-1 (pecam-1). Identification of immunoreceptor tyrosine-based inhibitory motif-like binding motifs and substrates, J. Biol. Chem. 273 (1998) 28332–28340.

References

[1] Heart, T.
[2] Fung, Y.-c., 2013, Biomechanics: circulation, Springer Science & Business Media.
[3] BIDMC.
[4] Heron, M., 2013, "Deaths: leading causes for 2010," National vital statistics reports: from the Centers for Disease Control and Prevention, National Center for Health Statistics, National Vital Statistics System, 62(6), pp. 1-96.
[5] Harsh, M., 2010, Textbook of pathology, Jaypee Brothers Medical Publishers (P) Ltd.
[6] Basavaraju, S. R., and Jones, T. D., 1998, "Atherosclerotic risks from chemicals: part I. Toxicological observations and mechanisms of atherosclerosis," Archives of environmental contamination and toxicology, 35(1), pp. 152-164.
[7] Fox, C. S., Polak, J. F., Chazaro, I., Cupples, A., Wolf, P. A., D'Agostino, R. A., O'Donnell, C. J., and Framingham Heart, S., 2003, "Genetic and environmental contributions to atherosclerosis phenotypes in men and women:

heritability of carotid intima-media thickness in the Framingham Heart Study," Stroke; a journal of cerebral circulation, 34(2), pp. 397-401.
[8] Mustard, J., Rowsell, H., Murphy, E., and Downie, H., 1963, "Evolution of the Atherosclerotic Plaque.(edit by Jones, RJ) Chicago," University of Chicago Press.
[9] Fox, J. A., and Hugh, A. E., 1966, "Localization of atheroma: a theory based on boundary layer separation," Br Heart J, 28(3), pp. 388-399.
[10] Texon, M., 1960, "The hemodynamic concept of atherosclerosis," Bulletin of the New York Academy of Medicine, 36(4), p. 263.
[11] Mitchell, J. R. A., and Schwartz, C. J., 1965, Arterial disease, Blackwell Scientific Publications.
[12] Fry, D. L., 1968, "Acute vascular endothelial changes associated with increased blood velocity gradients," Circ Res, 22(2), pp. 165-197.
[13] Caro, C. G., Fitz-Gerald, J. M., and Schroter, R. C., 1971, "Atheroma and arterial wall shear. Observation, correlation and proposal of a shear dependent mass transfer mechanism for atherogenesis," Proc R Soc Lond B Biol Sci, 177(1046), pp. 109-159.
[14] Asakura, T., and Karino, T., 1990, "Flow patterns and spatial distribution of atherosclerotic lesions in human coronary arteries," Circ Res, 66(4), pp. 1045-1066.
[15] Caro, C. G., Fitz-Gerald, J. M., and Schroter, R. C., 1969, "Arterial wall shear and distribution of early atheroma in man," Nature, 223(5211), pp. 1159-1160.
[16] Montenegro, M. R., and Eggen, D. A., 1968, "Topography of atherosclerosis in the coronary arteries," Lab Invest, 18(5), pp. 586-593.
[17] Schwartz, C. J., and Mitchell, J. R., 1962, "Observations on localization of arterial plaques," Circ Res, 11, pp. 63-73.
[18] Chien, S., 2007, "Mechanotransduction and endothelial cell homeostasis: the wisdom of the cell," American journal of physiology. Heart and circulatory physiology, 292(3), pp. H1209-1224.
[19] Malek, A. M., Alper, S. L., and Izumo, S., 1999, "Hemodynamic shear stress and its role in atherosclerosis," JAMA, 282(21), pp. 2035-2042.
[20] Heo, K. S., Fujiwara, K., and Abe, J., 2014, "Shear stress and atherosclerosis," Mol Cells, 37(6), pp. 435-440.
[21] Cunningham, K. S., and Gotlieb, A. I., 2005, "The role of shear stress in the pathogenesis of atherosclerosis," Lab Invest, 85(1), pp. 9-23.
[22] Nomura, S., Tandon, N. N., Nakamura, T., Cone, J., Fukuhara, S., and Kambayashi, J., 2001, "High-shear-stress-induced activation of platelets and microparticles enhances expression of cell adhesion molecules in THP-1 and endothelial cells," Atherosclerosis, 158(2), pp. 277-287.
[23] Fujiwara, K., 2006, "Platelet endothelial cell adhesion molecule-1 and mechanotransduction in vascular endothelial cells," Journal of internal medicine, 259(4), pp. 373-380.
[24] Sumpio, B. E., Yun, S., Cordova, A. C., Haga, M., Zhang, J., Koh, Y., and Madri, J. A., 2005, "MAPKs (ERK½, p38) and AKT can be phosphorylated by shear stress independently of platelet endothelial cell adhesion molecule-1 (CD31) in vascular endothelial cells," Journal of Biological Chemistry, 280(12), pp. 11185-11191.
[25] Osawa, M., Masuda, M., Kusano, K., and Fujiwara, K., 2002, "Evidence for a role of platelet endothelial cell adhesion molecule-1 in endothelial cell mechanosignal transduction: is it a mechanoresponsive molecule?," The Journal of cell biology, 158(4), pp. 773-785.
[26] Tzima, E., Irani-Tehrani, M., Kiosses, W. B., Dejana, E., Schultz, D. A., Engelhardt, B., Cao, G., DeLisser, H., and Schwartz, M. A., 2005, "A mechanosensory complex that mediates the endothelial cell response to fluid shear stress," Nature, 437(7057), pp. 426-431.
[27] Tsuboi, H., Ando, J., Korenaga, R., Takada, Y., and Kamiya, A., 1995, "Flow stimulates ICAM-1 expression time and shear stress dependently in cultured human endothelial cells," Biochemical and biophysical research communications, 206(3), pp. 988-996.
[28] Kishimoto, T. K., and Rothlein, R., 1994, "Integrins, ICAMs, and selectins: role and regulation of adhesion molecules in neutrophil recruitment to inflammatory sites," Advances in pharmacology, 25, pp. 117-169.

[29] Harrison, M., Smith, E., Ross, E., Krams, R., Segers, D., Buckley, C. D., Nash, G. B., and Rainger, G. E., 2013, "The role of platelet-endothelial cell adhesion molecule-1 in atheroma formation varies depending on the site-specific hemodynamic environment," Arteriosclerosis, thrombosis, and vascular biology, 33(4), pp. 694-701.
[30] Dewey, C. F., Jr., Bussolari, S. R., Gimbrone, M. A., Jr., and Davies, P. F., 1981, "The dynamic response of vascular endothelial cells to fluid shear stress," Journal of biomechanical engineering, 103(3), pp. 177-185.
[31] Rouleau, L., Farcas, M., Tardif, J. C., Mongrain, R., and Leask, R. L., 2010, "Endothelial cell morphologic response to asymmetric stenosis hemodynamics: effects of spatial wall shear stress gradients," Journal of biomechanical engineering, 132(8), p. 081013.
[32] Heo, K. S., Fujiwara, K., and Abe, J., 2011, "Disturbed-flow-mediated vascular reactive oxygen species induce endothelial dysfunction," Circ J, 75(12), pp. 2722-2730.
[33] Husmann, L., Leschka, S., Desbiolles, L., Schepis, T., Gaemperli, O., Seifert, B., Cattin, P., Frauenfelder, T., Flohr, T. G., and Marincek, B., 2007, "Coronary Artery Motion and Cardiac Phases: Dependency on Heart Rate—Implications for CT Image Reconstruction 1," Radiology, 245(2), pp. 567-576.
[34] Azuma, N., Duzgun, S. A., Ikeda, M., Kito, H., Akasaka, N., Sasajima, T., and Sumpio, B. E., 2000, "Endothelial cell response to different mechanical forces," J Vasc Surg, 32(4), pp. 789-794.
[35] Riehl, B. D., Park, J. H., Kwon, I. K., and Lim, J. Y., 2012, "Mechanical stretching for tissue engineering: two-dimensional and three-dimensional constructs," Tissue Eng Part B Rev, 18(4), pp. 288-300.
[36] Fujiwara, K., 2003, "Mechanical stresses keep endothelial cells healthy: beneficial effects of a physiological level of cyclic stretch on endothelial barrier function," Am J Physiol Lung Cell Mol Physiol, 285(4), pp. L782-784.
[37] Jufri, N. F., Mohamedali, A., Avolio, A., and Baker, M. S., 2015, "Mechanical stretch: physiological and pathological implications for human vascular endothelial cells," Vasc Cell, 7, p. 8.
[38] Sinha, R., Verdonschot, N., Koopman, B., and Rouwkema, J., 2017, "Tuning cell and tissue development by combining multiple mechanical signals," Tissue Eng Part B Rev.
[39] Safar, M., and Frohlich, E. D., 2007, Atherosclerosis, large arteries and cardiovascular risk, Karger Medical and Scientific Publishers.
[40] Benbrahim, A., L'Italien, G. J., Kwolek, C. J., Petersen, M. J., Milinazzo, B., Gertler, J. P., Abbott, W. M., and Orkin, R. W., 1996, "Characteristics of Vascular Wall Cells Subjected to Dynamic Cyclic Strain and Fluid Shear Conditions< i> in Vitro</i>," Journal of Surgical Research, 65(2), pp. 119-127.
[41] Peng, X., Recchia, F. A., Byrne, B. J., Wittstein, I. S., Ziegelstein, R. C., and Kass, D. A., 2000, "In vitro system to study realistic pulsatile flow and stretch signaling in cultured vascular cells," American Journal of Physiology-Cell Physiology, 279(3), pp. C797-C805.
[42] Zhao, S., Suciu, A., Ziegler, T., Moore, J. E., Bürki, E., Meister, J.-J., and Brunner, H. R., 1995, "Synergistic effects of fluid shear stress and cyclic circumferential stretch on vascular endothelial cell morphology and cytoskeleton," Arteriosclerosis, thrombosis, and vascular biology, 15(10), pp. 1781-1786.
[43] Benbrahim, A., L'Italien, G. J., Milinazzo, B. B., Warnock, D. F., Dhara, S., Gertler, J. P., Orkin, R. W., and Abbott, W. M., 1994, "A compliant tubular device to study the influences of wall strain and fluid shear stress on cells of the vascular wall," Journal of vascular surgery, 20(2), pp. 184-194.
[44] Owatverot, T. B., Oswald, S. J., Chen, Y., Wille, J. J., and Yin, F. C., 2005, "Effect of combined cyclic stretch and fluid shear stress on endothelial cell morphological responses," Journal of biomechanical engineering, 127(3), pp. 374-382.
[45] Azuma, N., Duzgun, S. A., Ikeda, M., Kito, H., Akasaka, N., Sasajima, T., and Sumpio, B. E., 2000, "Endothelial cell response to different mechanical forces," Journal of vascular surgery, 32(4), pp. 789-794.
[46] Moore Jr, J. E., Bürki, E., Suciu, A., Zhao, S., Burnier, M., Brunner, H. R., and Meister, J.-J., 1994, "A device for subjecting vascular endothelial cells to both fluid shear stress and circumferential cyclic stretch," Annals of biomedical engineering, 22(4), pp. 416-422.
[47] Ives, C., Eskin, S., and McIntire, L., 1986, "Mechanical effects on endothelial cell morphology: in vitro assessment," In vitro cellular & developmental biology, 22(9), pp. 500-507.
[48] Tarbell, Y. Q. J. M., 2000, "Interaction between Wall Shear Stress and Circumferential Strain Affects Endothelial Cell Biochemical Production."

[49] Estrada, R., Giridharan, G. A., Nguyen, M.-D., Roussel, T. J., Shakeri, M., Parichehreh, V., Prabhu, S. D., and Sethu, P., 2011, "Endothelial cell culture model for replication of physiological profiles of pressure, flow, stretch, and shear stress in vitro," Analytical chemistry, 83(8), pp. 3170-3177.
[50] Estrada, R., Giridharan, G. A., Nguyen, M. D., Roussel, T. J., Shakeri, M., Parichehreh, V., Prabhu, S. D., and Sethu, P., 2011, "Endothelial cell culture model for replication of physiological profiles of pressure, flow, stretch, and shear stress in vitro," Anal Chem, 83(8), pp. 3170-3177.
[51] Van Dyke, W. S., Sun, X., Richard, A. B., Nauman, E. A., and Akkus, O., 2012, "Novel mechanical bioreactor for concomitant fluid shear stress and substrate strain," Journal of biomechanics, 45(7), pp. 1323-1327.
[52] Maeda, E., Hagiwara, Y., Wang, J. H., and Ohashi, T., 2013, "A new experimental system for simultaneous application of cyclic tensile strain and fluid shear stress to tenocytes in vitro," Biomedical microdevices, 15(6), pp. 1067-1075.
[53] Breen, L. T., McHugh, P. E., McCormack, B. A., Muir, G., Quinlan, N. J., Heraty, K. B., and Murphy, B. P., 2006, "Development of a novel bioreactor to apply shear stress and tensile strain simultaneously to cell monolayers," Review of scientific instruments, 77(10), p. 104301.
[54] Sinha, R., Le Gac, S., Verdonschot, N., Van Den Berg, A., Koopman, B., and Rouwkema, J., 2016, "Endothelial cell alignment as a result of anisotropic strain and flow induced shear stress combinations," Scientific reports, 6.
[55] Toda, M., Yamamoto, K., Shimizu, N., Obi, S., Kumagaya, S., Igarashi, T., Kamiya, A., and Ando, J., 2008, "Differential gene responses in endothelial cells exposed to a combination of shear stress and cyclic stretch," J Biotechnol, 133(2), pp. 239-244.
[56] Thacher, T. N., Silacci, P., Stergiopulos, N., and da Silva, R. F., 2010, "Autonomous effects of shear stress and cyclic circumferential stretch regarding endothelial dysfunction and oxidative stress: an ex vivo arterial model," Journal of vascular research, 47(4), pp. 336-345.
[57] Berardi, D. E., and Tarbell, J. M., 2009, "Stretch and Shear Interactions Affect Intercellular Junction Protein Expression and Turnover in Endothelial Cells," Cellular and molecular bioengineering, 2(3), pp. 320-331.
[58] Walsh, P., Gow, B., Odell, R., and Schindhelm, K., "Morphological response of endothelial cells to combined pulsatile shear stress plus cyclic stretch," Proc. [Engineering in Medicine and Biology, 1999. 21st Annual Conference and the 1999 Annual Fall Meetring of the Biomedical Engineering Society] BMES/EMBS Conference, 1999. Proceedings of the First Joint, IEEE, p. 11 vol. 11.
[59] Go, A. S., Mozaffarian, D., Roger, V. L., Benjamin, E. J., Berry, J. D., Blaha, M. J., Dai, S., Ford, E. S., Fox, C. S., and Franco, S., 2014, "Heart disease and stroke statistics--2014 update: a report from the American Heart Association," Circulation, 129(3), p. e28.
[60] Ferenczi, E., Aggarwal, R., and Muirhead, N., 2007, One Stop Doc Cardiology, Taylor & Francis Limited.
[61] CDC, N., 1999, "Underlying Cause of Death 1999-2013 on CDC WONDER Online Database, released 2015," Data are from the Multiple Cause of Death Files, 2013.
[62] VanderLaan, P. A., Reardon, C. A., and Getz, G. S., 2004, "Site specificity of atherosclerosis: site-selective responses to atherosclerotic modulators," Arterioscler Thromb Vasc Biol, 24(1), pp. 12-22.
[63] Davies, P. F., Shi, C., Depaola, N., Helmke, B. P., and Polacek, D. C., 2001, "Hemodynamics and the focal origin of atherosclerosis: a spatial approach to endothelial structure, gene expression, and function," Ann N Y Acad Sci, 947, pp. 7-16; discussion 16-17.
[64] Glagov, S., Zarins, C., Giddens, D. P., and Ku, D. N., 1988, "Hemodynamics and atherosclerosis. Insights and perspectives gained from studies of human arteries," Arch Pathol Lab Med, 112(10), pp. 1018-1031.
[65] Schaar, J. A., De Korte, C. L., Mastik, F., Strijder, C., Pasterkamp, G., Boersma, E., Serruys, P. W., and Van Der Steen, A. F., 2003, "Characterizing vulnerable plaque features with intravascular elastography," Circulation, 108(21), pp. 2636-2641.
[66] Meza, D., Abejar, L., Rubenstein, D. A., and Yin, W., 2016, "A Shearing-Stretching Device That Can Apply Physiological Fluid Shear Stress and Cyclic Stretch Concurrently to Endothelial Cells," J Biomech Eng, 138(3), p. 4032550.
[67] Vis, M. A., Sipkema, P., and Westerhof, N., 1995, "Modeling pressure-area relations of coronary blood vessels embedded in cardiac muscle in diastole and systole," Am J Physiol, 268(6 Pt 2), pp. H2531-2543.

[68] Tecelao, S. R., Zwanenburg, J. J., Kuijer, J. P., and Marcus, J. T., 2006, "Extended harmonic phase tracking of myocardial motion: improved coverage of myocardium and its effect on strain results," J Magn Reson Imaging, 23(5), pp. 682-690.
[69] Reneman, R. S., and Hoeks, A. P., 2008, "Wall shear stress as measured in vivo: consequences for the design of the arterial system," Medical & biological engineering & computing, 46(5), pp. 499-507.
[70] Stalder, A. F., Russe, M. F., Frydrychowicz, A., Bock, J., Hennig, J., and Markl, M., 2008, "Quantitative 2D and 3D phase contrast MRI: optimized analysis of blood flow and vessel wall parameters," Magnetic resonance in medicine, 60(5), pp. 1218-1231.
[71] Markl, M., Wegent, F., Zech, T., Bauer, S., Strecker, C., Schumacher, M., Weiller, C., Hennig, J., and Harloff, A., 2010, "In vivo wall shear stress distribution in the carotid artery: effect of bifurcation geometry, internal carotid artery stenosis, and recanalization therapy," Circulation. Cardiovascular imaging, 3(6), pp. 647-655.
[72] van der Giessen, A. G., Schaap, M., Gijsen, F. J., Groen, H. C., van Walsum, T., Mollet, N. R., Dijkstra, J., van de Vosse, F. N., Niessen, W. J., de Feyter, P. J., van der Steen, A. F., and Wentzel, J. J., 2010, "3D fusion of intravascular ultrasound and coronary computed tomography for in-vivo wall shear stress analysis: a feasibility study," The international journal of cardiovascular imaging, 26(7), pp. 781-796.
[73] Hanekom, L., Cho, G.-Y., Leano, R., Jeffriess, L., and Marwick, T. H., 2007, "Comparison of two-dimensional speckle and tissue Doppler strain measurement during dobutamine stress echocardiography: an angiographic correlation," European heart journal.
[74] Hoit, B. D., 2011, "Strain and strain rate echocardiography and coronary artery disease," Circulation. Cardiovascular imaging, 4(2), pp. 179-190.
[75] Leung, E., Baldewsing, R., Mastik, F., Schaar, J., Gisolf, A., and van der Steen, T., 2005, "Motion compensation for intravascular ultrasound palpography for in vivo vulnerable plaque detection."
[76] Maurice, R. L., Soulez, G., Giroux, M. F., and Cloutier, G., 2008, "Noninvasive vascular elastography for carotid artery characterization on subjects without previous history of atherosclerosis," Medical physics, 35(8), pp. 3436-3443.
[77] Shehata, M., Adel, W., Mansour, S., Samir, S., and Elmahalawy, N., 2014, "Use of Strain Imaging to Predict Myocardial Function Recovery after Percutaneous Revascularization of Infarct Related Artery," International Journal of Cardiovascular Research.
[78] Veress, A. I., Weiss, J. A., Gullberg, G. T., Vince, D. G., and Rabbitt, R. D., 2002, "Strain measurement in coronary arteries using intravascular ultrasound and deformable images," Journal of biomechanical engineering, 124(6), pp. 734-741.
[79] Miyatake, K., Yamagishi, M., Tanaka, N., Uematsu, M., Yamazaki, N., Mine, Y., Sano, A., and Hirama, M., 1995, "New method for evaluating left ventricular wall motion by color-coded tissue Doppler imaging: in vitro and in vivo studies," Journal of the American College of Cardiology, 25(3), pp. 717-724.
[80] Sutherland, G. R., Di Salvo, G., Claus, P., D'hooge, J., and Bijnens, B., 2004, "Strain and strain rate imaging: a new clinical approach to quantifying regional myocardial function," Journal of the American Society of Echocardiography, 17(7), pp. 788-802.
[81] Yip, G., Abraham, T., Belohlavek, M., and Khandheria, B. K., 2003, "Clinical applications of strain rate imaging," journal of the american society of echocardiography, 16(12), pp. 1334-1342.
[82] Hoffmann, R., Marwick, T., Poldermans, D., Lethen, H., Ciani, R., van der Meer, P., Tries, H., Gianfagna, P., Fioretti, P., and Bax, J., 2002, "Refinements in stress echocardiographic techniques improve inter-institutional agreement in interpretation of dobutamine stress echocardiograms," European heart journal, 23(10), pp. 821-829.
[83] Hoffmann, R., Lethen, H., Marwick, T., Arnese, M., Fioretti, P., Pingitore, A., Picano, E., Buck, T., Erbel, R., and Flachskampf, F. A., 1996, "Analysis of interinstitutional observer agreement in interpretation of dobutamine stress echocardiograms," Journal of the American College of Cardiology, 27(2), pp. 330-336.
[84] de Korte, C. L., Hansen, H. H., and van der Steen, A. F., 2011, "Vascular ultrasound for atherosclerosis imaging," Interface Focus, 1(4), pp. 565-575.
[85] Torii, R., Wood, N. B., Hadjiloizou, N., Dowsey, A. W., Wright, A. R., Hughes, A. D., Davies, J., Francis, D. P., Mayet, J., and Yang, G. Z., 2009, "Fluid–structure interaction analysis of a patient-specific right coronary artery

with physiological velocity and pressure waveforms," Communications in numerical methods in engineering, 25(5), pp. 565-580.
[86] Taylor, C. A., and Figueroa, C. A., 2009, "Patient-specific modeling of cardiovascular mechanics," Annu Rev Biomed Eng, 11, pp. 109-134.
[87] Hasan, M., Rubenstein, D. A., and Yin, W., 2013, "Effects of cyclic motion on coronary blood flow," J Biomech Eng, 135(12), p. 121002.
[88] Tang, D., Yang, C., Kobayashi, S., Zheng, J., Woodard, P. K., Teng, Z., Billiar, K., Bach, R., and Ku, D. N., 2009, "3D MRI-based anisotropic FSI models with cyclic bending for human coronary atherosclerotic plaque mechanical analysis," J Biomech Eng, 131(6), p. 061010.
[89] Westerhof, N., Boer, C., Lamberts, R. R., and Sipkema, P., 2006, "Cross-talk between cardiac muscle and coronary vasculature," Physiological Reviews, 86(4), pp. 1263-1308.
[90] Spaan, J. A., 1993, "Heart Contraction and Coronary Blood Flow," Recent Advances in Coronary Circulation, Springer, pp. 60-68.
[91] Zhang, W., Herrera, C., Atluri, S. N., and Kassab, G. S., 2004, "Effect of surrounding tissue on vessel fluid and solid mechanics," J Biomech Eng, 126(6), pp. 760-769.
[92] Smith, N. P., 2004, "A computational study of the interaction between coronary blood flow and myocardial mechanics," Physiological measurement, 25(4), p. 863.
[93] Ohayon, J., Gharib, A. M., Garcia, A., Heroux, J., Yazdani, S. K., Malve, M., Tracqui, P., Martinez, M. A., Doblare, M., Finet, G., and Pettigrew, R. I., 2011, "Is arterial wall-strain stiffening an additional process responsible for atherosclerosis in coronary bifurcations?: an in vivo study based on dynamic CT and MRI," Am J Physiol Heart Circ Physiol, 301(3), pp. H1097-1106.
[94] Oviedo, C., Maehara, A., Mintz, G. S., Araki, H., Choi, S. Y., Tsujita, K., Kubo, T., Doi, H., Templin, B., Lansky, A. J., Dangas, G., Leon, M. B., Mehran, R., Tahk, S. J., Stone, G. W., Ochiai, M., and Moses, J. W., 2010, "Intravascular ultrasound classification of plaque distribution in left main coronary artery bifurcations: where is the plaque really located?," Circ Cardiovasc Interv, 3(2), pp. 105-112.
[95] Zandwijk, J., 2014, "Dynamic geometry and plaque development in the coronary arteries."
[96] Gradus-Pizlo, I., Bigelow, B., Mahomed, Y., Sawada, S. G., Rieger, K., and Feigenbaum, H., 2003, "Left anterior descending coronary artery wall thickness measured by high-frequency transthoracic and epicardial echocardiography includes adventitia," Am J Cardiol, 91(1), pp. 27-32.
[97] Holzapfel, G. A., Gasser, T. C., and Ogden, R. W., 2000, "A new constitutive framework for arterial wall mechanics and a comparative study of material models," Journal of elasticity and the physical science of solids, 61(1-3), pp. 1-48.
[98] Bathe, K., 2015, "Theory and modeling guide," Watertown, MA: ADINA R & D.: Inc.
[99] Kural, M. H., Cai, M., Tang, D., Gwyther, T., Zheng, J., and Billiar, K. L., 2012, "Planar biaxial characterization of diseased human coronary and carotid arteries for computational modeling," J Biomech, 45(5), pp. 790-798.
[100] Karimi, A., Navidbakhsh, M., Yamada, H., and Razaghi, R., 2014, "A nonlinear finite element simulation of balloon expandable stent for assessment of plaque vulnerability inside a stenotic artery," Med Biol Eng Comput, 52(7), pp. 589-599.
[101] Florenciano-Sanchez, R., de la Morena-Valenzuela, G., Villegas-Garcia, M., Soria-Arcos, F., Rubio-Paton, R., Teruel-Carrillo, F., Hurtado, J., and Valdes-Chavarri, M., 2005, "Noninvasive assessment of coronary flow velocity reserve in left anterior descending artery adds diagnostic value to both clinical variables and dobutamine echocardiography: a study based on clinical practice," Eur J Echocardiogr, 6(4), pp. 251-259.
[102] Watanabe, N., 2017, "Noninvasive assessment of coronary blood flow by transthoracic Doppler echocardiography: basic to practical use in the emergency room," J Echocardiogr.
[103] Shanmugavelayudam, S. K., Rubenstein, D. A., and Yin, W., 2010, "Effect of geometrical assumptions on numerical modeling of coronary blood flow under normal and disease conditions," J Biomech Eng, 132(6), p. 061004.
[104] Javadzadegan, A., Yong, A. S., Chang, M., Ng, M. K., Behnia, M., and Kritharides, L., 2017, "Haemodynamic assessment of human coronary arteries is affected by degree of freedom of artery movement," Computer Methods in Biomechanics and Biomedical Engineering, 20(3), pp. 260-272.

[105] Dhawan, S. S., Avati Nanjundappa, R. P., Branch, J. R., Taylor, W. R., Quyyumi, A. A., Jo, H., McDaniel, M. C., Suo, J., Giddens, D., and Samady, H., 2010, "Shear stress and plaque development," Expert Rev Cardiovasc Ther, 8(4), pp. 545-556.
[106] Eshtehardi, P., McDaniel, M. C., Suo, J., Dhawan, S. S., Timmins, L. H., Binongo, J. N., Golub, L. J., Corban, M. T., Finn, A. V., Oshinski, J. N., Quyyumi, A. A., Giddens, D. P., and Samady, H., 2012, "Association of coronary wall shear stress with atherosclerotic plaque burden, composition, and distribution in patients with coronary artery disease," J Am Heart Assoc, 1(4), p. e002543.
[107] Wang, Y., Qiu, J., Luo, S., Xie, X., Zheng, Y., Zhang, K., Ye, Z., Liu, W., Gregersen, H., and Wang, G., 2016, "High shear stress induces atherosclerotic vulnerable plaque formation through angiogenesis," Regen Biomater, 3(4), pp. 257-267.
[108] Hetterich, H., Jaber, A., Gehring, M., Curta, A., Bamberg, F., Filipovic, N., and Rieber, J., 2015, "Coronary computed tomography angiography based assessment of endothelial shear stress and its association with atherosclerotic plaque distribution in-vivo," PLoS One, 10(1), p. e0115408.
[109] Yamamoto T, I. K., Arai J, Umezu M 2015, "A Study of the Proximal Left Anterior Descending Coronary Artery Motion," J Med Diagn Meth 4(1000).
[110] Liang, Y., Zhu, H., Gehrig, T., and Friedman, M. H., 2008, "Measurement of the transverse strain tensor in the coronary arterial wall from clinical intravascular ultrasound images," J Biomech, 41(14), pp. 2906-2911.
[111] Valgimigli, M., Rodriguez-Granillo, G. A., Garcia-Garcia, H. M., Vaina, S., De Jaegere, P., De Feyter, P., and Serruys, P. W., 2007, "Plaque composition in the left main stem mimics the distal but not the proximal tract of the left coronary artery: influence of clinical presentation, length of the left main trunk, lipid profile, and systemic levels of C-reactive protein," J Am Coll Cardiol, 49(1), pp. 23-31.
[112] Prosi, M., Perktold, K., Ding, Z., and Friedman, M. H., 2004, "Influence of curvature dynamics on pulsatile coronary artery flow in a realistic bifurcation model," J Biomech, 37(11), pp. 1767-1775.
[113] Yang, C., Bach, R. G., Zheng, J., Naqa, I. E., Woodard, P. K., Teng, Z., Billiar, K., and Tang, D., 2009, "In vivo IVUS-based 3-D fluid-structure interaction models with cyclic bending and anisotropic vessel properties for human atherosclerotic coronary plaque mechanical analysis," IEEE Trans Biomed Eng, 56(10), pp. 2420-2428.
[114] Gradus-Pizlo, I., Bigelow, B., Mahomed, Y., Sawada, S. G., Rieger, K., and Feigenbaum, H., 2003, "Left anterior descending coronary artery wall thickness measured by high-frequency transthoracic and epicardial echocardiography includes adventitia," The American journal of cardiology, 91(1), pp. 27-32.
[115] Raut, S. S., Jana, A., De Oliveira, V., Muluk, S. C., and Finol, E. A., 2013, "The importance of patient-specific regionally varying wall thickness in abdominal aortic aneurysm biomechanics," J Biomech Eng, 135(8), p. 81010.
[116] Joshi, A. K., Leask, R. L., Myers, J. G., Ojha, M., Butany, J., and Ethier, C. R., 2004, "Intimal thickness is not associated with wall shear stress patterns in the human right coronary artery," Arteriosclerosis, thrombosis, and vascular biology, 24(12), pp. 2408-2413.
[117] Selvarasu, N., and Tafti, D. K., 2012, "Investigation of the effects of dynamic change in curvature and torsion on pulsatile flow in a helical tube," Journal of biomechanical engineering, 134(7), p. 071005.
[118] Cunningham, K. S., and Gotlieb, A. I., 2004, "The role of shear stress in the pathogenesis of atherosclerosis," Lab Invest, 85(1), pp. 9-23.
[119] Chiu, J.-J., Usami, S., and Chien, S., 2009, "Vascular endothelial responses to altered shear stress: pathologic implications for atherosclerosis," Annals of medicine, 41(1), pp. 19-28.
[120] Alexander, R. W., 1995, "Hypertension and the pathogenesis of atherosclerosis oxidative stress and the mediation of arterial inflammatory response: a new perspective," Hypertension, 25(2), pp. 155-161.
[121] Frangos, S. G., Gahtan, V., and Sumpio, B., 1999, "Localization of atherosclerosis: role of hemodynamics," Archives of Surgery, 134(10), pp. 1142-1149.
[122] Hunt, B. J., and Jurd, K. M., 1998, "Endothelial cell activation. A central pathophysiological process," Bmj, 316(7141), pp. 1328-1329.
[123] Sipkema, P., van der Linden, P. J., Westerhof, N., and Yin, F. C., 2003, "Effect of cyclic axial stretch of rat arteries on endothelial cytoskeletal morphology and vascular reactivity," Journal of biomechanics, 36(5), pp. 653-659.

[124] Barron, V., Brougham, C., Coghlan, K., McLucas, E., O'Mahoney, D., Stenson-Cox, C., and McHugh, P. E., 2007, "The effect of physiological cyclic stretch on the cell morphology, cell orientation and protein expression of endothelial cells," Journal of materials science. Materials in medicine, 18(10), pp. 1973-1981.
[125] Michel, J. B., 2003, "Anoikis in the cardiovascular system: known and unknown extracellular mediators," Arteriosclerosis, thrombosis, and vascular biology, 23(12), pp. 2146-2154.
[126] Lacolley, P., Challande, P., Boumaza, S., Cohuet, G., Laurent, S., Boutouyrie, P., Grimaud, J. A., Paulin, D., Lamaziere, J. M., and Li, Z., 2001, "Mechanical properties and structure of carotid arteries in mice lacking desmin," Cardiovascular research, 51(1), pp. 178-187.
[127] Korff, T., Aufgebauer, K., and Hecker, M., 2007, "Cyclic stretch controls the expression of CD40 in endothelial cells by changing their transforming growth factor-beta1 response," Circulation, 116(20), pp. 2288-2297.
[128] Yin, W., and Rubenstein, D., 2009, "Dose Effect of Shear Stress on Platelet Complement Activation in a Cone and Plate Shearing Device," Cellular and molecular bioengineering, 2(2), pp. 274-280.
[129] Banes, A. J., Gilbert, J., Taylor, D., and Monbureau, O., 1985, "A new vacuum-operated stress-providing instrument that applies static or variable duration cyclic tension or compression to cells in vitro," Journal of cell science, 75, pp. 35-42.
[130] Vande Geest, J. P., Di Martino, E. S., and Vorp, D. A., 2004, "An analysis of the complete strain field within Flexercell membranes," Journal of biomechanics, 37(12), pp. 1923-1928.
[131] Ethier, C. R., and Simmons, C. A., 2007, "Introductory biomechanics: from cells to organisms," Cambridge University Press, pp. 82-86.
[132] Yin, W., Shanmugavelayudam, S. K., and Rubenstein, D. A., 2011, "The effect of physiologically relevant dynamic shear stress on platelet and endothelial cell activation," Thrombosis research, 127(3), pp. 235-241.
[133] Fung, Y.-c., 1977, "A first course in continuum mechanics," Englewood Cliffs, NJ, Prentice-Hall, Inc., 1977. 351 p., 1, pp. 112-124.
[134] Maria, Z., Yin, W., and Rubenstein, D. A., 2014, "Combined effects of physiologically relevant disturbed wall shear stress and glycated albumin on endothelial cell functions associated with inflammation, thrombosis and cytoskeletal dynamics," Journal of diabetes investigation, 5(4), pp. 372-381.
[135] Ng, C. P., Hinz, B., and Swartz, M. A., 2005, "Interstitial fluid flow induces myofibroblast differentiation and collagen alignment in vitro," Journal of cell science, 118(20), pp. 4731-4739.
[136] Sternberg, S. R., 1983, "Biomedical image processing," Computer, 16(1), pp. 22-34.
[137] Ng, C. P., Hinz, B., and Swartz, M. A., 2005, "Interstitial fluid flow induces myofibroblast differentiation and collagen alignment in vitro," J Cell Sci, 118(Pt 20), pp. 4731-4739.
[138] Caille, N., Thoumine, O., Tardy, Y., and Meister, J. J., 2002, "Contribution of the nucleus to the mechanical properties of endothelial cells," Journal of biomechanics, 35(2), pp. 177-187.
[139] Martinelli, R., Zeiger, A. S., Whitfield, M., Sciuto, T. E., Dvorak, A., Van Vliet, K. J., Greenwood, J., and Carman, C. V., 2014, "Probing the biomechanical contribution of the endothelium to lymphocyte migration: diapedesis by the path of least resistance," Journal of cell science, 127(Pt 17), pp. 3720-3734.
[140] Tojkander, S., Gateva, G., and Lappalainen, P., 2012, "Actin stress fibers--assembly, dynamics and biological roles," Journal of cell science, 125(Pt 8), pp. 1855-1864.
[141] Liu, Z., Tan, J. L., Cohen, D. M., Yang, M. T., Sniadecki, N. J., Ruiz, S. A., Nelson, C. M., and Chen, C. S., 2010, "Mechanical tugging force regulates the size of cell-cell junctions," Proc Natl Acad Sci U S A, 107(22), pp. 9944-9949.
[142] Chen, C. S., Tan, J., and Tien, J., 2004, "Mechanotransduction at cell-matrix and cell-cell contacts," Annu. Rev. Biomed. Eng., 6, pp. 275-302.
[143] Chatzizisis, Y. S., Coskun, A. U., Jonas, M., Edelman, E. R., Feldman, C. L., and Stone, P. H., 2007, "Role of endothelial shear stress in the natural history of coronary atherosclerosis and vascular remodeling: molecular, cellular, and vascular behavior," Journal of the American College of Cardiology, 49(25), pp. 2379-2393.
[144] Maalej, N., and Folts, J. D., 1996, "Increased Shear Stress Overcomes the Antithrombotic Platelet Inhibitory Effect of Aspirin in Stenosed Dog Coronary Arteries," Circulation, 93(6), pp. 1201-1205.

[145] Zhao, S., Suciu, A., Ziegler, T., Moore, J. E., Jr., Burki, E., Meister, J. J., and Brunner, H. R., 1995, "Synergistic effects of fluid shear stress and cyclic circumferential stretch on vascular endothelial cell morphology and cytoskeleton," Arterioscler Thromb Vasc Biol, 15(10), pp. 1781-1786.
[146] Levesque, M. J., and Nerem, R. M., 1985, "The elongation and orientation of cultured endothelial cells in response to shear stress," J Biomech Eng, 107(4), pp. 341-347.
[147] Potter, C. M., Schobesberger, S., Lundberg, M. H., Weinberg, P. D., Mitchell, J. A., and Gorelik, J., 2012, "Shape and compliance of endothelial cells after shear stress in vitro or from different aortic regions: scanning ion conductance microscopy study," PLoS One, 7(2), p. e31228.
[148] Levesque, M. J., Liepsch, D., Moravec, S., and Nerem, R. M., 1986, "Correlation of endothelial cell shape and wall shear stress in a stenosed dog aorta," Arteriosclerosis, 6(2), pp. 220-229.
[149] Ohashi, T., and Sato, M., 2005, "Remodeling of vascular endothelial cells exposed to fluid shear stress: experimental and numerical approach," Fluid dynamics research, 37(1), pp. 40-59.
[150] Wang, J. H., Goldschmidt-Clermont, P., Wille, J., and Yin, F. C., 2001, "Specificity of endothelial cell reorientation in response to cyclic mechanical stretching," J Biomech, 34(12), pp. 1563-1572.
[151] Moore, J. E., Bürki, E., Suciu, A., Zhao, S., Burnier, M., Brunner, H. R., and Meister, J.-J., 1994, "A device for subjecting vascular endothelial cells to both fluid shear stress and circumferential cyclic stretch," Annals of biomedical engineering, 22(4), pp. 416-422.
[152] Wang, C., Baker, B. M., Chen, C. S., and Schwartz, M. A., 2013, "Endothelial cell sensing of flow direction," Arterioscler Thromb Vasc Biol, 33(9), pp. 2130-2136.
[153] Hatami, J., Tafazzoli-Shadpour, M., Haghighipour, N., Shokrgozar, M., and Janmaleki, M., 2013, "Influence of cyclic stretch on mechanical properties of endothelial cells," Experimental Mechanics, 53(8), pp. 1291-1298.
[154] Lu, D., and Kassab, G. S., 2011, "Role of shear stress and stretch in vascular mechanobiology," J R Soc Interface, 8(63), pp. 1379-1385.
[155] Breen, L. T., McHugh, P. E., and Murphy, B. P., 2009, "Multi-axial mechanical stimulation of HUVECs demonstrates that combined loading is not equivalent to the superposition of individual wall shear stress and tensile hoop stress components," Journal of biomechanical engineering, 131(8), p. 081001.
[156] Breen, L. T., McHugh, P. E., and Murphy, B. P., 2010, "HUVEC ICAM-1 and VCAM-1 synthesis in response to potentially athero-prone and athero-protective mechanical and nicotine chemical stimuli," Ann Biomed Eng, 38(5), pp. 1880-1892.
[157] Breen, L. T., McHugh, P. E., and Murphy, B. P., 2010, "HUVEC ICAM-1 and VCAM-1 synthesis in response to potentially athero-prone and athero-protective mechanical and nicotine chemical stimuli," Annals of biomedical engineering, 38(5), pp. 1880-1892.
[158] Jo, H., Sipos, K., Go, Y. M., Law, R., Rong, J., and McDonald, J. M., 1997, "Differential effect of shear stress on extracellular signal-regulated kinase and N-terminal Jun kinase in endothelial cells. Gi2- and Gbeta/gamma-dependent signaling pathways," The Journal of biological chemistry, 272(2), pp. 1395-1401.
[159] Tseng, H., Peterson, T. E., and Berk, B. C., 1995, "Fluid shear stress stimulates mitogen-activated protein kinase in endothelial cells," Circulation research, 77(5), pp. 869-878.
[160] Woodfin, A., Voisin, M. B., and Nourshargh, S., 2007, "PECAM-1: a multi-functional molecule in inflammation and vascular biology," Arterioscler Thromb Vasc Biol, 27(12), pp. 2514-2523.
[161] Chiu, Y.-J., 2009, "Identification of the Kinase for Flow-and Stretch-elicited Phosphorylation of Platelet Endothelial Cell Adhesion Molecule-1 in Endothelial Cells."
[162] Ueki, Y. a., Sakamoto, N., Ohashi, T., and Sato, M., 2009, "Morphological responses of vascular endothelial cells induced by local stretch transmitted through intercellular junctions," Experimental mechanics, 49(1), p. 125.
[163] Plotnikov, A., Zehorai, E., Procaccia, S., and Seger, R., 2011, "The MAPK cascades: signaling components, nuclear roles and mechanisms of nuclear translocation," Biochimica et biophysica acta, 1813(9), pp. 1619-1633.
[164] Kyriakis, J. M., and Avruch, J., 2012, "Mammalian MAPK signal transduction pathways activated by stress and inflammation: a 10-year update," Physiological reviews, 92(2), pp. 689-737.
[165] Li, Y.-S., Shyy, J., Li, S., Lee, J., Su, B., Karin, M., and Chien, S., 1996, "The Ras-JNK pathway is involved in shear-induced gene expression," Molecular and Cellular Biology, 16(11), pp. 5947-5954.

[166] Jalali, S., Li, Y.-S., Sotoudeh, M., Yuan, S., Li, S., Chien, S., and Shyy, J. Y., 1998, "Shear stress activates p60src-Ras-MAPK signaling pathways in vascular endothelial cells," Arteriosclerosis, thrombosis, and vascular biology, 18(2), pp. 227-234.
[167] Wu, J., Thabet, S. R., Kirabo, A., Trott, D. W., Saleh, M. A., Xiao, L., Madhur, M. S., Chen, W., and Harrison, D. G., 2014, "Inflammation and mechanical stretch promote aortic stiffening in hypertension through activation of p38 mitogen-activated protein kinase," Circulation research, 114(4), pp. 616-625.
[168] Li, L. F., Ouyang, B., Choukroun, G., Matyal, R., Mascarenhas, M., Jafari, B., Bonventre, J. V., Force, T., and Quinn, D. A., 2003, "Stretch-induced IL-8 depends on c-Jun NH2-terminal and nuclear factor-kappaB-inducing kinases," American journal of physiology. Lung cellular and molecular physiology, 285(2), pp. L464-475.
[169] Li, Y.-S. J., Haga, J. H., and Chien, S., 2005, "Molecular basis of the effects of shear stress on vascular endothelial cells," Journal of biomechanics, 38(10), pp. 1949-1971.
[170] Wang, J. G., Miyazu, M., Matsushita, E., Sokabe, M., and Naruse, K., 2001, "Uniaxial cyclic stretch induces focal adhesion kinase (FAK) tyrosine phosphorylation followed by mitogen-activated protein kinase (MAPK) activation," Biochem Biophys Res Commun, 288(2), pp. 356-361.
[171] Correa-Meyer, E., Pesce, L., Guerrero, C., and Sznajder, J. I., 2002, "Cyclic stretch activates ERK1/2 via G proteins and EGFR in alveolar epithelial cells," Am J Physiol Lung Cell Mol Physiol, 282(5), pp. L883-891.
[172] Pedrigi, R. M., Papadimitriou, K. I., Kondiboyina, A., Sidhu, S., Chau, J., Patel, M. B., Baeriswyl, D. C., Drakakis, E. M., and Krams, R., 2017, "Disturbed Cyclical Stretch of Endothelial Cells Promotes Nuclear Expression of the Pro-Atherogenic Transcription Factor NF-kappaB," Ann Biomed Eng, 45(4), pp. 898-909.
[173] Hajra, L., Evans, A. I., Chen, M., Hyduk, S. J., Collins, T., and Cybulsky, M. I., 2000, "The NF-κB signal transduction pathway in aortic endothelial cells is primed for activation in regions predisposed to atherosclerotic lesion formation," Proceedings of the National Academy of Sciences, 97(16), pp. 9052-9057.
[174] Gareus, R., Kotsaki, E., Xanthoulea, S., van der Made, I., Gijbels, M. J., Kardakaris, R., Polykratis, A., Kollias, G., de Winther, M. P., and Pasparakis, M., 2008, "Endothelial cell-specific NF-κB inhibition protects mice from atherosclerosis," Cell metabolism, 8(5), pp. 372-383.
[175] Riou, S., Mees, B., Esposito, B., Merval, R., Vilar, J., Stengel, D., Ninio, E., van Haperen, R., de Crom, R., Tedgui, A., and Lehoux, S., 2007, "High pressure promotes monocyte adhesion to the vascular wall," Circulation research, 100(8), pp. 1226-1233.
[176] Sucosky, P., Balachandran, K., Elhammali, A., Jo, H., and Yoganathan, A. P., 2009, "Altered shear stress stimulates upregulation of endothelial VCAM-1 and ICAM-1 in a BMP-4–and TGF-β1–dependent pathway," Arteriosclerosis, thrombosis, and vascular biology, 29(2), pp. 254-260.
[177] Golledge, J., Turner, R. J., Harley, S. L., Springall, D. R., and Powell, J. T., 1997, "Circumferential deformation and shear stress induce differential responses in saphenous vein endothelium exposed to arterial flow," Journal of Clinical Investigation, 99(11), p. 2719.
[178] Tzima, E., Irani-Tehrani, M., Kiosses, W. B., Dejana, E., Schultz, D. A., Engelhardt, B., Cao, G., DeLisser, H., and Schwartz, M. A., 2005, "A mechanosensory complex that mediates the endothelial cell response to fluid shear stress," Nature, 437(7057), pp. 426-431.
[179] Hashimoto, K., Kataoka, N., Nakamura, E., Tsujioka, K., and Kajiya, F., 2007, "Oxidized LDL specifically promotes the initiation of monocyte invasion during transendothelial migration with upregulated PECAM-1 and downregulated VE-cadherin on endothelial junctions," Atherosclerosis, 194(2), pp. e9-e17.
[180] Meza, D., Shanmugavelayudam, S. K., Mendoza, A., Sanchez, C., Rubenstein, D. A., and Yin, W., 2017, "Platelets modulate endothelial cell response to dynamic shear stress through PECAM-1," Thromb Res, 150, pp. 44-50.